Universidade de Aveiro
2014
Departamento de Engenharia de Materiais e Cerâmica

Kyle Jacob Debelak

ZnO NP e compósitos PU/ZnO NP para libertação controlada de Ibuprofeno

Universidade de Aveiro Departamento de Engenharia de Materiais e Cerâmica
2014

Kyle Jacob Debelak

ZnO NP e compósitos PU/ZnO NP para libertação controlada de Ibuprofeno

ZnO NP and PU/ZnO NP composites for controlled delivery of Ibuprofen

Dissertação apresentada à Universidade de Aveiro para cumprimento dos requisitos necessários à obtenção do grau de Mestre em Ciência e Engenharia de Materiais, realizada sob a orientação científica das Doutoras Maria Elizabete Jorge Vieira da Costa, Professora Auxiliar, e Maria Helena Figueiras Vaz Fernandes, Professora Associada, ambas do Departamento de Engenharia de Materiais e Cerâmica da Universidade de Aveiro.

Dissertation presented to the University of Aveiro to obtain the Master degree in Materials Science and Engineering, under scientific supervision of Dr. Maria Elizabete Jorge Vieira Costa, Auxiliary Professor and Dr. Maria Helena Figueiras Vaz Fernandes, Associate Professor, both of the Department of Materials and Ceramics Engineering of the University of Aveiro.

Jury Members

President

Profª Doutora Ana Margarida Madeira Viegas de Barros Timmons
Professor Auxiliar da Universidade de Aveiro

Doutora Ana Luísa Daniel da Silva
Equiparado a Investigador Auxiliar da Universidade de Aveiro

Profª Doutora Maria Elizabete Jorge Vieira da Costa
Professor Auxiliar da Universidade de Aveiro

Acknowledgements

I would like to express my gratitude to the following, whose support has been integral to the completion of this work:

the European Commission, EMMI Institute, and FAME Consortium, for their financial and academic support

my supervisors Elizabete Costa and Helena Fernandes, for their endless encouragement and insight

my gregarious lab colleagues Alicia Alves, Nathalie Barroca, and Priscila Melo, for their beauty and camaraderie that drew me to the laboratory each day

my coursemates Mikalai Zhuk and Hugues Mondesért, for their emotional support as we completed this adventure together

my Erasmus family, for providing the distractions that allowed me to keep balance through this journey

my parents, for everything.

palavras-chave

Óxido de zinco, poliuretano, ibuprofeno, sistemas de libertação de fármacos

resumo

Para projectar um sistema de entrega de fármacos, em que se pretende armazenar uma grande quantidade de fármaco a ser libertada durante um período de tempo longo, é vantajoso recorrer a nanoestruturas com elevada área específica para o carregamento do fármaco por processos adsortivos. Além disso, a combinação de transportadores nanoestruturados com materiais poliméricos, formando sistemas compósitos para a entrega de fármacos pode proporcionar o controlo de certos parâmetros associados à libertação do fármaco. Entre as várias combinações possíveis, o óxido de zinco (ZnO) e o poliuretano (PU) oferecem um particular interesse dado ser possível preparar ZnO nanoestruturado e o PU ser um polímero com reconhecida aptidão para aplicações médicas.

Neste trabalho, estudaram-se vários aspectos do processo de libertação de um fármaco modelo (o ibuprofeno) a partir de nanoestruturas de óxido de zinco e de compositos ZnO/PU. Em particular, estudaram-se os efeitos da variação da carga do fármaco usando soluções etanólicas com diferentes concentrações do fármaco,i.e. 1, 2, 10, e 20 mg de ibuprofeno / mL de etanol, tendo-se demonstrado que por esta via se pode controlar a carga do fármaco , o que é importante para personalização da dose em sistemas de entrega de fármacos. Além disso, a importância dos procedimentos de lavagem das nanoestruturas após carregamento do fármaco foi também avaliada, concluindo-se que tais procedimentos condicionam a carga de fármaco por remoção das camadas de fármaco fracamente adsorvidas. Estudou-se também a libertação de ibuprofeno a partir das nanoestruturas de óxido de zinco puro e dos compositos ZnO/PU, medindo a variação no tempo da quantidade de fármaco libertada em solução tampão de fosfato. Os perfis de libertação do fármaco aliados às imagens de microscopia electrónica (SEM) dos materiais obtidas no fim de diferentes períodos de tempo de libertação são usados neste trabalho para discutir os mecanismos de libertação do fármaco e avaliar a sua relacção com a degradação do material em análise.

keywords

Zinc Oxide, Polyurethane, Ibuprofen, Drug Delivery Systems

abstract

For the design of drug delivery systems, in which a large amount of drug should be stored and released over a sustained period of time, utilization of nanostructures is frequently advantageous as their high specific surface areas are beneficial for adsorptive drug loading. Additionally, the use of nanostructured drug carriers in concert with polymeric materials in composite drug delivery systems affords control over the drug release characteristics. While many combinations of materials can be imagined, the use of zinc-oxide and poly(urethane) is of particular interest in that nanostructures based on the former are easily producible and the latter is already an established material in biomedical applications.

In this investigation, various aspects of the drug delivery properties were examined. In particular, the effects of altering the amount of drug loaded (by loading in solutions of 1, 2, 10, and 20 mg ibuprofen/mL ethanol) were studied and it was demonstrated that the amount of drug loaded can be controlled, which is important for customizing dosages in drug delivery systems. Additionally, the role of a washing procedure after loading the nanoparticles was examined in order to show that these procedures influence the drug loading by removal of loosely bound layers of drug.

In completion of this study, the release of ibuprofen from both pure zinc oxide nanoparticles and the composites with poly(urethane) was investigated by tracking the concentration of drug present in a phosphate buffered saline solution containing the drug carrier with respect to time. In order better understand the mechanisms of drug release and analyze the degradation processes of the drug carrier, SEM images were produced for the samples at various times during the drug release process.

Table of Contents

List of Figures

List of Tables

Abbreviations

ATR-FTIR – Attenuated Total Reflectance Fourier Transform Infrared Spectroscopy

BET – Model of Brunauer, Emmet, and Teller

DDS – Drug Delivery System

DMF – *N,N*-dimethylformamide

DPM – Di(ethylenediamineplatinum)medronate

ETH – Ethanol

FTIR – Fourier Transform Infrared Spectroscopy

FWHM – Full-Width at Half-Maximum

IBU – Ibuprofen

MIC – Minimum Inhibitory Concentration

PBS – Phosphate Buffered Saline

SEM – Scanning Electron Microscopy

TGA – Thermogravimetric Analysis

UV-VIS – Ultraviolet-Visible Spectroscopy

XRD – X-ray diffraction

Chapter 1

Introduction and Objectives

1. Introduction and Objectives

1.1. Motivation

With the advances in modern medicine and associated increases in quality of life as well as life expectancy, a further expansion of the paradigm for common treatment practices is necessary. In the case of hard tissue engineering, post operation drug-delivery is integral to recovery and rehabilitation. For this purpose, much research is focused on the topics of targeted and sustained drug delivery systems (SDDs), which can locally and consistently administer a drug to a desired location within the body over the course of an extended time period. Unfortunately, modern practices often fall short in achieving the therapeutic goals set out for drug treatment. Namely, conventional systems may not effectively target the desired site and, if this is indeed the case, the delivery is frequently characterized by a fast, burst-type drug release [1]. Addressing these two problems is the heart of current research trends in drug delivery systems.

While many drug delivery systems (DDSs) can be envisioned, the focus of this thesis will be on ceramic nanostructured particles and composite materials comprising said nanostructured particles within a polymer matrix. Specifically, the material system of zinc oxide/poly(urethane) is the material of interest. Each component has established application in biomedicine and preliminary studies on the composite system based on embedment of zinc oxide nanoparticles in a polyurethane matrix offer promising results [2].

In studies on drug delivery systems, the unfortunate reality is the non-standardized methodology in sample preparation and experimental design. Naturally, the synthesis procedures must vary for the fabrication of an array of materials and sample types. However, significant ambiguity lies in the steps taken with the resulting drug delivery materials. For example, a common technique for loading the model drug into the DDS prescribes suspending the DDS in a drug-containing solution and allowing it to soak for a specified duration. Following collection of the powder, however, some authors report washing the DDS, often under the high forces of an ultracentrifuge. While such minor

differences in experimental procedure may seem insignificant, altering the initial state of the DDS before performing drug release experiments can complicate comparisons between different systems.

1.2. Objectives

While previous works have focused on the characterization and biocompatibility of the ZnO/PU nanostructured, composite DDSs, as well as on the various influences of alternative synthesis routes [2,3], the objective of this study will be to more specifically explore the drug release properties of both the nanostructured zinc oxide as well as the composite systems. Namely, investigations on the effect of the drug-loading environment will take place, where the concentration of drug in the solution will be varied in order to determine the extent to which the drug-loading amount can be controlled. Secondly, the effect of washing the nanostructured particles post-loading will be investigated in order to see if there exists some merit in this procedural step frequently reported in literature. Thirdly, drug release studies will be performed on composite samples of different weight ratios (relative amounts of ZnO and PU) in order to explore the effect the polymer plays in the drug release mechanics of the system as a whole. Finally, mathematical modeling of the data will be performed in an attempt to draw connections between the various release studies. For this, proposed equations commonly found in literature will be used.

1.3. Thesis Structure

This thesis will continue with a review of the state-of-affairs in the literature regarding DDSs in order to develop a background in the topic. Following will be an overview of the experimental procedures for material synthesis, characterization, and drug release experiments, after which the experimental data will be presented as well as a discussion of the results. Finally, a review of the main points will be given in the conclusion along with suggestions for future work.

Chapter 2

Literature Review

2. Literature Review

2.1. Drug Delivery Systems

At its root, the concept of drug delivery is rather simple in that the end goal is simply to introduce a drug to the body in order to obtain the desired effects from the drug. However, the routes taken to achieve this goal differ greatly in both methodology as well as complexity. For example, orally administering a drug encapsulated in a pill is quite simple in comparison to the creative techniques envisioned for targeted drug delivery. One can easily imagine the advantages of targeted drug delivery, especially for the archetypical example of chemotherapy-based cancer treatments. With targeted drug delivery, the drug would be administered solely to the desired location, reducing the negative side effects associated with a general, non-targeted drug delivery. However, the ease of use for the delivery of drugs through methods such as inhalation, ingestion, or injection should not be overlooked.

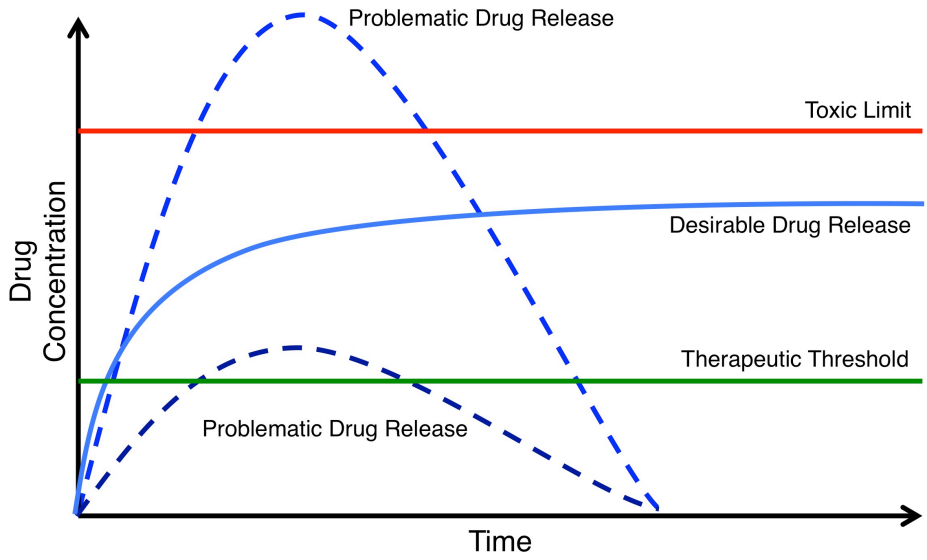

Figure 1: Comparison of controlled drug release with conventional drug administration

As can be seen in figure 1, problems arise when little control is provided for the drug release. In the two extreme cases, either the drug concentration surpasses the toxic limit

in order to achieve a prolonged release or the drug concentration remains above the therapeutic threshold for only a short amount of time in order to ensure that the drug concentration does not surpass the toxic limit. These lines correspond to non-controlled drug release, such as would occur through oral or general administration of a drug—non-targeted drug delivery systems. The ideal case, falling in the middle of the therapeutic threshold and toxic limit, is given for a controlled release system where the drug concentration within the body can be maintained between the two limits for an extended duration.

In terms of targeted drug delivery, the range of techniques also varies quite drastically. While the group's interest lies in zinc oxide-based nanostructures and their associated composites, techniques such as the use of liposomes, fullerenes, or carbon nanotubes have been proposed [4]. In these examples, the drugs are loaded into fabricated vesicles, which serve to transport a drug or other agent of interest in a cage-like structure. While fullerenes and carbon nanotubes can be categorized as carbon nanostructures, the basis of the liposome structure is a bilayer of lipids, small organic molecules typically associated with ampiphilicity. Through functionalization of these vessels with various ligands, the carrier structure can target specific cells for drug delivery. As the targeting nature of the nanocarriers allows a reduction in the adverse side effects expected for small molecule drugs such as the platinates, camptothecins, or adriamycins (commonly used cancer treatments), much research is focused on such delivery systems [5]. In this case, the drug delivery system functions by forcing the drug movement throughout the body to a specific location after administering the system in a general manner. The drug release can then commence once the system arrives at the site of interest.

However, while these notable examples indeed offer promising application in the realm of targeted drug delivery, they would first be generally introduced into the body and the targeting would then follow based on the chemistry of the carriers. Alternatively, the targeting aspect of drug delivery could include physical administration of the drug to the desired site. Indeed, this is how the delivery would take place for the ZnO/PU system, with the drug loaded into a composite material applied directly to the target site as a part of a surgical procedure, for example.

In the case where the targeted delivery is completed by direct application of the drug carrier to the target site, developing a system in which the drug delivery can continue for long durations is also desirable. It is therefore imperative to improve the capabilities of the delivery systems to promote sustained drug release in addition to simply developing the targeting in general. More specifically, the goal is to enable continuous and consistent delivery of the drug of interest. Or rather, the goal is to be able to control the release of the drug in order to fine-tune both the dosage and duration of drug delivery so that the DDS can be useful for several applications.

The heading of “targeted drug delivery systems” can thus be split into two categories, depending on the method by which the targeting occurs: “smart” carriers, and direct application devices. The term “smart carriers” describes devices, typically of a nanoscale, which respond to some external signal in order to deliver the drug to the target site. This means that, while the system could be administered generally, the drug activity would be limited to the area of interest. For example, a carrier could be functionalized so that the drug release would be triggered on pH changes. As tumorous cancer cells exhibit a lower pH than healthy cells, the delivery of antitumoral drugs could be restricted to tumorous cells through the use of a “smart” delivery system. Further external triggers could include application of a magnetic field, ultrasound, electric field, temperature change, light, or mechanical forces [6]. For the second category, the direct application of a drug delivery system describes a method for containing the drug activity simply by limiting the location of the drug delivery device in the body. Such would be the case for implant materials, transdermal patches, or wound dressings, among others [7].

As previously mentioned, in terms of post-operation therapy, maintaining a continuous pharmaceutical level above a certain minimum concentration is necessary in order to ensure the most effective treatment. For example, with antibacterial treatment, a minimum inhibitory concentration (MIC) must be maintained, which is analogous to the previously introduced term “therapeutic threshold”; below this value, the drug is no longer effective. Furthermore, this concentration must be maintained at the specific target site. With non-targeted delivery, a high concentration of drug will be present throughout the entire body, resulting in negative side effects due to the widespread presence of drug, as occurs when the drug concentration surpasses the toxic limit.

To highlight the efficacy of targeted, sustained delivery systems, it is useful to compare the drug concentration profiles as shown in figure 2. Additionally, this type of graphic will serve as the basis for comparison of the various drug delivery systems investigated in the literature review. While the graphic specifies release profiles for proteins, these curves are representative for any type of release. Furthermore, these hand-drawn curves are simply intended to serve as examples for the various types of release profiles; they are not associated with any particular set of experimental data, which is also valid for figure 1.

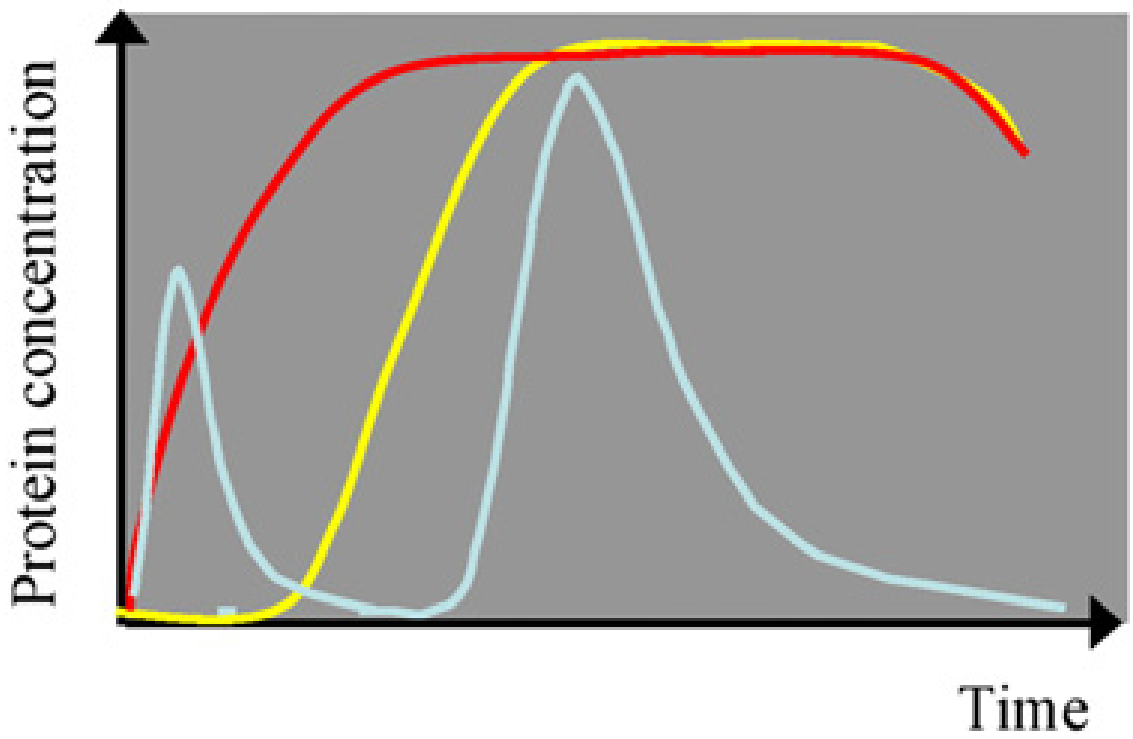

Figure 2: Types of delivery profiles, adapted from [8]
Red: continuous delivery, Yellow: delayed delivery, Blue: pulse-like delivery

In general, continuous administration of the drug can be ensured by repeated doses, characterized by a pulse-like profile of the drug concentration within the body, shown as the blue line in the figure. An extension of this profile as seen in the figure would describe the familiar example of “take two pills, twice daily” associated with a doctor’s instructions for prescribed medication. However, for cases where the drug is administered directly to the targeted site, as would occur by introducing the drug delivery system during a surgery, repeated dosage is not a viable solution to ensure continuous drug availability; once the concentration reduces below the MIC, it is no longer realistically possible to reintroduce

the drug. Additionally, as was seen in figure 1, problems often arise when the drug concentrations exceed the toxic limit. When this repeatedly occurs problems may arise regarding drug side effects. To address this problem, the drug release should be sustained for the treatment duration. A release profile for a sustained release can be seen as the red line in the figure 2. This type of release profile is described by an initial steep increase in concentration followed by a plateau at a maximum concentration. Additionally, for a third situation, the yellow line in figure 2 displays the profile for a delayed release, which is similar to the continuous delivery, but the initial step is offset by a delay time.

Although the reported delivery systems (these will be discussed in following sections) generally displayed release profiles coinciding with the continuous release curve, the differences in time-scale are what necessitate the engineering of advanced delivery systems. Namely, the optimal release curve requires maintenance of the plateau concentration for the duration of treatment. It is of little use if the continuous delivery is concluded after only a few hours when the ideal therapy involves several days of drug administration. Additionally, a consistent delivery is also desired for the optimal release profile. Perhaps the greatest challenging to designing effective delivery systems is to reduce the typical ‘initial burst’ seen by a surge of drug released within a short amount of time followed by a reduced release rate. Finally, the drug loading capacity for a delivery system must be considered. This property simply refers to the amount of drug that can be stored in a delivery system and is typically given as a weight ratio between the drug loaded and the carrier itself.

2.1.1 Use of Nanoparticles in a Delivery System

It should now be apparent that the crux of designing the delivery systems lies in enabling a continuous release for a sustained period and maximizing the drug loading capacity. For the proposed system of ZnO/PU, or ceramic/polymer composites in general, the main mechanism for the drug-uptake relies on the adsorption of the drug molecules onto the surface of porous, inorganic nanoparticles. Because of this, a key parameter will be the surface area to volume ratio of the particles, which can be maximized by a reduction in the particle size.

However, a reduction in size of a material can also be associated with a change in the material properties, such as a change in the absorbance spectrum for gold nanoparticles [9]. With this in mind, the toxicity of the inorganic nanoparticles must be considered, as the toxicological properties of the inorganic nanoparticles may not necessarily correlate with those of the bulk material. Additionally, the toxicological properties of nanoparticles changes upon incorporation into a composite material; toxicity is important for isolated nanoparticles.

2.1.2 Use of Polymers in a Nanocomposite Delivery System

To address the challenge of achieving a sustained drug release, novel techniques must be employed in order to optimize the release profile. A promising method relies on the use of polymeric materials in a nanocomposite with inorganic nanoparticles. In this way, the polymeric matrix could serve as a diffusion barrier for the drugs, increasing the time scale of the drug release and suppressing the initial burst. Additionally, the drugs could be stored in a biodegradable polymer, and the drug release would coincide with the biodegradation of the polymeric material. It is one of the goals for the study of the ZnO/PU system to determine the role that the poly(urethane) plays in terms of drug loading and release. Appropriate results from literature regarding the use of polymers in drug delivery systems will be discussed.

2.2 Drugs of Interest in Drug Delivery Systems

Naturally, the goal of a delivery system is to introduce a specific chemical into the body in a controlled manner. Drugs of particular interest for tissue engineering include, but are not limited to, proteins, growth factors, antibiotics, anti-inflammatory, and anticancer drugs. With the introduction of these compounds to the body, recovery may be facilitated through promotion of tissue regeneration, prevention of infections, and alleviation of pain caused

by the procedure. Of course, tissue engineering is not the sole application envisioned for drug delivery systems. For example, administration of drugs through the skin via fiber mats in a transdermal patch serves as an additional use for drug delivery systems [10].

However, with the assortment of attractive drugs for various therapeutic applications, it must not be forgotten that their different properties determine their respective loading and release behavior in a delivery system; the chemistry of the drug molecule dictates the kinetics of the delivery process, as well as the drug loading mechanisms and degradation of the loaded system. That is to say, an ideal delivery system tailored to one species may not (and likely will not) necessary prove effective for a second drug. Differences in molecular structure (size, geometry, hydrophobicity, etc.) and electrostatic properties mean that each drug should be treated on a case-by-case basis. This must also be remembered when comparing the systems proposed in literature, as the standards set for gentamicin delivery systems differ from those for salicylic acid, for example.

Fortunately a large number of studies have used ibuprofen as the model drug. Ibuprofen is an anti-inflammatory drug often taken to alleviate pain associated with rheumatoid arthritis as well as to treat mild aches associated with fever, headaches, or common cold [11]; it is of particular interest in this study due to its broad range of application, such as effectiveness in reducing post-operation swelling and associated pain for bone surgeries. The chemical structure of ibuprofen is presented below in figure 3, and the molecule is characterized by empirical formula of $C_{13}H_{18}O_2$, a molecular weight of 206.26, and a melting point between 75-77°C [12].

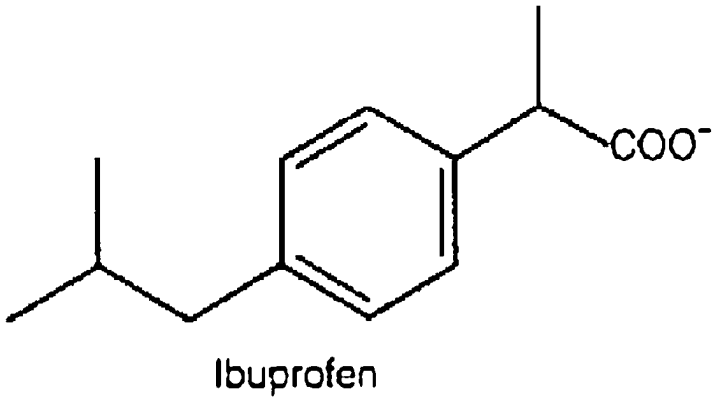

Figure 3: Molecular Structure of Ibuprofen, adapted from [13]

In terms of loading ibuprofen, it is important to note the polarity of the molecule, as this property may dictate its ability to adsorb onto certain drug delivery systems. For example, the –COOH groups of ibuprofen tend to form electrostatic bonds with Ca^{2+} species in calcium silicate hydrate based drug delivery systems [14]. Additionally, the size of the molecule can play a role where geometrical constraints are considered, as is the case for mesoporous drug carriers with channels of small diameters. These and other factors will be discussed in further detail with respect to particular delivery systems later in this report.

Though ibuprofen is frequently used as a model drug in studies related to drug delivery, the array of other drug types should not be overlooked, as each has its place in modern medicine. In examples of bone replacement, delivery of antibiotics is commonly desired in order to prevent bone degradation due to periodontis or other related infections [15]. Additionally, the administration of growth factors and proteins can serve to promote growth of natural bone in order to slowly remodel a bone defect [16]. Naturally, the use for drugs extends well beyond tissue engineering, such as the use of antitumoral drugs in cancer treatment [4].

2.3 Factors that Influence Drug Release

The drug release is influenced by many factors, especially those that relate to the adsorption properties of the system such as porosity of the drug carrier, chemical interactions between the drug and surface of the carrier, and the use of diffusion barriers such as polymer coatings. Several systems have been reviewed which allow analysis of these factors. Namely, inorganic DDSs based on calcium phosphate materials were of interest due to their prevalence in biomedical research and chemical similarity to natural bone inorganic phase; systems based on mesoporous silica (SiO_2) are also of interest, as these oxide materials, when characterized by nanoscopic morphologies, could function similar to ZnO nanoparticles.

2.3.1. Porosity of the Drug Delivery System

The porosity of the DDS plays a large role in the drug release profile; furthermore, the pore morphology, including pore size, tortuosity, and interconnectivity also influence the drug release. When considering porosity, the pore scale is of importance, as the pore sizes may range from a few nanometers in the case of mesoporous silicates, to hundreds of microns for hydroxyapatite scaffolds.

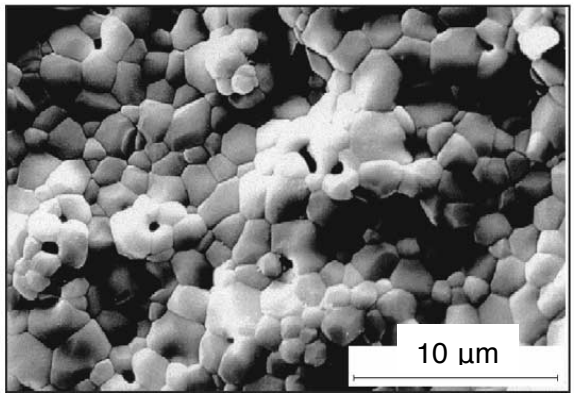

Figure 4: SEM of a porous scaffold as produced by Palazzo et al. showing the microporosity on the walls of the macropores, adapted from [17]

To begin, hydroxyapatite scaffolds offer attractive potential for applications in bone implant materials and drug delivery devices due to their structural similarities to the mineral phase of natural bone [17, 18]. A typical scaffold used as a DDS can be seen in figure 4, with the porous nature of the material clearly observable. It was found that variations in processing parameters affected the drug release profile. Namely, the type of drug loaded, the porosity of the scaffolds, and the amount of drug loaded were investigated. The respective drug release profiles are shown in figure 5. Beginning with the topmost graph, the influence of the type of drug is shown and the idea is reinforced that a delivery system optimized for one type of drug may not necessarily be the best system for a different drug. It can be seen that the release of ibuprofen is more complete, meaning that less residual drug remains in the delivery system after the drug release plateaus. For hydrocortisone, less than 80% of the drug releases, even after 300 minutes. Furthermore, the initial drug release is more evident in the case of hydrocortisone. Both of these results are due to the higher steric hindrance of hydrocortisone, which hinders the diffusion of the molecule through the porous network of the scaffold, resulting in the slower overall release seen by the incomplete drug release after 300 minutes. For the same reason, the drug tends to concentrate on outer macroporous walls, leading to the rapid initial burst release.

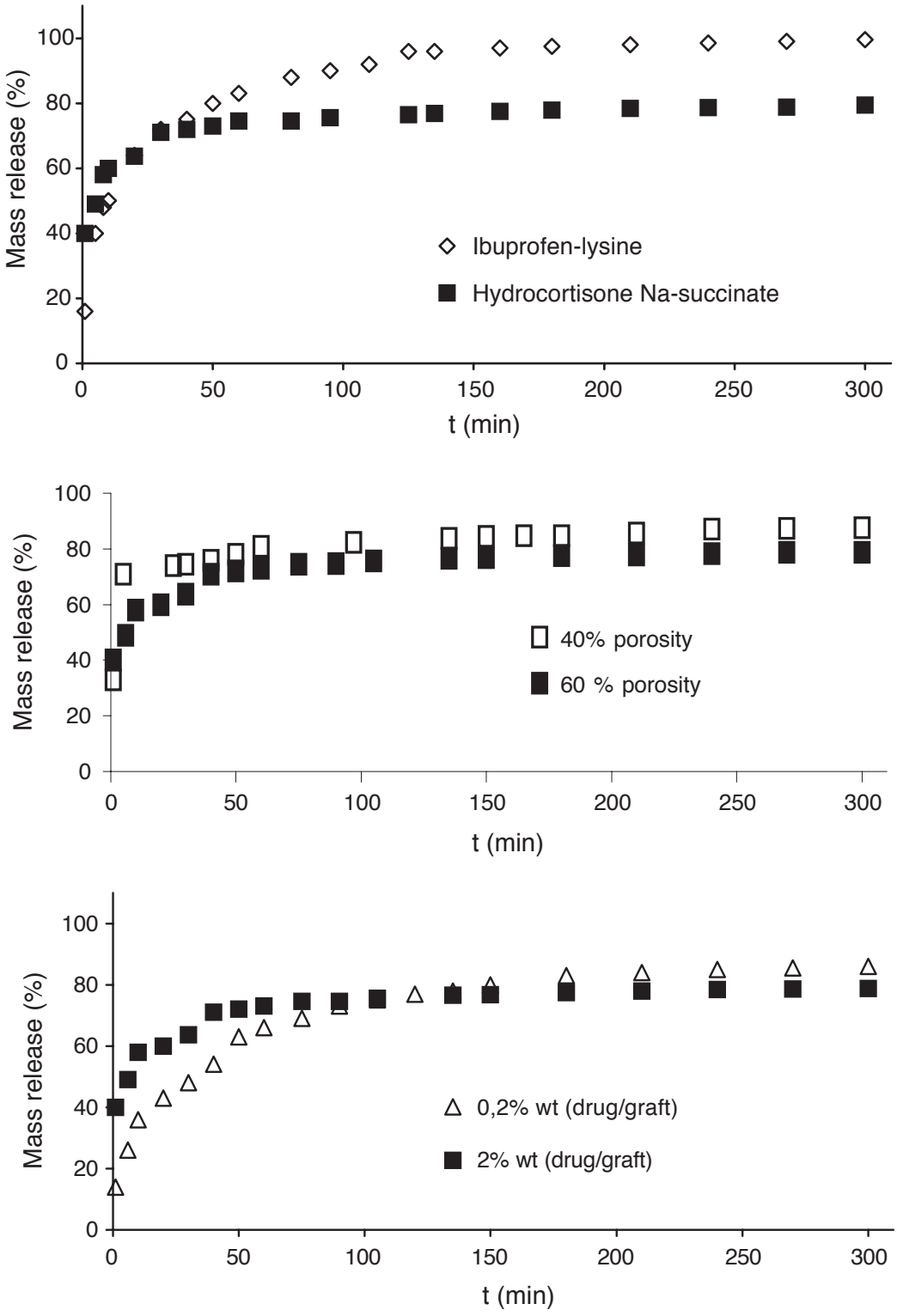

Figure 5: Drug release profiles for hydroxyapatite scaffolds as prepared by Palazzo et al. From top to bottom: effect of drug type, effect of total porosity, and effect of amount of drug loaded, adapted from [17]

In the middle graph can be seen the effect of porosity observed in the study. Note that the graphs were produced using hydrocortisone. Here, the initial burst is seen to be higher for the materials of lower porosity, as well as the overall faster release shown by the more complete drug release. In this case, the initial burst is also promoted by the higher concentration of drug on the external macropore walls. It follows that with a less porous scaffold, more of the drug must be concentrated on external walls and a higher burst type release will thus be observed. Indeed, this is the case. The effect of drug loading amount also plays on this same phenomenon. As more drug is loaded and the micropores are filled, the drug must adsorb to the walls of the macropores, resulting in the higher burst release observed for the sample loaded with more drug [17].

The study of scaffolds can be extended to analyze the influence of nanopore size within the scaffolds themselves [18]. The initial burst release was seen to be particularly dependent on these pore sizes. Figure 6 shows the ibuprofen drug release profiles for two samples from another study where drug release properties of hydroxyapatite-based materials, Sp3 and Sp4, are investigated. These samples differed in their preparation by variation of microemulsion content, which translated to different pore morphologies in the final materials. More specifically, the sample Sp3 had smaller pores with an average diameter of 60 nm and a porosity of 54.7% while sample Sp4 had pores with an average diameter of 146.4 nm and a porosity of 64.6%. Furthermore, the tortuosity reported for the Sp3 samples was higher, meaning that the diffusion pathways inside the sample included more twists and turns. Shown by the black line in the figure, the data for Sp4 is presented in the curve showing the higher burst release, being steeper at times less than four hours. The first observation one may notice is that the role of porosity has the opposite effect as was observed by Palazzo. However, it must be remembered that the pores here are of a different size scale than the macroscopic pores of the previous data. Another important difference is that in the scaffolds prepared by Öner et al., the pores were more or less uniform. Therefore, with the larger pores, the diffusion of ibuprofen was much easier than for smaller pores. Because of this, the initial burst effect was more pronounced in the samples of higher porosity.

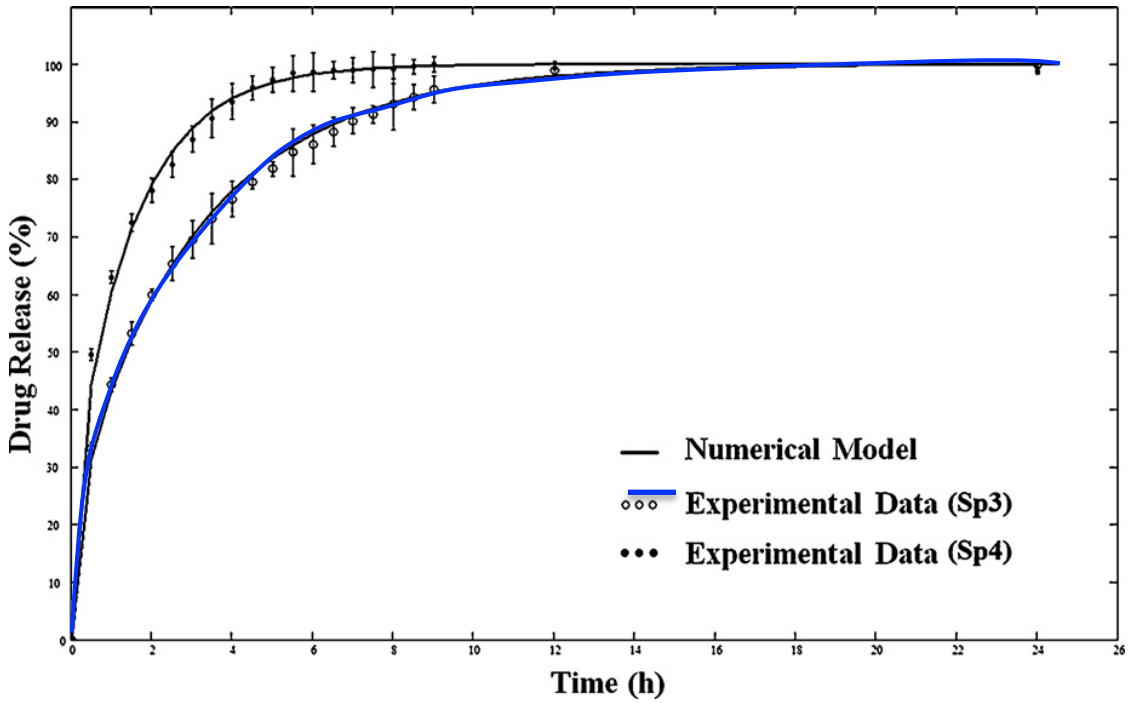

Figure 6: Drug release profiles for hydroxyapatite scaffolds as prepared by Öner et al. showing the effect of porosity, adapted from [18]

The investigation of the effect of pore morphology on drug release is the focus of many studies on the use of mesoporous silicate-based DDSs. The typical silicate structures in the present discussion are characterized by having strongly ordered porous networks, with pore diameters less than 100 nm [19-22].

In materials where the pore sizes are on a similar order of magnitude as the size of the drug molecule, diffusion and drug release properties are frequently limited simply by geometrical constraints. In MCM-41 synthesized with pore diameters of 2.5 nm, the ibuprofen molecules cannot overlap for efficient adsorption in the pore channels [22]. This effect can be seen in figure 7. However, for the MCM-41 sample with 3.6 nm pore diameters, the ibuprofen could efficiently pack on the pore surfaces. The relationship this has with the release profile can be seen in figure 8.

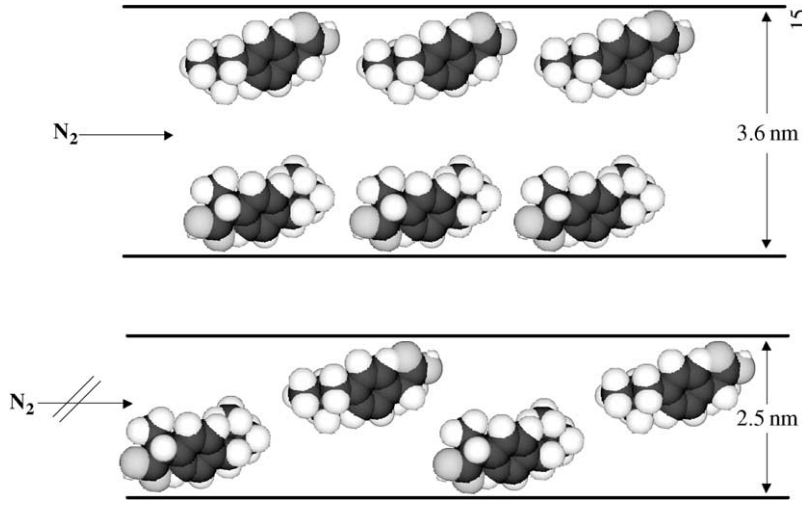

Figure 7: Effect of Pore diameter in mesoporous channels on the drug loading of MCM-41, adapted from [22]

It can be seen from the release profiles that the drug release rate for the larger-pored samples is significantly faster. For the samples MCM-$41_{8(70\%)\text{-}10(30\%)}$ and MCM-$41_{8(85\%)\text{-}10(15\%)}$ the authors reported incomplete delivery even after three weeks, while the other two samples had completely released the ibuprofen after three days. TG data were taken after the drug loading to determine the weight percent of drug loaded, and the release rate was determined by observing when the total drug released compared to this value. Additionally, the total amount of drug release is higher for the MCM-41_{16} and MCM-41_{12} samples, due to the larger pore volume in the samples with a larger pore diameter. This follows from simple geometrical considerations. As various samples were synthesized by using different surfactants, it is possible to control the pore sizes by adjusting the ratios of surfactants. Furthermore, the pore volume and subsequent amount of drug loaded are also controlled by the surfactants used in synthesis. Therefore, the drug dosage and delivery rate can be engineered based on the synthesis procedure.

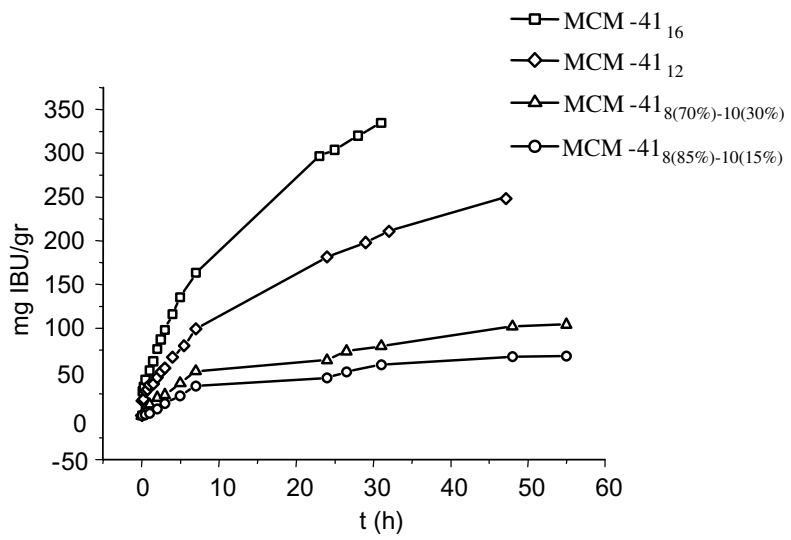

Figure 8: Effect of pore diameter on release profile. Diameters are as follows (in nm): MCM-41$_{16}$ = 3.6, MCM-41$_{12}$ = 3.3, MCM-41$_{8(70\%)-10(30\%)}$ = 2.7, MCM-41$_{8(85\%)-10(15\%)}$ = 2.5, adapted from [22]

An identical conclusion to the relationship between pore size and drug delivery rate was reached by comparing the release profiles for the mesoporous silicates MCM-48 and LP-*Ia3d* [20]. Here, the analysis was extended with the realization that the pore size alone does not determine the drug delivery rate, but the relationship in size between the drug molecule and pore diameter. That is, the larger the drug molecule with respect to the pore channels, the slower the drug delivery rate. However, with the suppression of delivery rate, the maximum drug loading also decreases. The effect of pore size was also confirmed by Ukmar et al. in the comparison of MCM-41 with an average pore diameter of 3.1 nm having a slower release than SBA-15 with an average pore diameter of 9.2 nm [21].

These studies were extended by investigating the effect of surface functionalization of the mesoporous silicates on the drug release profiles [19]. The delivery profiles for five variations of mesoporous silicates are shown in 9. Here, the “a” after the material name denotes that the sample was aged at 363K at a pH of 10 for five days after the material synthesis. The “μ” symbol before the material name denotes a microporous material, while “m” describes a mesoporous material. Finally, the “c” in cMCM-41a denotes that the material was synthesized in the presence of decanoic acid and toluene; the material is cationic. The first observation from the figure is that the dependence on pore size shown by the previous studies is confirmed in that the microporous materials display a significantly faster release than the mesoporous carriers. Secondly, the functionalization of

the MCM-41 with cationic surface significantly suppresses the initial burst and sustains the drug delivery for roughly 400 hours, or over two weeks.

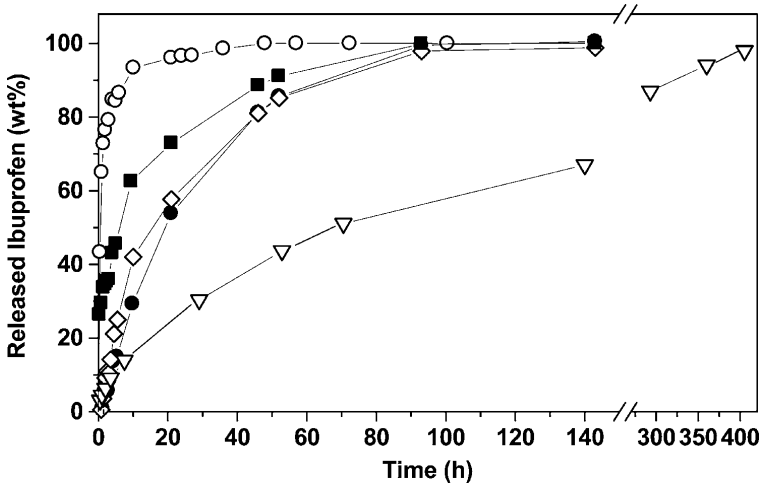

Figure 9: Drug release profile for various mesoporous silicates: open triangles = cMCM-41a, open diamonds = μSBA-1, open circles = MCM-41a, closed circles = μSBA3, closed squares = mSBA-3, adapted from [19]

It was found that the drug loading capacity for the microporous materials was lower than that for the mesoporous materials. This is due to the pore sizes of >2nm for the microporous materials, the size constraints resulted in steric hindrance of the drug molecules, preventing high drug loadings. So long that the pores are large enough for efficient packing, maximizing the surface area allows the highest drug loading as the process is adsorption based [22]. It was also suggested that the drug loading is based on adsorption mechanisms based on hydrogen bonding of the carboxyl group of ibuprofen and silanol groups of the silica [19]. For the case of the slow release of c-MCM-41a, the authors suggest that the synthesis forms 1D cage like pores, which, combined with the small pore diameter and high relative loading per surface area, results in slow diffusion kinetics and a sustained drug release.

From these studies, it can be seen that the reduction in pore size is advantageous for suppressing the burst release observed in drug delivery systems with large pores such as was seen in the case of the calcium phosphate based scaffolds. The porosity and its associated properties will likely play a large role for the drug release of the nanostructured zinc oxide particles under study.

2.3.2 Interactions between drug and DDS surface

As has been discussed previously, the type of drug loaded in the system plays a role in the drug release properties and a system optimized for a specific drug may not necessarily be optimal for a different drug. This is due to the differences in interactions between the drug and surface of the delivery system. Namely, the strength of the interaction plays a strong role in the drug release properties [23, 24].

For a system based on hydroxyapatite nanocrystals, it can be observed that the release rates for three different drugs (*cis*-platin, alendronate, and di(ethylenediamineplatinum)medronate [DPM]) vary drastically [23]. The chemical structure of the drugs and the corresponding release profiles are shown in figures 10 and 11, respectively.

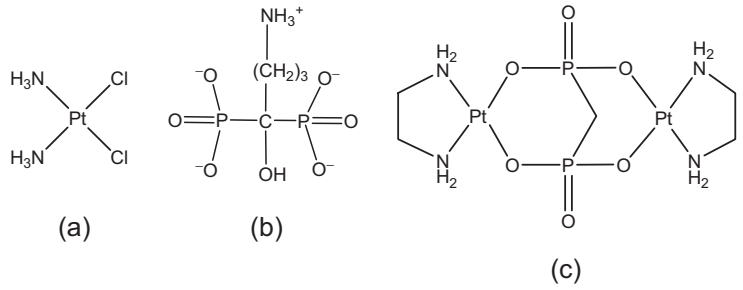

Figure 10: Chemical structure of a) *cis*-platin b) alendronate, and c) di(ethylenediamineplatinum)medronate (DPM), adapted from [23]

The difference in drug release kinetics is caused by the different mechanisms of adsorption of the drug onto the surface of the hydroxyapatite nanoparticles. Namely, the stronger the interaction between the drug and carrier, the slower the drug release process will be. It can be seen in figure 11 that the release rate is fastest for DPM and slowest for alendronate. This is because the alendronate molecule fixes to the hydroxyapatite surface by strong electrostatic interactions between the negatively charged bisphosphonate groups of the alendronate and positively charged Ca^{2+} ions of the hydroxyapatite. In contrast, the *cis*-platin molecule hydrolizes to form a positively charged species, which more weakly fixates to the overall negatively charged hydroxyapatite surface. Thus, while

the drug release is characterized by a prolonged release with suppressed initial burst for alendronate, its drug release properties for DPM are not as ideal. Comparison of the open to closed symbols distinguishes between the release profiles for needle-shaped particles with plate-shaped particles, respectively, which doesn't relate to interactions between the drug and DDS.

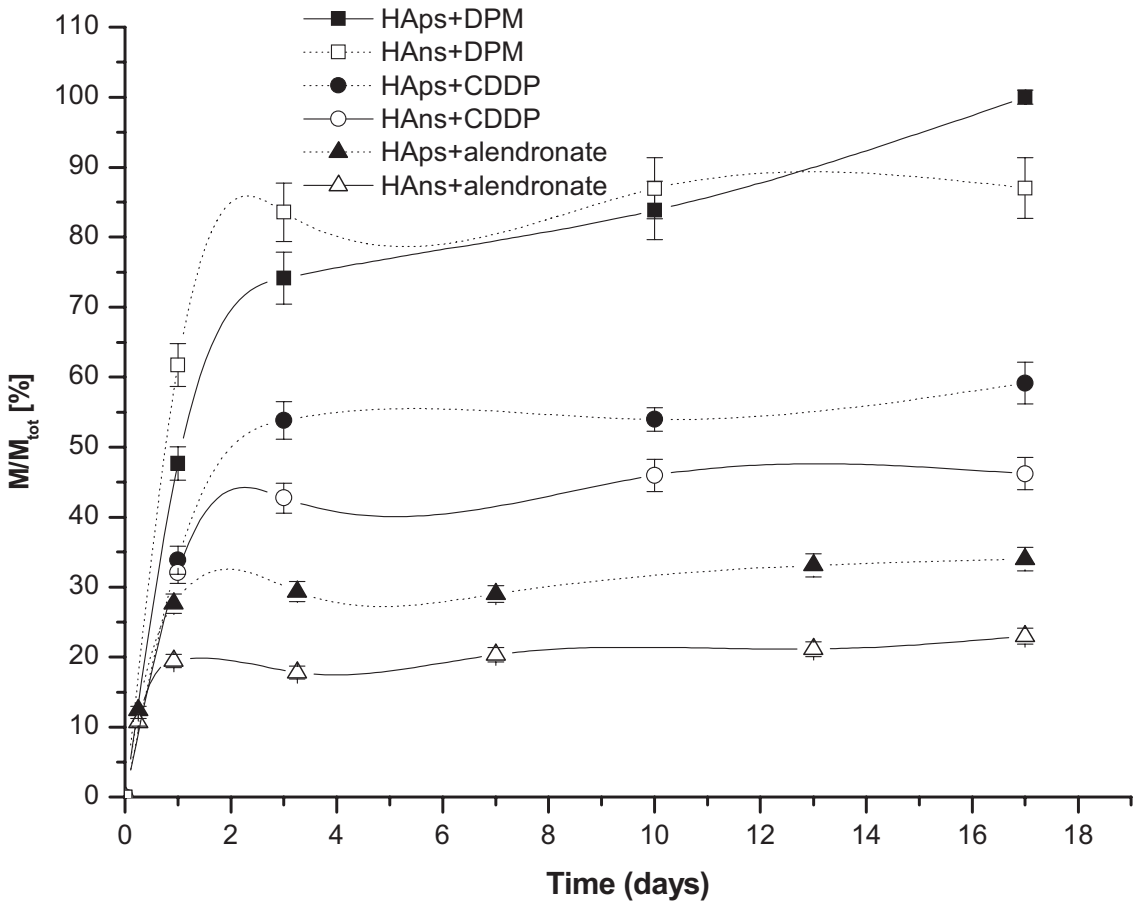

Figure 11: Drug release profile for hydroxyapatite nanoparticles loaded with *cis*-platin, alendronate, and DPM, adapted from [23]

In addition to the variation of the drug for the same drug delivery system, varying composition of the DDS also affects the release properties [25]. Here, the synthesis procedure was varied to produce various samples from different initial concentrations of ibuprofen and OH^-, as well as variety in the pH values of the reaction. These conditions subsequently controlled the drug loading efficiency, which is, notably, the highest of the studies presented so far. With various precursor ratios, samples were produced with various ratios of amorphous calcium phosphate to hydroxyapatite to octacalcium

phosphate. Namely, for the CP-IBU_5 sample (mixture of octacalcium phosphate and hydroxyapatite), for which the release profile is shown in the upper graph of figure 12, the drug loading content was 47% and 196% for CP-IBU_{13} (pure hydroxyapatite). This means that 1.96 grams of ibuprofen was loaded for every gram of calcium phosphate in the carrier system. For the CP-IBU_5 system, the ibuprofen concentration was 0.1 mol/L and OH^- concentration was 0.07 mol/L with a reaction pH of 6.6; the CP-IBU_{13} system was produced with an ibuprofen concentration of 0.6 mol/L, OH^- concentration of 0.18 mol/L, and a reaction pH of 5.7.

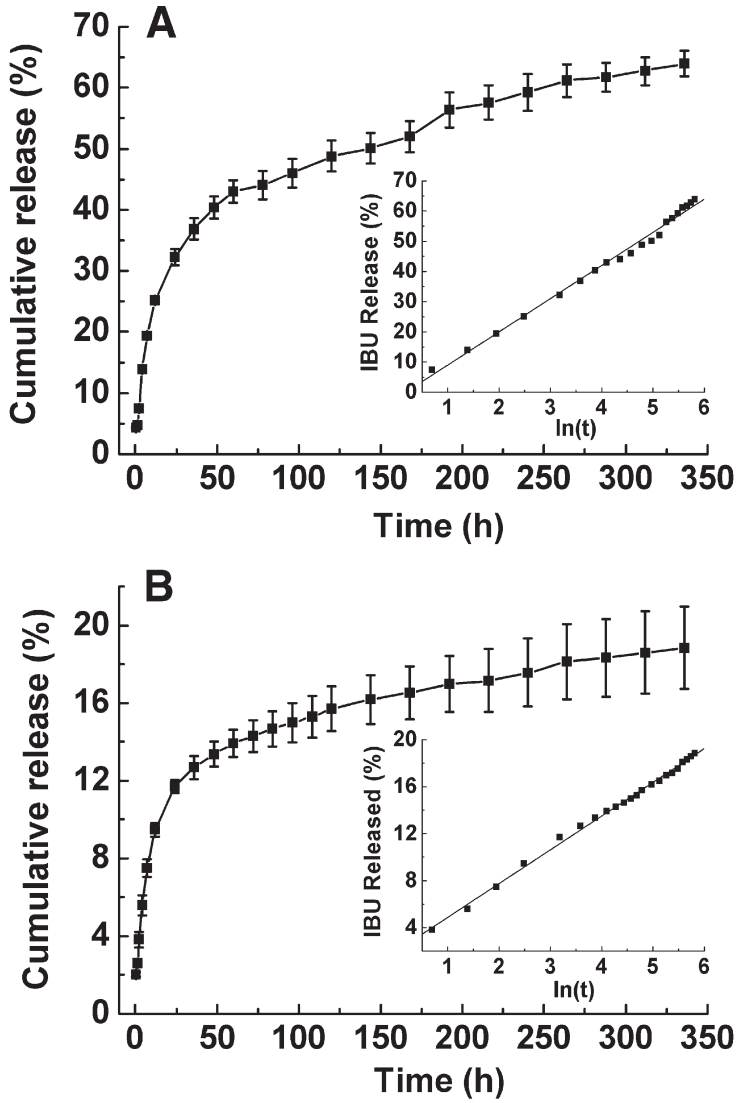

Figure 12: Drug release profiles for ibuprofen-loaded calcium phosphate drug delivery systems produced by one-step synthesis by Tang et al. for CP-IBU_5 (top) and CP-IBU_{13} (bottom), adapted from [25]

The first observation in comparing the two delivery profiles is the difference in cumulative release, with the CP-IBU_5 sample releasing nearly 60% of the ibuprofen by the end of the study compared to roughly 18% for CP-IBU_{13}. These results indicate the ability of this system to sustain prolonged release of ibuprofen, with 350 hours corresponding to a period of 2 weeks. Secondly, the authors denote the loading capacity of the CP-IBU_{13} sample as "ultrahigh." This can be explained by figure 13, where it can be seen that the drug is entrapped within the system, and not solely adsorbed on the surface of the carrier. FTIR studies suggested that there were both strongly and weakly bounded ibuprofen species, which explains the relatively low drug release; only the weakly bounded species were released and the strongly bonded molecules remained in the carrier.

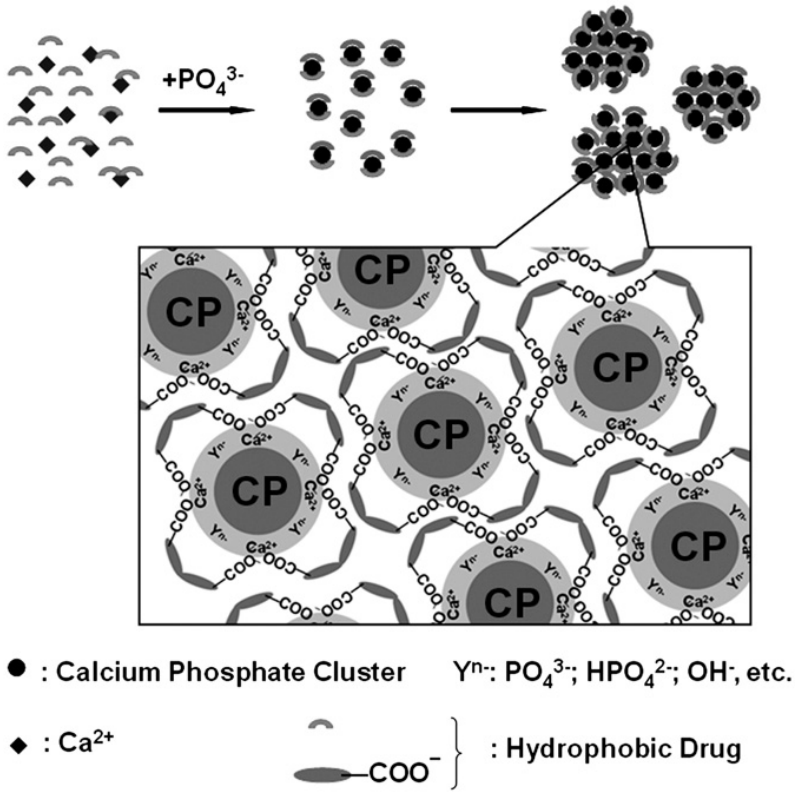

Figure 13: Drug loading mechanism proposed by Tang et al. for calcium phosphate system based on one-step synthesis procedure, adapted from [25]

By varying the synthesis parameters, the authors were able to tune the drug release properties, control of which is desirable for the application of a drug delivery system. Indeed, the prolonged release combined with the high drug loading ability shown by this system is attractive and lends itself well to use as a drug delivery system.

2.3.3. Addition of diffusion barriers

When the drug must move out of the DDS through diffusion, the addition of barriers to this process can control the drug delivery profile. By forming composites with the addition of polymeric materials, the drug delivery properties may be even more finely controlled. Referring back to the hydroxyapatite scaffolds presented earlier, it was hypothesized that the addition of a polymer coating on the scaffold walls would serve to suppress the initial burst of the drug release [26, 27]. To test this, the authors impregnated their scaffolds with various polymers with various thicknesses. Though different drugs were used—Loca et al. studied gentamicin and Dubnika et al. studied lidocaine—both results showed that the addition of polymer layers suppressed the initial burst and sustained the drug release over longer time periods.

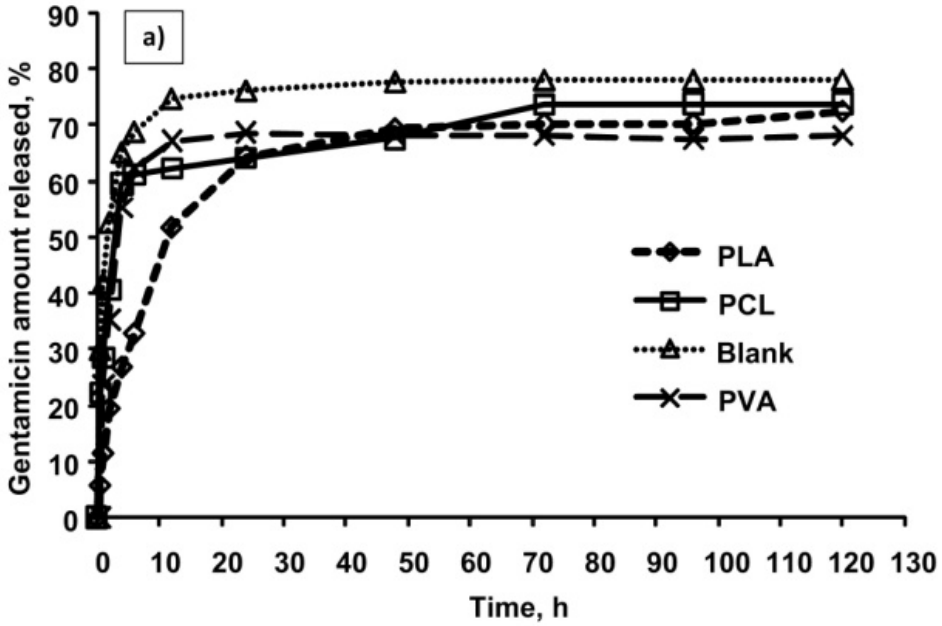

Figure 14a: Drug release profiles for polymer coated scaffolds, adapted from Loca et al. [27]

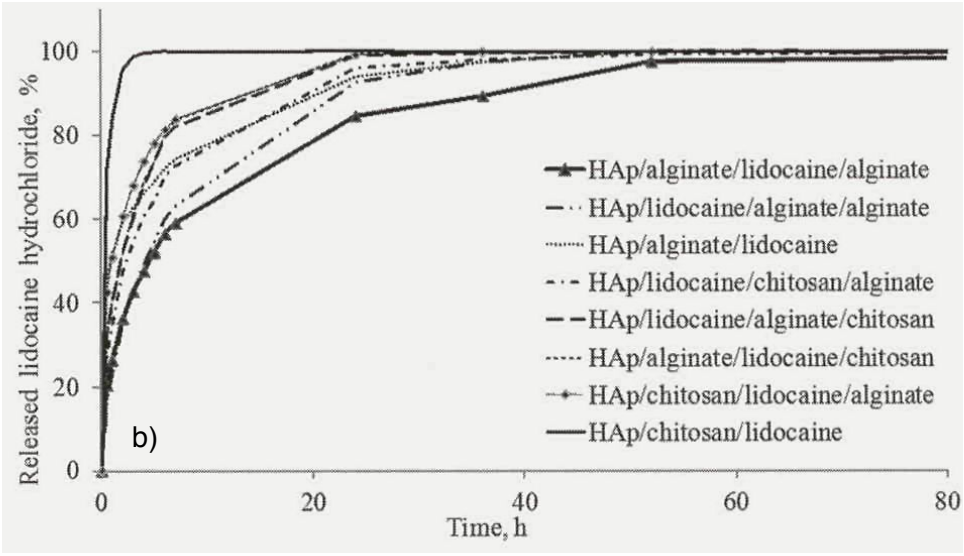

Figure 15b: Drug release profiles for polymer coated scaffolds, adapted from Dubnika et al. [26].

It can be seen from figure 14b that the impregnation of alginate into the scaffold significantly suppressed the burst release and even sustained the release to 60 hours. While these values remain much faster than was observed for the mesoporous silicates, it is a significant improvement on the drug release provided by the hydroxyapatite scaffold coated with chitosan preloading. The study by Loca et al. confirms the effectiveness of adding a polymer layer to the hydroxyapatite scaffold, with PLA being especially beneficial in suppressing the initial burst release. Similarly, Kim et al. coated hydroxyapatite scaffolds with a composite of hydroxyapatite and PCL and also found that the coating suppressed the initial burst and sustained the drug release [28].

When considering the use of polymers for biomedical applications such as drug delivery systems, an important consideration is biodegradability. For example, while PMMA beads have been used for delivery of antibiotics to treat bone infections post surgery, they are not biodegradable and required a second surgery to remove the beads after the antibiotic delivery was complete [29, 30]. Furthermore, beads based on PMMA displayed “unacceptably low” drug release, meaning that a very small fraction of the loaded drug was finally delivered.

Biodegradable polymer microspheres were utilized in a study on composite microparticles of PLA, PGLA, and PCL [31]. It was found that the complexity of their materials afforded more favorable drug release properties; by embedding polymeric ibuprofen-loaded PCL

nanoparticles within polymeric microparticles of PLGA, it was possible to suppress the burst release and sustain drug release for over 96 hours. This can be observed in figure 16, where the closed diamonds representing this composite material show an optimized release profile in comparison to the unencapsulated nanoparticles of ibuprofen-loaded PCL. The suppression of burst release can be explained by the double polymer layer hindering the drug diffusion. As the ibuprofen is loaded in the PCL nanoparticles, it must first diffuse out of these. Then, as the nanoparticles are loaded into the microparticles, the drug must subsequently diffuse out of the matrix.

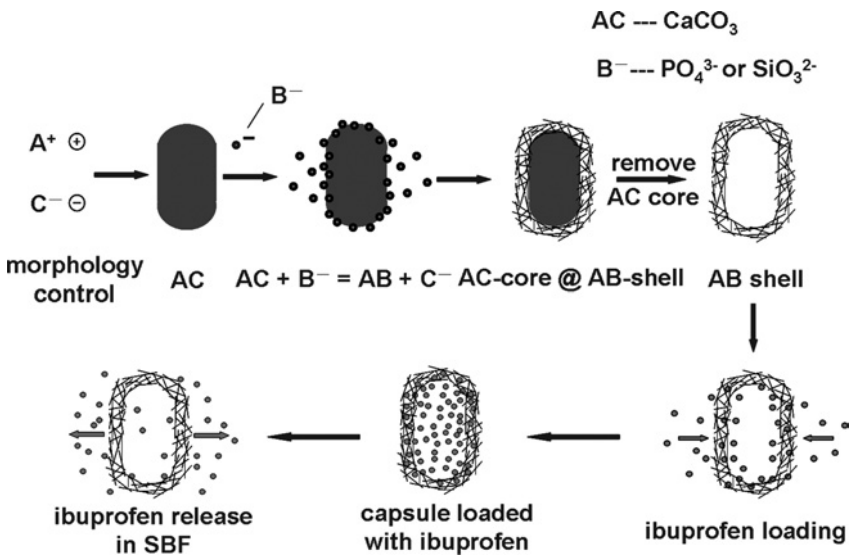

Figure 16: Schematic illustration of the synthesis procedure used by Ma et al. in forming hollow nanocapsules, adapted from [24]

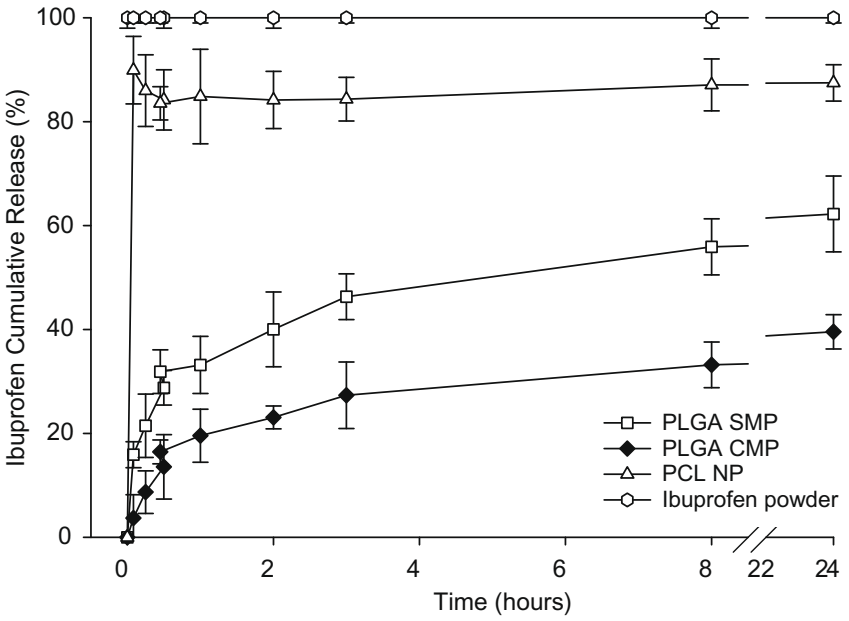

Figure 17: Release profile for biodegradable polymeric drug delivery systems, adapted from [31] PLGA SMP denotes poly(lactide-co-glycolide) simple microparticles, PLGA CMP denotes poly(lactide-co-glycolide) composite microparticles, and PCL NP denotes poly(ε-caprolactone) nanoparticles

In the case of nanocapsules based on hydroxyapatite, the capsule shell acts as a diffusion barrier to the drug loaded within [24]. A schematic for the structure of these nanostructures is shown in figure 15 and the corresponding drug release profile is shown in figure 17. Clearly, compared the drug release profile of simple ibuprofen, the release of discs compacted of the nanocapsules shows a more sustained release with a suppressed initial burst. Furthermore, the study reported achieving a loading of 45.95 wt.%, a value much higher than those reported in the aforementioned scaffolds. However, the drug release was not complete and in fact relatively low, with less than 40% drug released after 100 hours. The authors suggest that bonding occurs between the –COOH group of the ibuprofen molecules with the –OH groups of the hydroxyapatite capsules. Despite this relatively low release, the modest release of a large amount of stored drug is more favorable than the total release of a very small amount of loaded drug. It is proposed that the drug is stored internally within the nanocapsules and that the shell acts as a diffusion barrier to the drug release. The release is thus more complex than the simple surface desorption proposed for the scaffold-based systems.

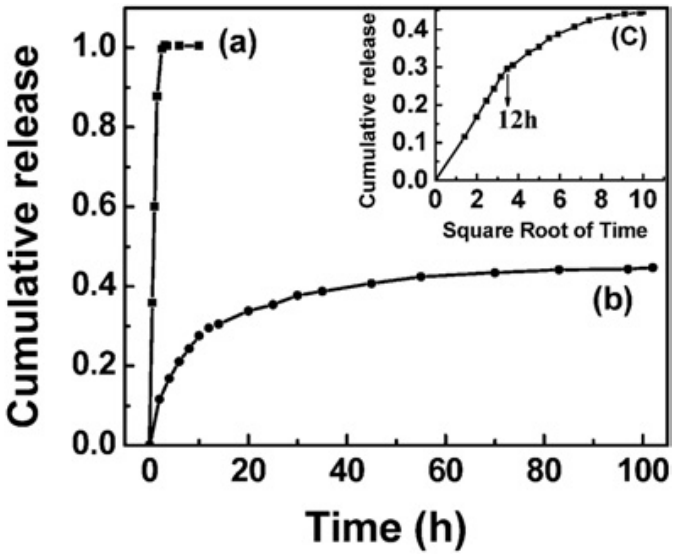

Figure 18: Drug release profile for a) pure ibuprofen and b) ibuprofen loaded ellipsoidal nanocapsules and c) graph of b on axis showing square root of time, adapted from [24]

2.3.4. Engineering of the Drug Release Profile

From these presented release profiles, it can be seen that several key factors play a role in determining its shape. The takeaways from these studies will prove useful in optimizing the release profile for the nanocomposite system of ZnO/PU. To summarize: the burst effect is more pronounced in systems with larger pore sizes, as easy diffusion is enabled by the relatively large cross section of the pores. This was especially apparent in the case of mesoporous silicates, where a threshold pore size was found where the ibuprofen molecules could not efficiently pack on the pore surfaces due to geometrical constraints. Here, the initial burst was especially suppressed due to the difficult diffusion presented by the small pores. Finally, by adding additional components to the systems in the form of polymeric coatings, an additional diffusion barrier was implemented which suppressed the drug release even further. It will be investigated whether these trends apply to the system based on zinc oxide embedded in a polyurethane matrix.

2.4 Use of Zinc Oxide/Poly(urethane) Material System

As the drug delivery system based on ZnO nanoparticles embedded in a polyurethane matrix has been proposed, it would be prudent to justify the materials selection as well as to review the properties of the respective materials. In the case of zinc oxide, the production of monodispersed nanoparticles has shown possible through relatively simple synthesis procedures [2]. Additionally, it has been seen that ZnO nanoparticles can be loaded with drug for drug delivery applications [32]. Finally, as ZnO is a heavily researched material, much is known with respect to its toxicological properties in the human body, and, while it has been observed to be a “selective killer” towards cancer cells, the nanoparticles are quite safe in the body, especially in the case where they are embedded in a polymer matrix [33]. Polyurethane is attractive due to its stability in the body and wide range of biomedical applications already reported [34]. Thus, the combination of these two materials to form a nanostructured composite drug delivery device is a sensible extension of the applications of the individual materials.

2.4.1. ZnO

While zinc oxide is a popular research topic for semiconducting applications due to its wide direct band gap and large exciton binding energy, its use in biomedical applications is also prevalent [35]. Specifically, the synthesis of ZnO nanostructures such as nanowires, nanorings, and nanoflowers allows development of devices such as field effect transistors and even biosensors [36]. ZnO with macroscopic morphologies has use in an array of fields ranging from catalysis to cosmetics [43]. In terms of biomedicine, ZnO is an attractive material due to its ability to selectively destroy tumor cells [33]. Especially for the case of chemotherapeutic drug delivery, the additional anti-cancer activity provided by the carrier itself (in the case of using ZnO nanoparticles as a drug delivery system) enhances the effect of the drug/carrier system as a whole.

Due to the semiconducting nature of zinc oxide, its reduction in size to the nanoscale results in the formation of quantum dots (QDs) as the particle diameter becomes smaller than the exciton Bohr radius. ZnO QDs are advantageous due to their nontoxicity as compared to the more common QDs based on cadmium-selenide of cadmium-telluride [38]. Applications in biomedicine envisioned for quantum dots include imaging (due to their fluorescence properties) as well as drug delivery (by functionalization of the QD surface).

2.4.2. PU

The polymer polyurethane, the structural unit for which is shown in figure 18, is formed via step-growth polymerization and is typically considered nonbiodegradable for the purposes of drug delivery systems due to the fact that the degradation time scale is much longer than that of the drug release [39]. Because of this, in cases of where the drug delivery system should be eliminated after the drug release (where it has first been implanted in the body), a second procedure may be required to remove the polymer. However, polyurethane is biocompatible, and has a range of applications in biomedicine ranging from vascular implant materials to injectable orthopedic scaffolds [40].

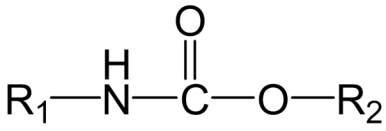

Figure 19: Urethane links, adapted from [39]

In terms of its application in drug delivery, systems based on polyurethane have been reported in which the drug loading occurs in the polymer itself [34]. This suggests that the use of polyurethane as a matrix material in a nanostructure composite drug delivery system has as consequence the result that the polyurethane may play an active role in the drug delivery process and not simply serve as a containment material for the drug-containing zinc oxide nanoparticles.

2.4.3. Notable Systems

For the delivery system based on zinc oxide nanoparticles, it is interesting to review the synthesis of various other zinc oxide nanostructures, as they could offer potential use in drug delivery systems. Furthermore, it is of interest to compare the synthesis strategy used in the present study with those used by other groups.

It has been seen that mesoporous silicates offer attractive potential for use as drug carriers due to their ordered, highly porous nature. The synthesis of analogous mesoporous nanospheres of zinc oxide was reported and their potential use as drug carriers was highlighted in a study of their use in drug delivery systems [32]. A TEM image of the structure can be seen in figure 19, where the ordered assembly of nanocrystals can be seen in the right-hand section of the image. It was determined that their system had mesopores of an average diameter of 28 nm, of a similar order of magnitude to the pores of the mesoporous silicates. These properties have been shown to be beneficial for use in drug carriers, and preliminary studies by Barick et al. confirm the potential for the material's use in drug delivery systems. Furthermore, the drug release was found to be pH sensitive, which can be utilized for chemotherapeutic uses as the pH values found in cancerous tumor cells are typically lower than those in healthy tissue.

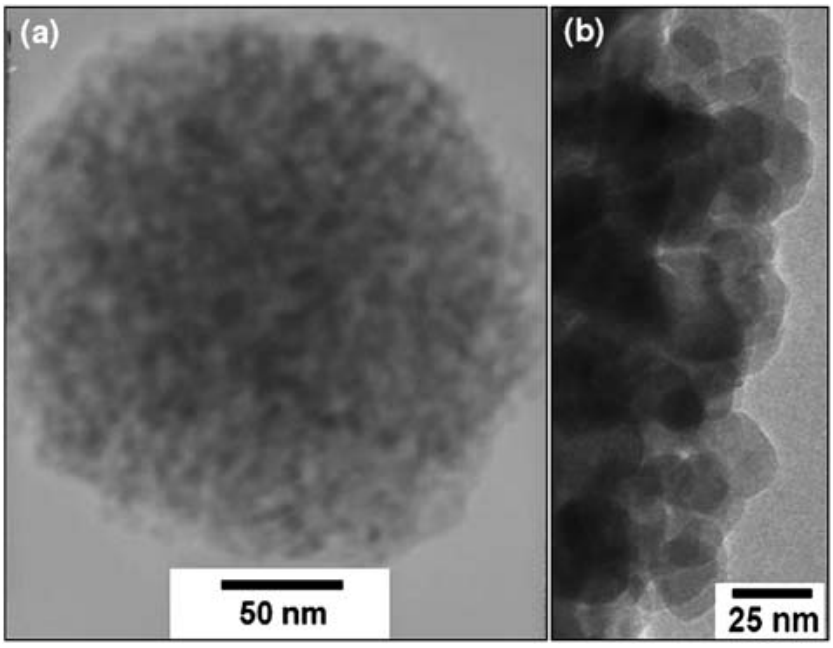

Figure 20: TEM images of mesoporous zinc oxide nanoparticles as synthesized by Barick et al., adapted from [32]

The reported synthesis procedure is relatively straightforward. Diethylene glycol containing acetate precursors was heated under reflux until ZnO nanocrystals precipitated after reaching temperatures of 160-165°C. After separation from the solution, the precipitate was thermally treated to remove excess solvent. This relatively simple synthesis procedure afforded itself well to the production of zinc oxide nanocrystals [32].

With biomedical applications in mind, Amna et al. synthesized composite spider web scaffolds of ZnO doped polyurethane [41]. The resulting structure, shown in figure 20, can be described by the addition of nanofibrous zinc oxide spider webs (shown by the green arrow) connecting polyurethane fibers (shown by the red arrow). These mats were found to have good biocompatibility through MTT assays, which are experiments to investigate cell compatibility. While the study didn't include any experimentation with drug release, it would be interesting to see how this composite material could be used with regard to drug delivery systems. Electrospinning was used for the material synthesis by ejecting a solution of polyurethane in *N,N*-dimethylformamide (DMF) with dispersed nanoparticles of zinc oxide from a syringe with a high voltage between the syringe tip and a polyethylene covered iron drum. This offers a cost-effective and simple method for creating a composite material with a complex morphology.

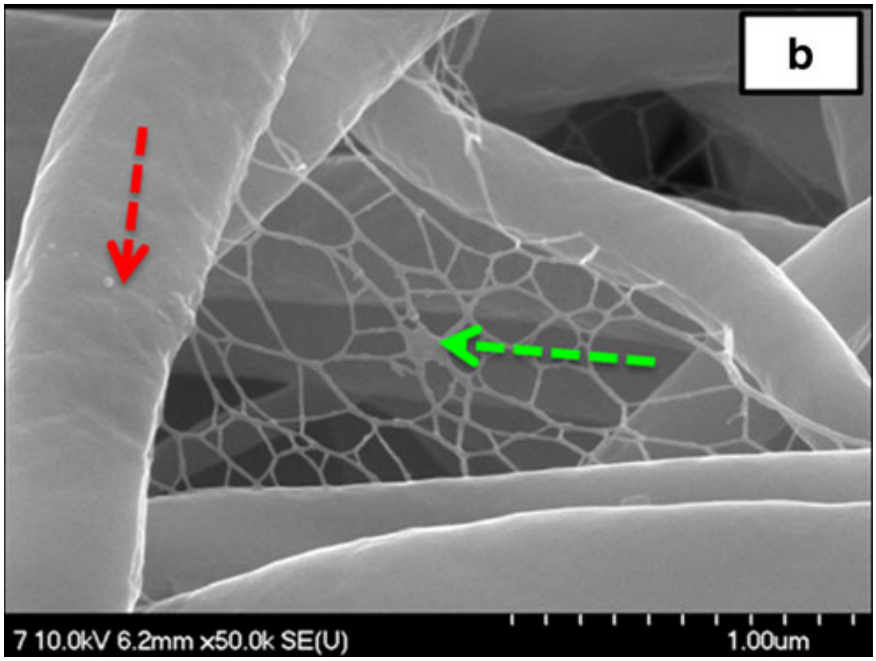

Figure 21:FE-SEM micrograph of ZnO doped polyurethane spider web nanostructures produced by electrospinning as reported by Amna et al., adapted from [41]

Recent publications (2013) even reported the synthesis of mesoporous nanospheres of ZnO for applications in drug delivery [42,43]. These studies have shown that the drug release for the carriers is similar to the results reported by Barick et al. and Zhang et al. for synthesized ZnO/polymer core/shell quantum dots loaded with doxorubicin [43]. The pH response, shown in figure 21 (A), was found to be due to the decomposition of the polymer shell at low pH values; the drug release was thus much higher at low pH values. The release at neutral pH values was speculated to be due to the weakly adsorbed surface molecules.

A pH response has also been reported for zinc oxide nanospheres, however here, the drug release of captopril was compared at pH values of 7.4 and 1.2, the drug release profiles for which can be seen in figure 21 (B) [43]. For this study, mesoporous nanospheres were synthesized by a soluble-starch-insertion method, in which $Zn(NO_3)_2$*$6H_2O$ was added drop wise to a solution of soluble starch dissolved in boiling water. By adjusting the pH, a white suspension was formed and the precipitate was subsequently separated and heat-treated to induce calcination and obtain ZnO.

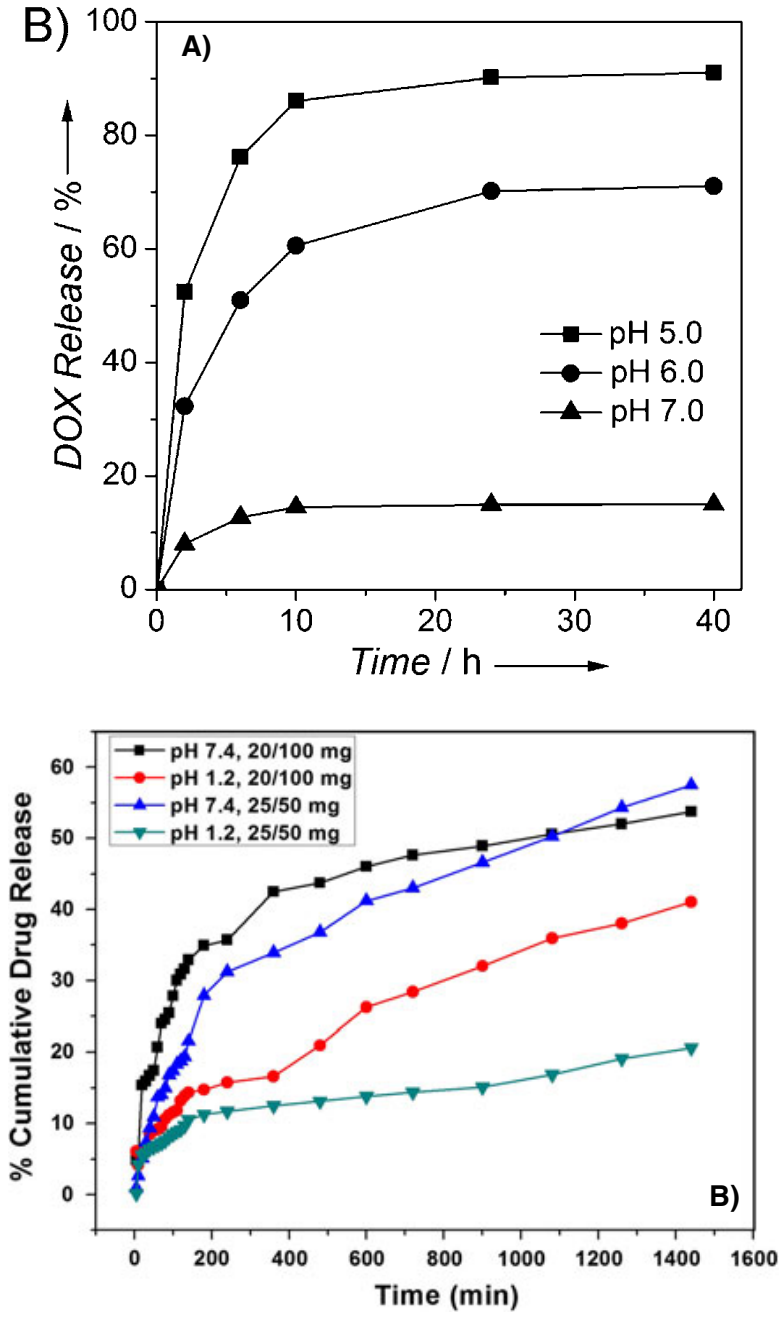

Figure 22: Drug release profile highlighting the pH dependence for doxorubicin (A) and captopril (B) release from ZnO nanoparticles, adapted from [43] (A) and [42] (B)

The captopril release behavior reported by Bakrudeen et al. [42] shows two dependencies: the degree of drug loading, either in a 1:5 or 1:2 ratio of drug to carrier, which is represented by the black/red and blue/green lines, respectively and the pH dependence of the drug release. Contrary to the study of doxorubicin release by Zhang et al., the lower pH suppressed the initial burst and sustained the drug release for captopril. This is due to the ionizability of the captropril molecule. In a more basic environment, the

diffusion is more rapid because of the increase in aqueous solubility due to the ionization of the –COOH and –SH groups [44]. This goes to show that the drug release can be controlled in different manners based on the chemistry of the drug molecule of interest.

2.4.4. Summary of Previous Results with ZnO/PU

The work by former master's student Ana Lúcia Mota Pires investigated the drug release behavior of a ZnO/PU system [2]. Composite systems were synthesized based on three different zinc oxide nanoparticles: a commercially obtained sample denoted ZnOC, a sample precipitated from a solution of $ZnCl_2$ and $C_6H_8O_7.H_2O$ with NaOH added drop wise from a burette, denoted ZnOA, and a sample precipitated from a similar solution with NaOH added via a pulverizer, denoted ZnOP. SEM images of the resulting loaded particles after being embedded in a polyurethane matrix are shown in figure 22. It can be seen that, while the size of the particles themselves is on the order of micrometers, they are formed by assemblies of nanoparticles, which confirms the nanostructured nature of the system. The corresponding drug release profiles are shown in figure 23. It can be seen that the addition of polyurethane had a significant effect on the suppression of the drug release as compared to the lone nanoparticles. Additionally, the drug release was more sustained for the precipitated samples compared to the commercially obtained powder.

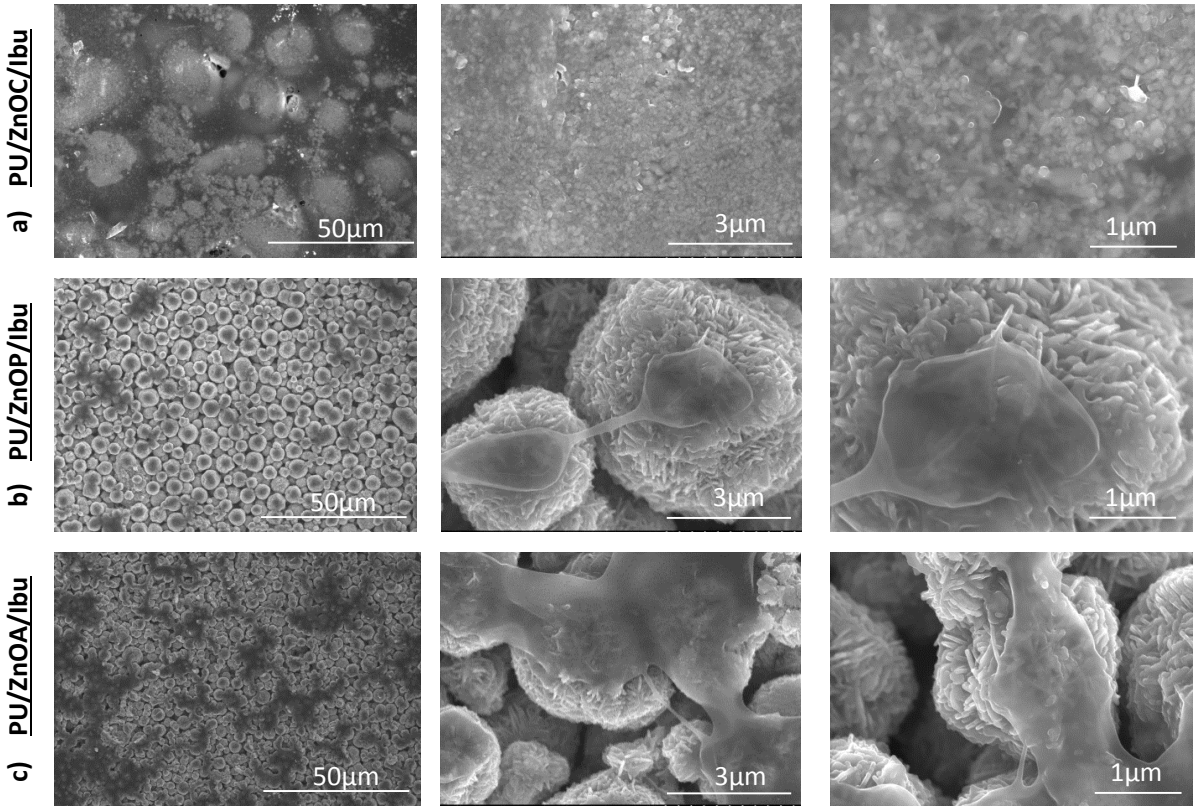

Figure 23: SEM images of ibuprofen-loaded zinc oxide nanoparticles embedded in a polyurethane matrix, adapted from [2]

It can be seen in figure 22 that the particle morphologies varied drastically between the commercially obtained powders and those synthesized in the laboratory. Namely, the synthesized particles were spherical shaped characterized by agglomerations of nanoplates. These resulted in high specific surface areas. The drug loading efficiency reported for these particles was roughly 85% for the ZnOC and ZnOA samples and 60% for ZnOP samples and it was suggested that the low loading was due to the adsorption of citrate ions on the sites where drug (in this case, ibuprofen) would otherwise have been adsorbed. Incomplete release—34% for ZnOA and 72% for ZnOC—was due to the strong interaction between the drug molecules and the surface of the ZnO carriers, forcing incomplete desorption of the drug molecules within the time of the study.

The effect of the polyurethane is easily observed in figure 26 by the drastically lowered release rate. This is due to the diffusion barrier provided by the polyurethane matrix. Comparing the two precipitated samples ZnOA and ZnOP on the release curves shows similar behavior. However, it was already pointed out that slightly different values for drug

loading efficiency were reported, with the ZnOA providing more efficient loading, likely due to the differences in specific surface area cause by the rate of addition of NaOH into the reaction solution during the synthesis procedure.

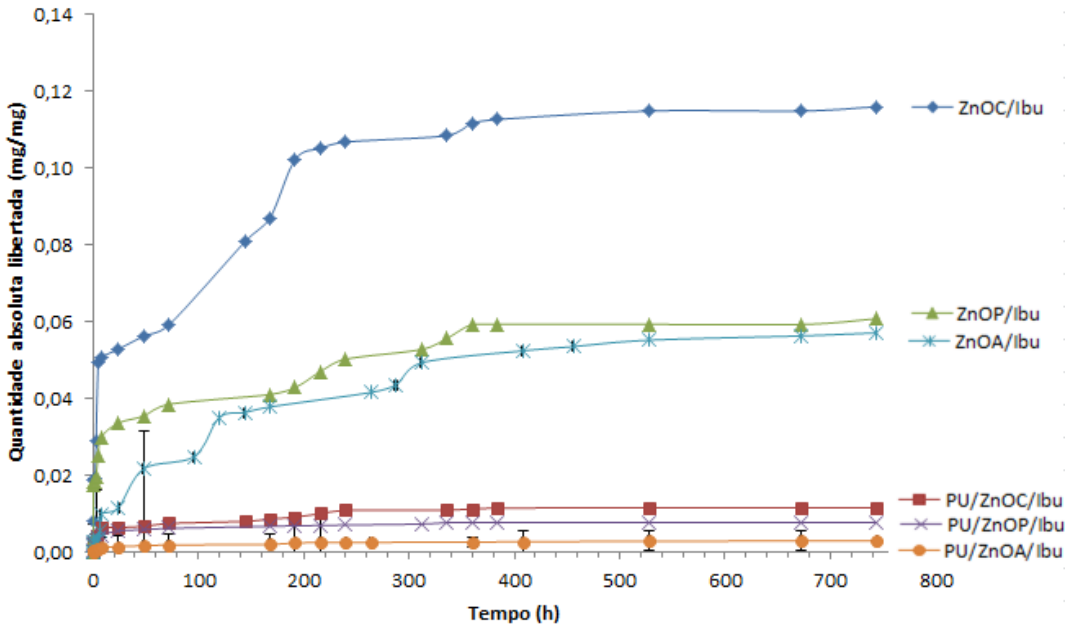

Figure 24: Release profile for ibuprofen-loaded zinc oxide nanoparticles of various compositions as well as for the same nanoparticles embedded in a polyurethane matrix, adapted from [2]

While the results from this study show the benefit of utilizing a composite drug delivery system in terms of suppressing the burst release and sustaining the drug delivery process in general, it remains desirable to optimize the system to promote a more complete drug release from these composite materials. For the current study, the particles designated as "ZnOP" will be produced and further investigated.

2.4.5. Toxicological Considerations

For medical materials such as drug delivery systems, the toxicology of novel systems must be considered, as the end use *in vivo* must not be harmful to the body [45, 46]. Evaluation of the PU is relatively simple, as its use as a matrix phase means that the toxicological properties correspond to those of its bulk form. However, evaluating the ZnO

nanoparticles may not be so straightforward. With the associated change in material properties due to size reduction of nanoparticles, the toxicological properties may not (and often do not) correlate to those of the material in bulk form.

Several studies have been performed on the toxicological properties of metal oxide nanoparticles especially due to their attractiveness as semiconducting materials to be used for quantum dots and the various envisioned applications for quantum dots [47, 48]. With respect to the use of zinc oxide nanoparticles in a drug delivery system, it was found that they are generally nontoxic to the body in general. However, both the studies by Chibber et al. and Chang et al. suggest that zinc oxide nanoparticles can be toxic to cancer cells, destroying them by the production of reactive oxygen species. These potential chemotherapeutic applications are due to the fact that cancer tumor cells are more susceptible to death induced by reactive oxygen species than healthy body cells. For the purposes of use of zinc oxide nanoparticles in a drug delivery system, it seems to be that the nanoparticles are biocompatible.

2.5 Modeling of Drug Release Profiles

Upon obtaining drug release profiles for DDSs, it is desirable to apply mathematical models to the experimental data in order to better understand the drug release mechanisms [49]. Namely, the constants found in these models can often be correlated to physical parameters of the system and, in this way, the drug release behavior can be predicted. A selection of models, which are commonly used in literature, is presented in table 1 below. In these equations, the term F is given as the fraction of drug released from the system at time t.

Table 1: Mathematical Models for Drug Delivery

Model	Equation
First Order	$F = 100 * (1 - e^{-k_1 * t})$
Higuchi	$F = k_H * t^{0.5}$
Korsmeyer-Peppas	$F = k_{KP} * t^n$
Baker-Lonsdale	$\frac{3}{2}\left[1 - \left(1 - \frac{F}{100}\right)^{2/3}\right] - \frac{F}{100} = k_{BL} * t$
Mankoid-Banaker	$F = k_{MB} * t^n * e^{-k*t}$

While many additional models exist, these have been selected due to provide a broad range of approaches to the models. The first order and Higuchi models are relatively simple, yet frequently used models in drug delivery. In the first order model, k_1 is simply an empirical constant selected in order to fit the data series. However, drug release which follows a first order model is known to occur through Fickian diffusion where perfect sink conditions are maintained (the drug concentration in the DDS is much higher than in the release medium), the drug permeability through the system remains constant, and the DDS does not swell or dissolve [50].

The famous Higuchi model, with the empirical constant k_H was developed to model the release of drug from thin film matrices. Because of this, it would be a surprise to find the model a good fit for drug release from nanostructured spheres. The Korsmeyer-Peppas model serves as an extension of the Higuchi model by removing the constraint of the power constant from 0.5. In this way, there are two constants in the Korsmeyer-Peppas model, k_{KP} and n. This allows one to account for the simultaneous diffusion of water into the system to induce swelling and drug diffusion out of the system [50]. The proportionality constant, k_{KP}, considers the geometry of the DDS, and n relates to the drug diffusion, with $n = 0.45$ designating Fickian diffusion and $0.45 < n < 0.89$ describing non-Fickian or anomalous diffusion [51].

In the fourth presented model of Baker and Lonsdale, a single constant exists, k_{BL}, which serves to represent physical properties. Namely, $k_{BL} = {3 * D * C_S}/{(r_0{}^2 * C_0)}$, where D is the drug diffusion coefficient, C_S the saturation solubility, r_0 the initial radius for a spherical DDS, and C_0 the initial drug loading concentration in the DDS.

Finally, the Mankoid-Banaker model includes three empirical constants, k_{MB}, n, and k. This is a very robust empirical model due to the inclusion of both power and exponential terms.

Chapter 3

Experimental Procedure

3. Experimental Procedure

3.1. Materials Used

The materials used in the various phases of the experimental work are listed below in table 2.

Table 2: List of Materials

Material	Chemical Formula	Source
Citric Acid	$C_6H_8O_7$	Sigma-Aldrich
Zinc Chloride	$ZnCl_2$	Merck
Sodium Hydroxide	NaOH	Sigma-Aldrich
Ethanol	C_2H_6O	Álcool E Géneros Alimentares SA
Ibuprofen	$C_{13}H_{18}O_2$	Aldrich
Poly(urethane)	Shown in figure 25, MW 90,000–140,000 kDa [X]	Fluka
Chloroform	$CHCl_3$	Carlo Erba Reagents
1,2-Dichloroethane	$C_2H_4Cl_2$	Fluka
Phosphate Buffered Saline	0.138 M NaCl, 0.0027 M KCl	Sigma-Aldrich

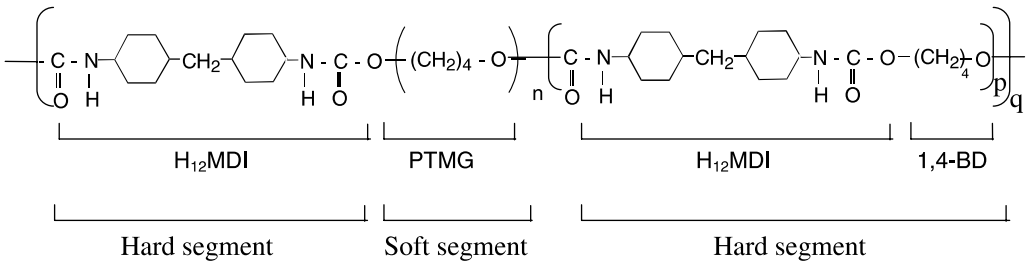

Figure 25: Chemical formula of Tecoflex SG80A polyurethane, adapted from [59]

3.2. Sample Preparation

3.2.1. Precipitation of ZnO

The nanostructured zinc oxide was produced via a chemical precipitation in which solutions of ethanolic sodium hydroxide and pure sodium hydroxide were sequentially added via a blowing nozzle to a solution of zinc chloride and citric acid, respectively. More specifically, a solution of 10 M sodium hydroxide was prepared by dissolving 80 g of NaOH pellets in 200 mL of distilled water and allowed to mix for approximately 20 minutes via magnetic stirring. Similarly, the ionic solution was prepared by measuring 17 g of citric acid and 3.674 g of zinc chloride powders and dissolving in 25 mL distilled water with magnetic stirring, ensuring a 3:1 ratio of citrate to zinc ions, respectively. The ethanolic solution of sodium hydroxide was prepared by measuring 20 mL of the prepared sodium hydroxide solution with 15 mL and then mixing these two solutions, also under magnetic stirring. Each solution was allowed to mix for a sufficient duration to ensure complete dissolution and mixing of the components, typically between 15 and 20 minutes.

As previously mentioned, the sequential combination of these solutions was completed by the addition of the ethanolic sodium hydroxide solution to the zinc chloride/citric acid solution and, after the complete addition, the pure sodium hydroxide solution was added in order to ensure that a sufficiently high pH was obtained in order to promote the precipitation of zinc oxide. These additions were completed with a blowing apparatus, in which the zinc chloride/citric acid solution was put in the base of a conical flask under stirring and the subsequent solutions were added under blowing at a pressure of roughly 1.25 bar. This blowing ensured dispersion of the liquid into the flask. The setup can be seen in figure 24. The hose coming from the right-hand side of the image connects to the buildings supply of compressed air in order to provide the blowing pressure. Prior to the precipitation, the connection between the blower and flask was wrapped in aluminum foil in order to hinder the escape of vapors that formed during the additions. After the total

addition of the pure sodium hydroxide and achievement of a sufficiently high pH, pure, crystalline zinc oxide precipitated and the previously transparent solution contained in the conical flask became opaque and milky-white.

Figure 26: Setup of blowing apparatus for chemical precipitation of nanostructured zinc oxide

The resulting suspension was then centrifuged at 10,000 rpm for 15 minutes in order to isolate and collect the zinc oxide powder. Following which, the powder was washed 5 times by additional centrifuge cycles with fresh batches of deionized water in order to remove remaining citrate and sodium ions from the powder. Finally, the powder was dried overnight at 50 °C to promote evaporation of remaining water molecules.

A visualization of the complete precipitation procedure is depicted in figure 25.

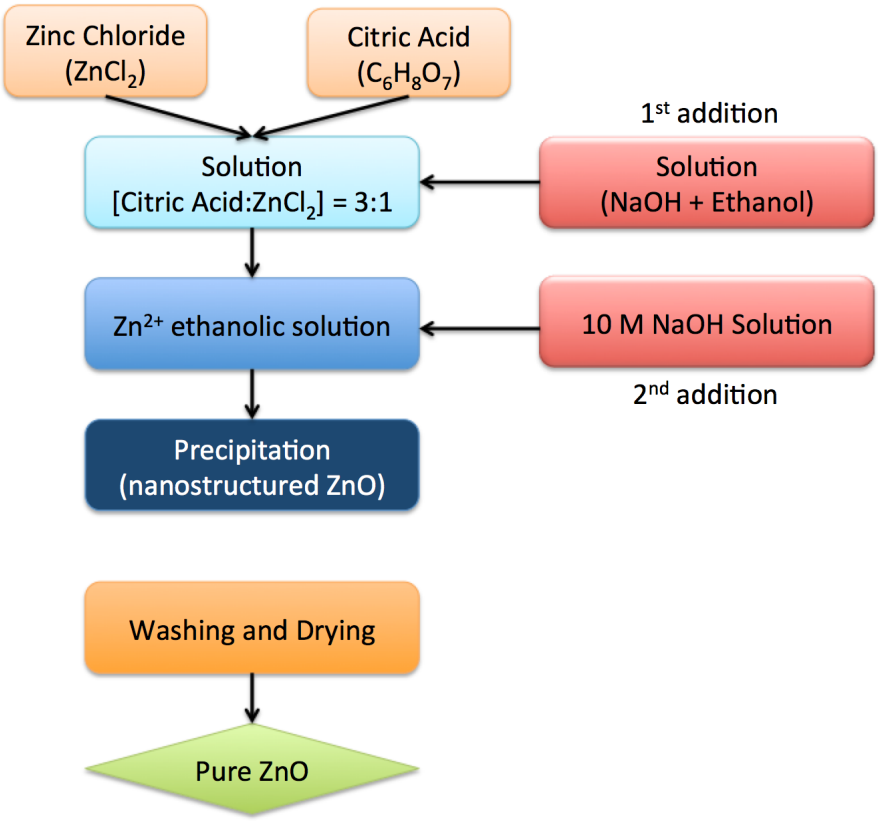

Figure 27: Flowchart outlining precipitation of nanostructured zinc oxide powder

3.2.2. Loading of nanostructured zinc oxide with Ibuprofen

After collecting the powder from the synthesis suspension, ibuprofen-loaded samples were prepared. This was simply done through an adsorption process by soaking the zinc oxide powder in solutions of ibuprofen dissolved in ethanol. Ibuprofen was first measured and weighed to appropriate values and allowed to dissolve in 50 mL of ethanol in order to produce loading solutions with concentrations of 1, 2, 10, and 20 mg/mL. These solutions of varied concentrations were prepared to examine the effects of loading concentration on drug release; for other experiments, a loading concentration of 10 mg/mL was used. It should be noted that the initial procedure specified the dissolution of ibuprofen in distilled water. However the solubility limit of ibuprofen in water was found to be <1 mg/mL, which is an impractically low value for the purposes of maximizing drug uptake into a drug

delivery system. It was found that ethanol provides optimal solvent properties for ibuprofen and allows the dissolution of high concentrations of ibuprofen.

It was observed during the loading procedure that the suspension of zinc oxide in the loading solution tended to settle to the bottom of the loading container. To ensure that the surface of the nanostructured particles were allowed contact with the solution, the loading suspensions were subjected to ultrasonic agitation for 60 minutes, twice per day. The overall loading process took place over the course of 3 days [2]. In figure 26 can be seen the loading suspensions held in the loading containers. These images were produced after shaking the containers in order to promote an even distribution of ZnO particles throughout the suspension.

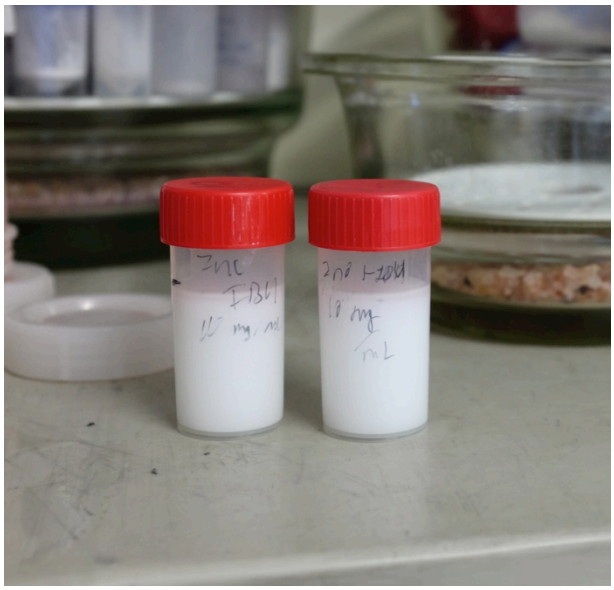

Figure 28: Loading containers for the loading of ibuprofen into nanostructured zinc oxide

As the ethanol evaporation rate was quite rapid, it was not possible to accurately determine the amount of ibuprofen remaining in the suspension (and therefore the amount loaded) via UV spectroscopy because the concentration change corresponding to the ethanol evaporation provided incorrect values. In other words, the measured concentration was not indicative of the initial ibuprofen concentration immediately after the drug loading due to the solvent evaporation. Other techniques were thus chosen in order to estimate the drug uptake.

3.2.3. Formation of ZnO/PU composites

The composite systems were formed based on a solvent evaporation method after the procedure described by Seil and Webster [52]. For this work, composites were made with 25 wt% ZnO as well as 50 wt% ZnO embedded in a polyurethane matrix. To summarize: commercial polyurethane was dissolved in chloroform with a weight ratio of 2.48 wt% PU under magnetic stirring for roughly 30 minutes or until the complete dissolution of the polymer could be observed. Then, the prescribed amount of zinc oxide was dispersed in 1,2-dichloroethane under sonication to form a uniform suspension. The suspension of ZnO and solution of dissolved PU were then mixed together with sonication until a homogenous mixture formed. This solution was then evenly distributed into 10 mL beakers so that the composite could be cast into small discs of roughly 500 µm in thickness at the bottom of the beakers. Finally, this was placed in a drying oven overnight at 37 °C to allow the solvents to evaporate. This procedure is visually depicted in figure 27.

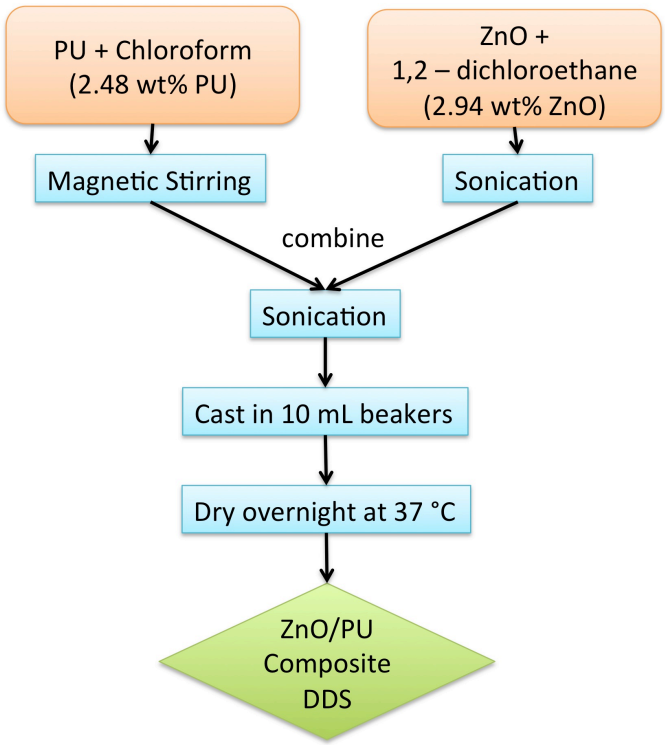

Figure 29: Flowchart outlining solvent evaporation procedure for production of ZnO/PU composites

3.3. Characterization Methods

3.3.1. Scanning electron microscopy

Scanning electron microscopy (SEM) images were produced in order to elucidate the morphologies of both the powder and composite drug delivery systems, which was of particular use in observing the degradation processes of the samples during the drug release experiments. For this, a Hitachi scanning electron microscope model S-4100 was used with a tungsten filament set to an accelerating voltage of 20 keV. The nanostructured zinc oxide powder, as it is a semiconducting material, could simply be placed on carbon tape attached to the aluminum sample holder with no additional preparation measures necessary (i.e. it was not necessary to sputter a conductive layer on top of the ZnO powder). The composite materials, on the other hand, underwent carbon sputtering with an Emitech K950 carbon evaporator in order to enable SEM imaging through formation of a conductive layer over the sample.

The particle sizes and nanoplatelet sizes were determined by averaging the dimensions from several samples, as shown in figure 28. Lines were drawn on top of the images and measured via the scale bar shown at the bottom of the images. Though not shown explicitly with its own figure, a similar technique was used for measuring the nanoplatelet width.

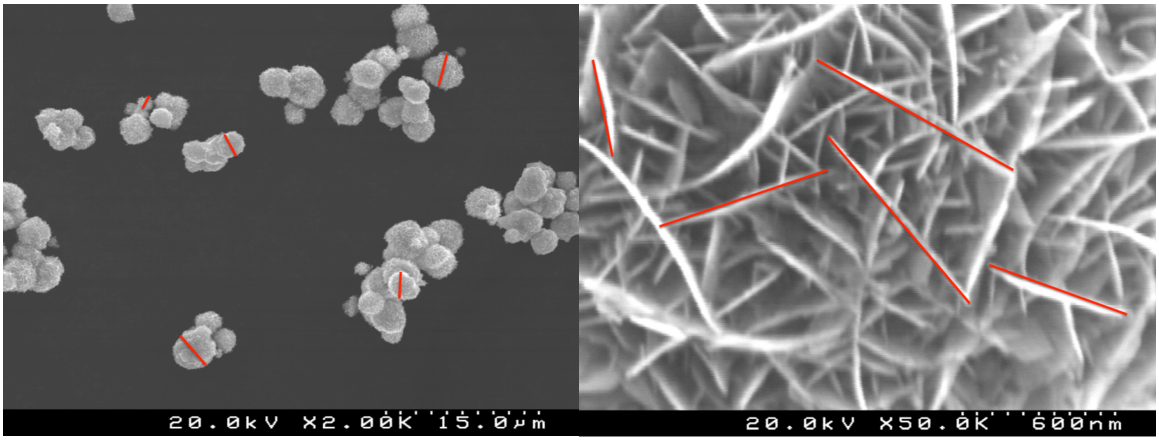

Figure 30: SEM images of ZnO particles with overlaid lines depicting how dimensions were determined

3.3.2 X-ray diffraction

X-ray diffraction (XRD) was used in order to provide insight into the crystal structure of the nanostructured zinc oxide powder. A Rigaku Geigerflex D/Max-SérieC was used with Cu Kα radiation corresponding to a wavelength of λ=1.54056 Å. The current and voltage applied were 30 mA and 40 kV, respectively.

In order to approximate the crystallite size based on the data obtained through the diffraction experiments the Debye-Scherrer equation was used and is given by:

$$Crystallite\ Size = \frac{K\lambda}{\beta \cos\theta}$$

where K is a shape constant taken to be 0.89 for spherical particles, λ is the radiation wavelength, β is the full-width at half-maximum (FWHM), and θ the diffraction angle. Though 0.89 is typically assumed to be valid for spherical particles, it is appropriate for estimating the size of indeterminate shapes, for which 0.9 is typically used. In the case of the particles, though they are spherical by nature, the actual crystallites would more likely be defined as the nanoplatelets that agglomerate to form the spherical ZnO particles. Secondly, the β constant is often taken as the FWHM including a correction due to instrumental peak broadening. However, for the purposes of simply using this equation as

an estimation tool for the crystallite size, the effect of the instrument was ignored and β was taken simply as the total FWHM, which simply refers to the width of the peak at half of its height. In total, the crystallite size was determined for the six largest peaks and the average value was taken to be the estimated crystallite size.

3.3.3. Fourier Transform Infrared Spectroscopy

To investigate the chemical bonding and properties of the samples of nanostructured zinc oxide as well as the composite drug delivery systems loaded with ibuprofen, Fourier transform infrared spectroscopy (FTIR) was used. As the typical FTIR spectroscopy is limited in applicability to solutions, ATR-FTIR (attenuated total reflectance FTIR) was utilized on the solid, composite samples. This technique relies on the total reflection of the light wave at the sample surface. Upon interacting with the sample, an evanescent wave forms within the sample and this is able to probe the chemical environment of the sample. The samples were sent to the department of chemistry at the university of Aveiro, where they were analyzed with a Bruker Tensor 27, scanning the range from 350-4000 cm^{-1}.

3.3.4. Thermogravimetric Analysis

Thermogravimetric Analysis (TGA) was used to quantify the weight changes of the various samples corresponding to temperature increase. The powder samples of nanostructured zinc oxide were measured with a Setaram Labsys DTA/TGA-DSC 1600, using a heating rate of 10 °C/minute over the temperature range of 50-400 °C.

With the data provided by TGA, it was possible to determine the amount of adsorbed species present in the loaded samples. This was done by subtracting the baseline provided by the TGA curve of pure nanostructured zinc-oxide powder from the various spectra of loaded samples. The weight loss occurring between 250-300 °C could then be attributed to the decomposition of the organic ibuprofen molecules [53]. However, as will be shown in the following chapter, this method provides complications in that the weight

loss step for the loaded samples cannot be attributed solely to ibuprofen, degradation of remaining citric acid must also be taken into consideration.

In order to minimize the amount of adsorbed water molecules, the samples were dried in an oven at 65 °C overnight prior to delivery to the technician responsible for TGA measurements.

3.3.5. Gas Sorption Analysis

Gas sorption experiments were used in probing the porosity of the nanostructured zinc oxide powders. A Micromeritics Gemini 2370V5 gas analyzer was used with measurement temperature of -195.85 °C and preparation evacuation rate of 1000 mmHg/min for 10 minutes. Adsorption isotherms were produced which compare the amount of gas adsorbed by the sample surfaces with respect to the relative pressure of the gas in the sample chamber. Here, N_2 was used as the analyzing gas.

3.3.6. Ultraviolet-Visible Light Spectroscopy

For the purposes of using UV-VIS spectroscopy to characterize drug delivery devices, the interest is not in using the spectrum for compositional determination, but to quantitatively determine concentrations of drug present in the elution solutions. For this, Beer's Law is used, which states that the amount of light absorbed is proportional to the number of molecules in the system, which can be written as the following equation:

$$T = e^{-kbc}$$

where T is the transmittance, k is a constant, b is the path length, and c is the concentration of the absorbing molecules. To use this equation to determine the drug concentration, the absorption is measured at a wavelength specific to the drug of interest. Finally, to create a drug release profile, a plot of the concentration values vs. time is

created, where time axis is enabled by taking samples at predetermined intervals after beginning a drug release experiment.

For measuring the concentration of ibuprofen in PBS, the 219 nm was chosen as the wavelength. This wavelength was selected due to the high signal of ibuprofen at this point, which was found by analyzing a spectrum from 190-350 nm. Sets of calibration curves were made to associate the respective absorption values at 219 nm with known concentrations of prepared samples. Thus, by using Beer's law, it was possible to determine the concentration of unknown samples by referencing the absorption value to the according calibration curve.

A Shimando UV-3100 was used with the software UVProbe 2.10 for these measurements. Although only the absorption at 219 nm was of interest, spectra from 190-350 nm were obtained for each sample. In this way, it was possible to compare the shape of the spectra to that of the prepared calibration samples for ibuprofen in PBS. Where the shape diverged significantly from that of the known samples, it was assumed to have had problems with contamination.

3.3. Drug Release Experiments

For the drug release experiments a standard procedure in the field of drug release studies was used in that the drug delivery systems were placed in a phosphate buffered saline solution (PBS) and aliquots of the release medium were taken at regular intervals for UV analysis to determine the drug concentration present at these times. Specifically, for the experiments on loaded powder (as opposed to the composite DDSs), 100 mg of loaded ZnO was measured and placed in a dialysis membrane with roughly 5 mL of PBS. The membrane was then submerged into 200 mL of PBS in a conical flask, as shown in figure 29. This setup was then placed on a shaking table and shaken at 125 rpm in an environmental chamber maintaining a constant body temperature of 37 °C.

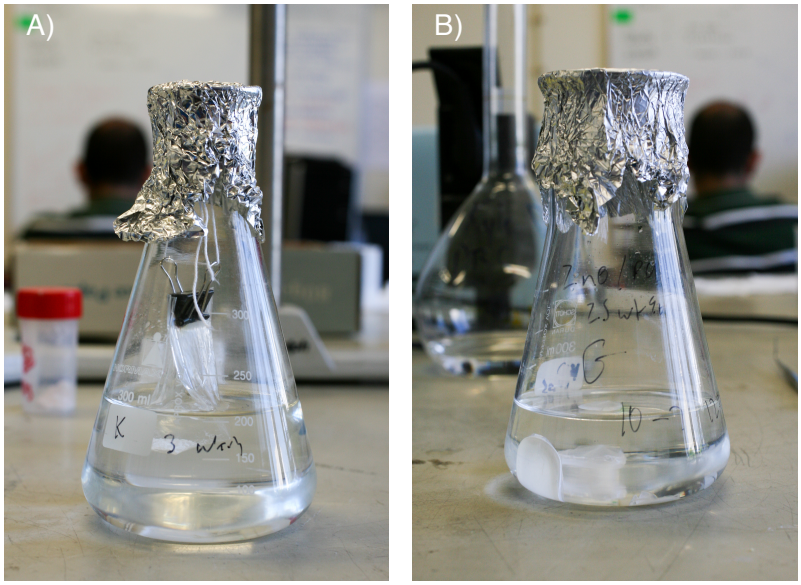

Figure 31: Setup for drug release experiments. A: Powder samples placed in dialysis membrane and then submerged in PBS; B: composite samples simply submerged in PBS

Similarly, for the drug release experiments with the composite DDSs, conical flasks containing 200 mL of PBS were used. However, for the composites, the DDSs were simply placed in the PBS solution without the use of dialysis membranes.

In both the cases for powder and composite samples, 4 mL samples were taken at predetermined intervals and analyzed via UV-VIS spectroscopy in order to determine the concentration of ibuprofen. Drug release curves were then built from these values.

3.4. Data Modeling

After obtaining the drug release curves for the experiments, it was attempted to fit various models found in literature to the experimental data. An assortment of reported models were selected and have been given with the corresponding equations in table 1, in chapter 2. The models were selected from [49] and the reasoning behind their selection was also presented in chapter 2.

The curve fitting was performed with Microsoft Excel, where the “Goal Seek” function was applied to the respective parameter(s) for each model in order to maximize the R^2 value

for the modeled data set. The optimized R^2 values are reported in the appendix in table 8. In other words, a data set was created to provide modeled ibuprofen concentrations at the same time points present in the various drug release experiments. Minimization of the difference between the modeled and experimental data set then allowed the parameters of the various models to be determined.

Chapter 4

Results and Discussion

4. Results and Discussion

To best report the experimental results in a logical fashion, this chapter will be divided into four sections. Firstly, the results from various characterization methods will be presented for the nanostructured ZnO particles, followed by the characterization results of the composite ZnO/PU drug delivery systems. Then, the drug release experimental results will be given, which includes those of both the systems based on pure nanostructured ZnO and the composites as well as the application of various models proposed in literature. Finally, this chapter will conclude with a discussion of the degradation behaviors observed during the drug release experiments for the particle and composite systems.

4.1 Characterization of the Nanostructured ZnO

4.1.1. X-Ray Diffraction

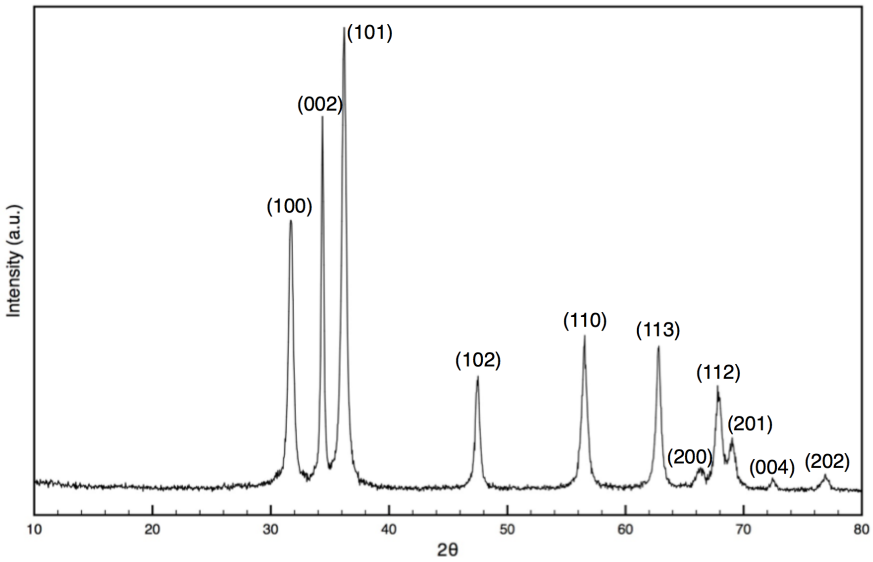

Figure 32: XRD Spectrum for pure nanostructured ZnO with peaks labeled according to diffraction planes

The XRD spectrum for the precipitated ZnO powder can be seen in figure 30. The peaks correspond well to the reported positions of literature for pure crystalline zinc oxide according to the JCPDS file number 00-036-1451. Using the Scherrer equation (eq. given in previous chapter) in order to determine average crystallite size suggests a crystallite size of 27 nm, which was calculated by averaging the values obtained for the six largest peaks.

The fact that pure, crystalline ZnO was produced is significant due to the fact that the synthesis of oxides frequently requires a calcination step, in which a heat treatment is applied to the material in order to promote oxidation [18, 42, 55]. In the present case, however, no additional high temperature steps were required to form pure zinc oxide. This would be advantageous in practical use in terms of ease of processing the drug delivery system.

4.1.2. Scanning Electron Microscopy

SEM images were produced in order to investigate the microstructure of the nanostructured ZnO particles. In figure 31 is shown SEM images for pure ZnO produced one day after the chemical precipitation. The left image shows the overall particle morphology and a magnified view of the particle surface is shown in the right section. The particles can be described by an agglomeration or assemblage of plate-shaped nanoscale pieces, which come together to form spherical forms of approximately 2.7 micrometers in diameter. It should be noted that the platelets present a radial orientation, meaning that one of the long edges points towards the center of the spherical particles, which provides channels and easy access to surfaces within the body of the particles. Because of these nanoscale features, it is expected that the nanostructured particles have a high specific surface area, which will be discussed in more detail in the section regarding gas sorption measurements.

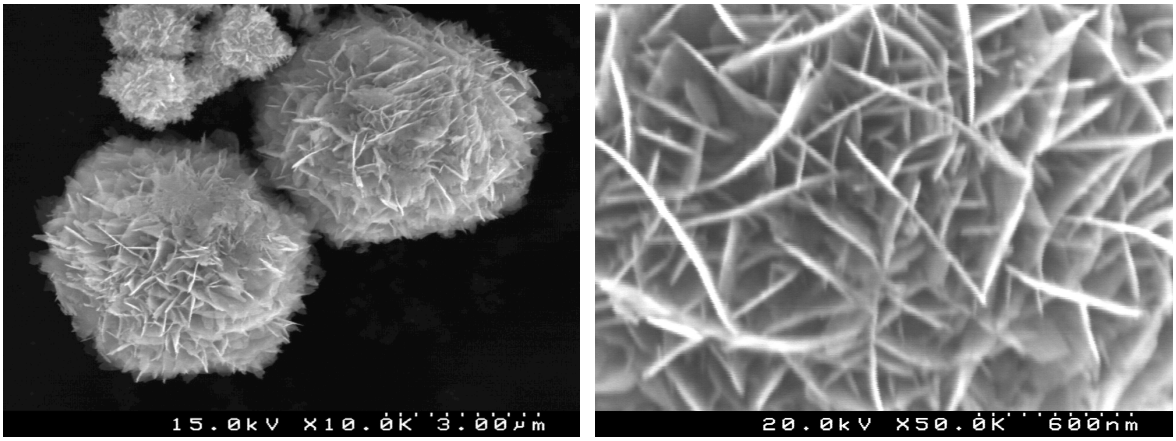

Figure 33: SEM image of pure nanostructured ZnO particles. Left: magnification of x10000 to show overall particle size; right: magnification of x50000 to show particle surface morphology

Following the procedure outlined in the experimental section, the particle dimensions were calculated and are shown in table 3.

Table 3: Dimensional details of ZnO nanostructured particles

Dimension	Calculated Value	Standard Deviation
Particle Diameter	2.7 µm	.9 µm
Nanoplatelet Length	680 nm	200 nm
Nanoplatelet Thickness	38 nm	12 nm

These platelet dimensions estimated from the micrographs are slightly larger than the 27 nm determined by the Scherrer equation based on the diffraction data discussed in the previous section. Though it has been proposed that the accuracy provided by the Scherrer equation leaves much to be desired [56], the estimation obtained based on the XRD data in fact provided a prediction for the average crystallite size that corresponds quite well to the thickness of the nanoplatelets. This suggests that indeed the particles are an assembly of individual nanoplatelets and that the designation as “nanostructured” can be justified. It can be noted that the nanoplatelet thickness (38nm) is very close to the average crystallite size (27nm) determined by the Scherrer equation.

Micrographs were produced for the loaded particles as well (containing ibuprofen). As can be seen in figure 32, the drug loading process does not alter the microstructure of the drug carrier. The particle size remains constant (no swelling and no disaggregation) and the

structure of agglomerated nanoplatelets' assemblage is maintained. In fact, the loaded particles are indistinguishable from their virgin counterparts.

Furthermore, in the left portion of figure 32 can be seen a less magnified view of the particles, where the uniformity of particle size can be observed. Comparing the images of figures 31 and 32 reveals the consistency in particle size, even between precipitation batches. Because of this, subsequent experiments with drug release could be made without concern that significant variation in particle morphology between synthesis batches would significantly impact the results.

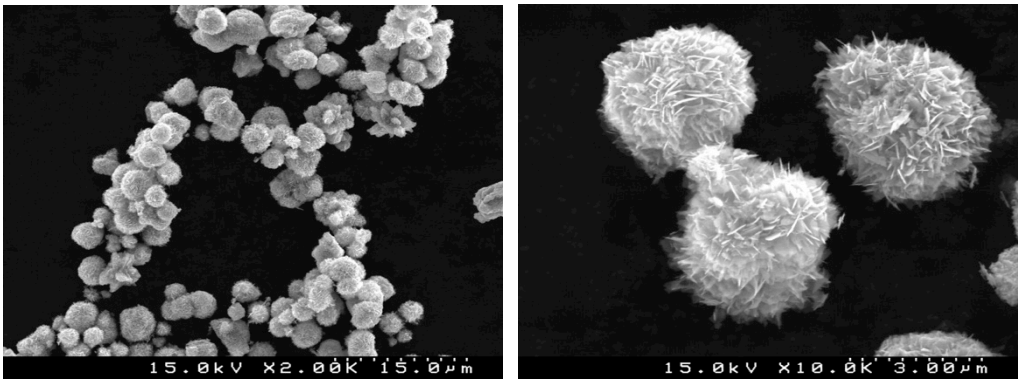

Figure 34: SEM images of nanostructured ZnO particles loaded with IBU at 800 ug/mL. Left: magnification of x2000; right: magnification of x10000

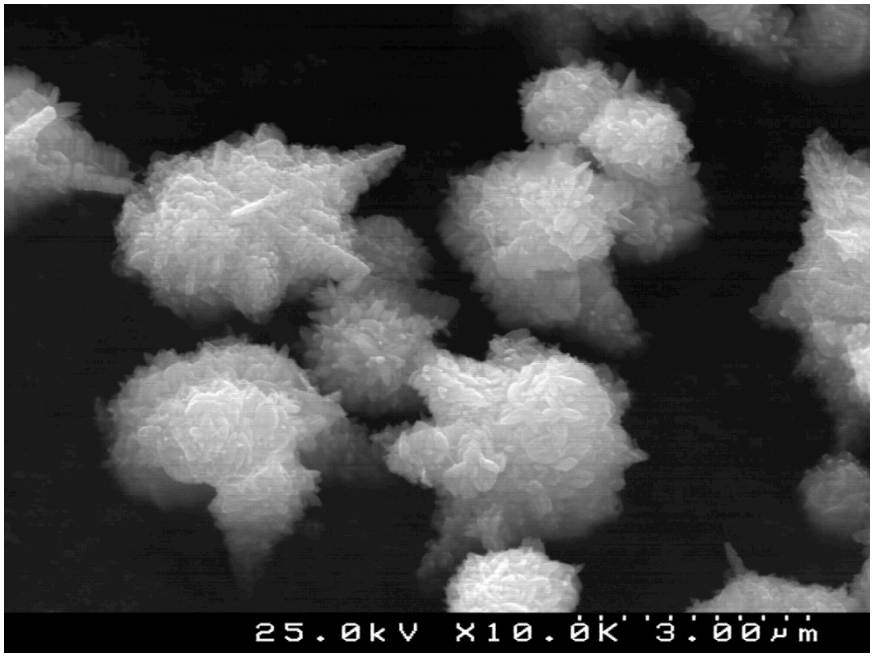

Figure 35: SEM of nanostructured ZnO particles precipitated from supernatant solution post-collection

To explore the process efficiency regarding the yield of ZnO precipitated during the procedure, after the initial powder was collected from the suspension resulting from the precipitation procedure the leftover supernatant was heated in order to promote the crystallization of additional zinc oxide. Indeed, this was possible; crystalline ZnO powder particles were precipitated, as confirmed by XRD and the microstructure of this ZnO is shown in figure 33. However, the amount of powder collected was too little for it to be viable for drug delivery experiments. As can be seen, the overall particle sizes of the ZnO precipitated from the supernatant are quite similar to the particles produced during the initial precipitation. However, the definition of the nanoplatelets is reduced; it can be seen that the spherical particles are, as in the initial precipitate, formed by an agglomeration of nanosized particles, but it cannot be said that these are nanoplatelets. The shape of these sub-particles is more ambiguous.

An explanation for this occurrence can be as follows. During the initial precipitation, the presence of citric acid ions, which is known to have a strong tendency to form chelated complexes with cations, gives rise to the formation of Zn-based complexes during the room-temperature precipitation. Thus, after the removal of the ZnO powder, an amount of Zn still is present in the supernatant solution. With a temperature increase, the complexes

of Zn and citric acid become unstable, releasing Zn^{2+} ions back into the solution, which leads to a supersaturation of Zn^{2+} and promotes the further precipitation of ZnO.

4.1.3. Fourier Transform Infrared Spectroscopy

To analyze the chemical bonding information in the samples, FTIR was used. Figures 34 and 35 show the spectra for the samples of pure nanostructured ZnO, ZnO loaded with ibuprofen at 1 mg/mL, and ZnO loaded with ibuprofen at 10 mg/mL, respectively. The characteristic absorption peak for the Zn—O bond occurs from 450-500 cm^{-1}, which can be seen in all cases as the sudden drop in that range, as the scanning range of the equipment did not account for the full peak. Additionally, the three samples show a broad absorption from 3000-3750 cm^{-1} that is due to O—H bonds from hydroxyl groups. The peaks labeled “b” and “c” can be assigned to the bending of water molecules and absorption of the C=O bond in carboxyl groups, respectively. The latter can be attributed to the presence of residual adsorbed citrate ions.

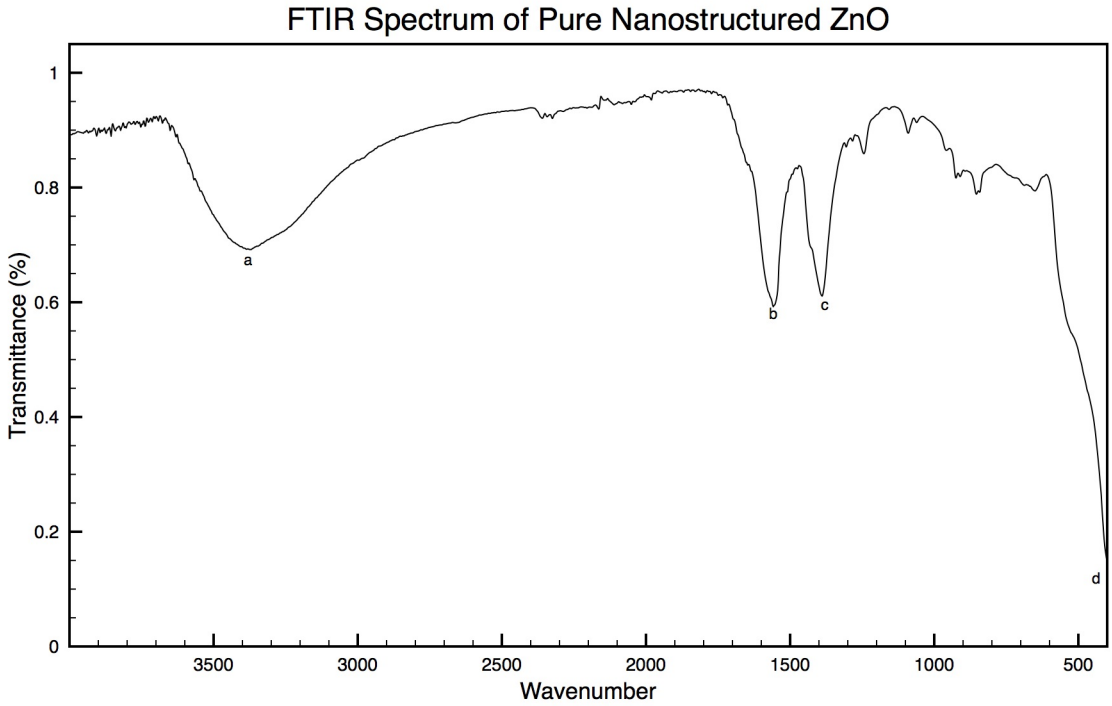

Figure 36: FTIR spectrum of pure nanostructured ZnO particles

Table 4: FTIR peak assignments for ZnO

Designation	wavenumber (cm^{-1})	Assignment [55,57,58]
a	3600	Characteristic absorption of hydroxyl (O-H) groups
b	1560	Bending of water molecules[1]
c	1396	Absorption of C=O[1]
d	< 500	Absorption of Zn-O bond

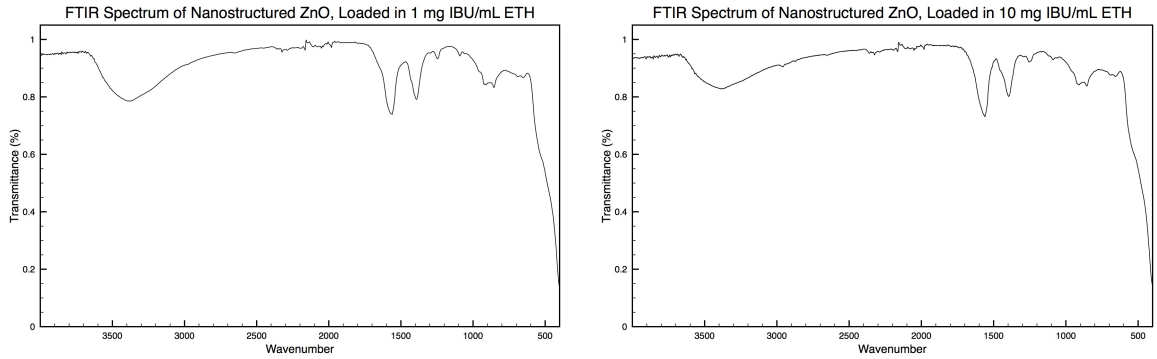

Figure 37: FTIR spectra of IBU loaded ZnO DDSs. Left: loaded in 1 mg/mL; right: loaded in 10 mg/mL

After the IBU loading, the resulting FTIR spectra show no significant deviation in the positions of absorption peaks. Though the shape of the peak attributed to Zn-O bonds located at the right extreme of the graphs remains consistent, the intensities of the three other main peaks diminishes slightly due to the drug loading. This can be seen especially well in peak “a” which was assigned to O-H hydroxyl groups, where the peak intensity decreases with a corresponding increase in amount of IBU. It could be that the attachment of residual water molecules post-precipitation is reduced with the replacement of IBU molecules on the same sites. The same decrease in peak intensity can be seen for that labeled “b.” As this signal intensity is proportional to the number of C=O bonds in the carboxyl groups, and citric acid has three C=O bonds while ibuprofen has only one, the decrease in the absorption at ~1400 cm^{-1} suggests the replacement of adsorbed citric acid with ibuprofen.

[1] These peaks are ambiguously reported in literature, however it is agreed that they are due to residual impurities due to atmospheric molecules such as H_2O or CO_2

Additionally, two small peaks appear in the spectra for IBU-loaded samples. These can be seen at ~2950 and ~2850 cm^{-1}, which can be assigned to the asymmetrical stretching of CH_3 groups and symmetrical stretching of CH_2 groups, respectively [53].

4.1.4. Gas Sorption Experiments

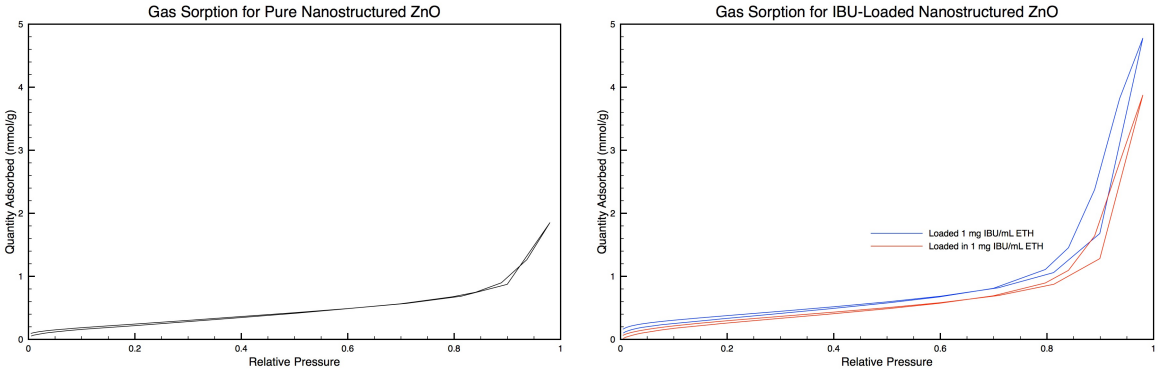

Figure 38: Gas sorption isotherms for powder ZnO DDSs. Left: Unloaded; right: loaded in 1 mg/mL (blue) and 10 mg/mL (red)

Gas sorption experiments, for which the isotherms are presented in figure 36, were performed in order to provide information regarding the porous nature of the nanostructured ZnO particles. From the isotherms it was possible to calculate important properties such as specific surface area, pore volume, and pore cross sections, which are presented in table 5.

Table 5: Porosity details of unloaded and loaded ZnO particles

Sample	BET SSA (m^2/g)	Pore Volume (cm^3/g)	Pore Cross Section (Å)
Pure ZnO	19	0.06	97
Loaded – 1 mg/mL	30	0.16	162
Loaded – 10 mg/mL	25	0.13	150

Comparisons between the loaded samples indicated that pore volume, cross section, and BET specific surface area are smaller for the sample that was subjected to higher loading

concentrations. It follows that, for the samples loaded in solutions of higher concentrations, the overall amount of drug present in the carrier post-loading should be higher. This can already be seen to be true in the gas sorption results, as the larger amount of loaded drug fills the pores more completely, closing the system and thereby reducing the apparent pore volume and cross section observed by the measurements. However, this trend is unfortunately contradicted by the data for unloaded ZnO, where it would be expected to have a larger pore volume and BET specific surface area than the loaded samples. This could indicate that the internal structure is not as consistent between synthesis batches as initially suggested by the SEM results; the data for the pure ZnO sample was taken for one of the first samples produced and was performed several months before the loaded samples.

Though, as shown by the FTIR spectra, the drug loading comes with an associated decrease in the amount of citric acid attached to the sample. A possible explanation for the increase of specific surface area associated with the loaded samples could be that the release of citric acid frees additional surface area in the sample more than that which is occupied by adsorbed ibuprofen.

4.1.5. Thermogravimetric Analyses

To investigate the thermal behavior of the samples, thermogravimetric analyses were performed, the results for which are presented in figures 37 and 39-43. Additionally, a differential thermal analysis spectrum is presented in the same figure for pure ibuprofen, shown in figure 38.

In the case of pure ZnO, the TGA for which can be seen in figure 37, a few important observations can be made. Namely, there is a constant general decrease in weight throughout the temperature change. At low temperature, up to roughly 250 °C, the weight loss can be attributed to the evaporation of physically and chemically adsorbed water molecules as well as remnant organic species from the precipitation procedure, mainly ethanol. A sharp step occurring between 260 and 270 °C can be accounted for by the decomposition of citric acid leftover from the synthesis. At higher temperatures, the weight

loss is also due to the continued combustion of citric acid, which continues through the range of the experiment. The broad steps can be explained by the fact that a constant heating rate is maintained throughout the experiment and that it takes time for the reaction products to escape the porous structure of the nanoparticles.

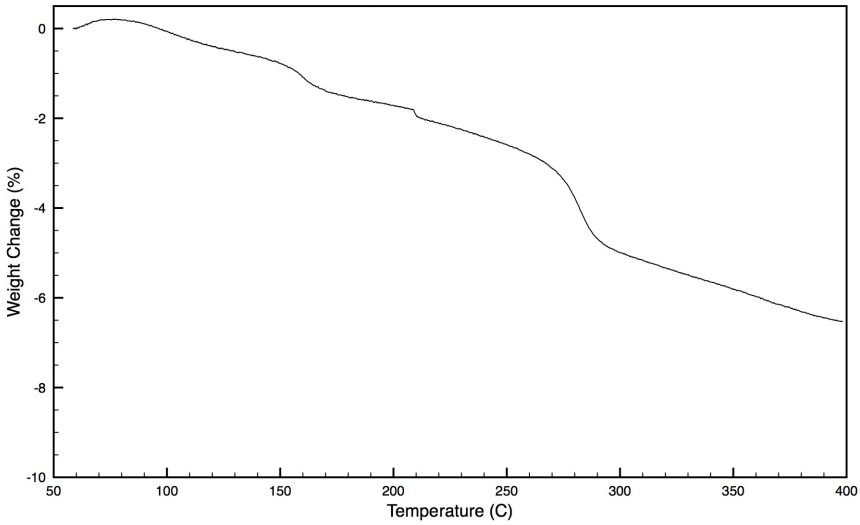

Figure 39: TGA curve for pure ZnO particles

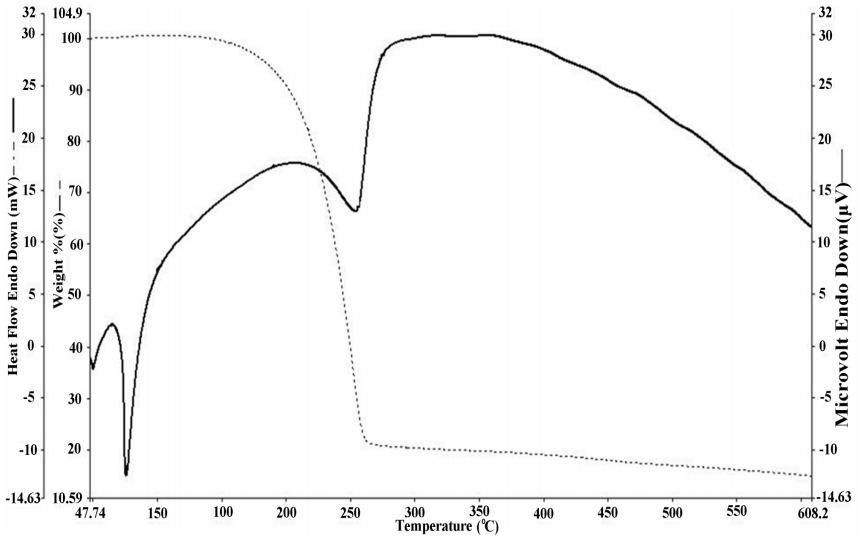

Figure 40: TGA (dotted line) and DTA (solid line) for pure IBU

The unfortunate circumstance is that the step due to decomposition of citric acid occurs in a similar position to that for the decomposition of ibuprofen, as seen in figure 38. This forces difficulties for the quantitative determination of the amount of ibuprofen loaded in

the samples. Additionally, it was seen in the FTIR results that the drug loading procedure is associated by replacement of adsorbed citric acid species, which prohibits the assumption that the step in the pure ZnO due to citric acid decomposition can be taken as a baseline step for all of the subsequent samples due to the different initial concentrations of adsorbed citric acid in the various samples. It would be beneficial to investigate methods of cleaning the citric acid from the precipitated ZnO particles in order to enable quantitative determination of ibuprofen loading through TGA.

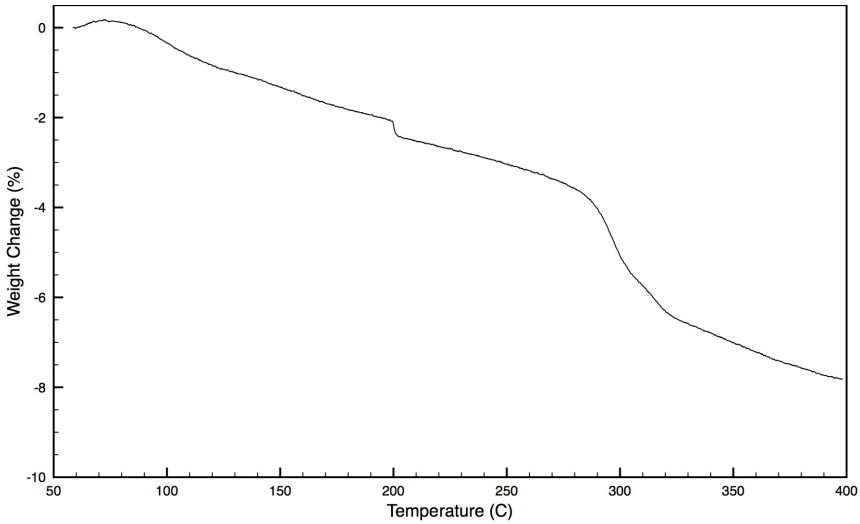

Figure 41: TGA curve for ZnO particles loaded with IBU at 1 mg/mL

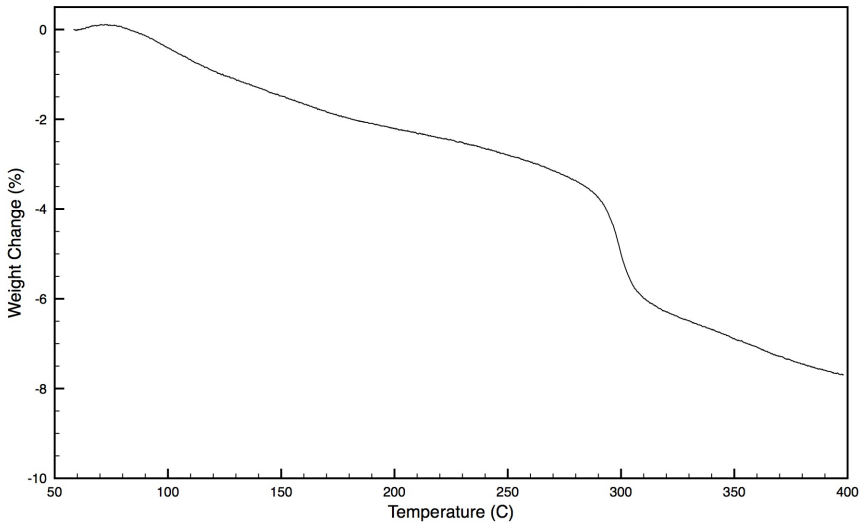

Figure 42: TGA curve for ZnO particles loaded with IBU at 2 mg/mL

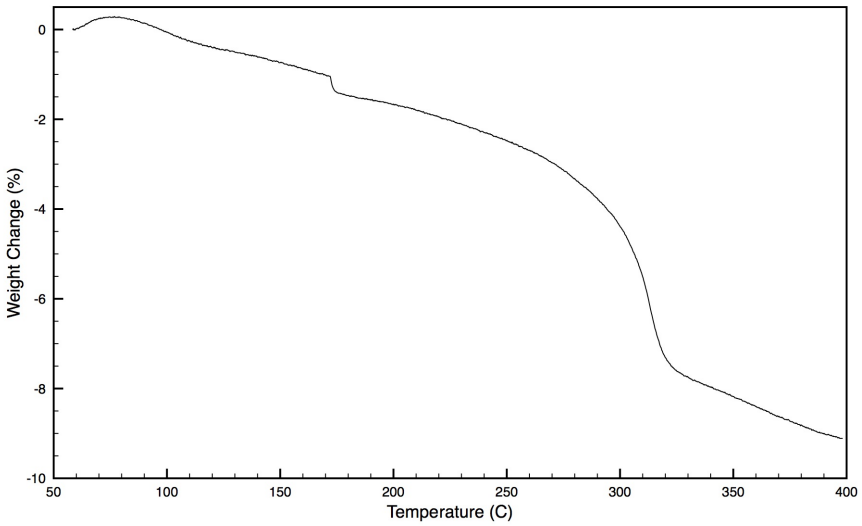

Figure 43: TGA curve for ZnO particles loaded with IBU at 10 mg/mL

Figures 39-41 show the TGA curves for the ZnO particles loaded with ibuprofen with various concentrations: 1, 2, and 10 mg/mL in ethanol. The three graphs share the general trend of broad weight losses occurring before and after the main step occurring at roughly 300 °C. These follow the same explanation as was given for the sample of pure ZnO with the slight exception that the decrease at high temperature also includes continued combustion of the organic ibuprofen molecules. The most significant point of comparison between these three figures is the steep step found at 300 °C. Namely, the height of this step differs between the three samples. Considering the hypothesis that the higher concentration of ibuprofen in the drug loading solution enables a higher loading, the larger step seen in figure 41 can be explained by the decomposition of a higher amount of ibuprofen.

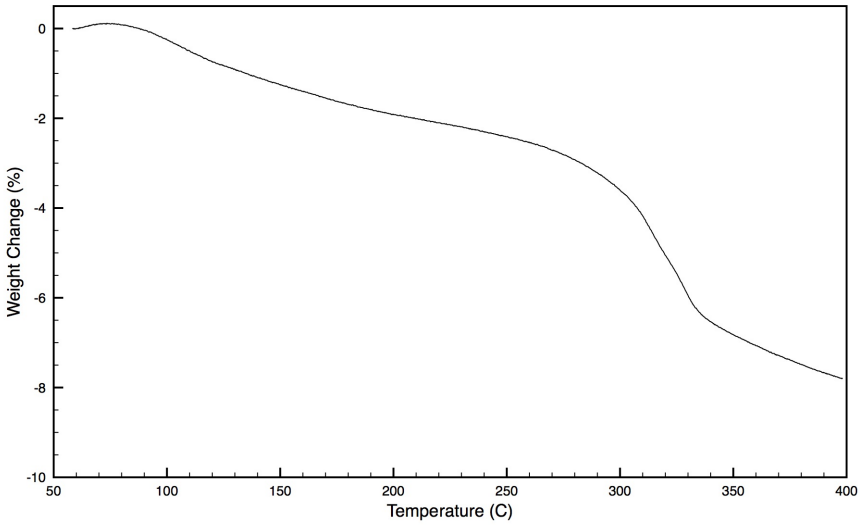

Figure 44: TGA curve of ZnO particles loaded with IBU at 10 mg/mL followed by 1 wash cycle

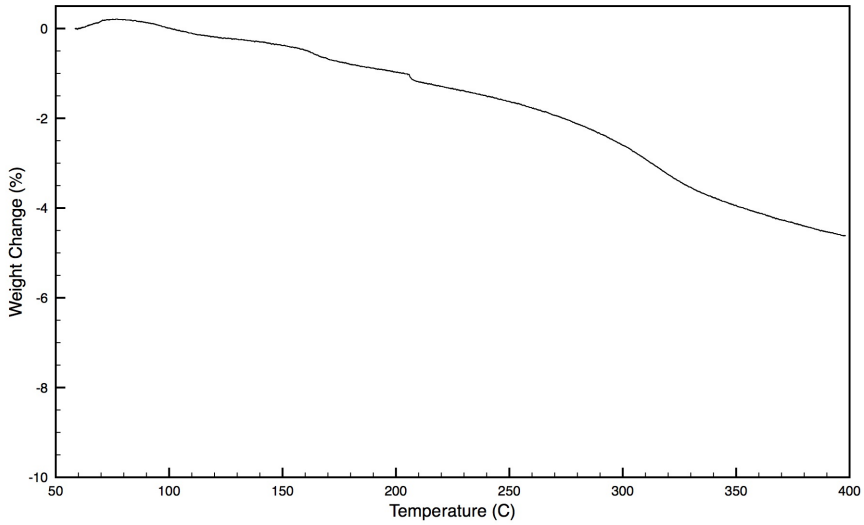

Figure 45: TGA curve of ZnO particles loaded with IBU at 10 mg/mL followed by 3 wash cycles

Comparison of figures 41-43 shows the effects of washing on the thermal properties of the ZnO particles. Again, the general behavior of the spectra follows the previous explanation and the point of interest is once more the step around 300 °C. Firstly, the step height is lower in the washed samples than in the unwashed sample. As the loading concentration for these samples, it can be concluded that the washing procedure serves to remove organic compounds. Though, whether it is citric acid, ibuprofen, or a combination of both that is removed remains unclear. Secondly, the onset of the weigh-loss step is shifted to higher temperatures in the washed samples. As the chemical history of the washed

samples was identical to the unwashed samples, an explanation for this could be that the washing procedure alters the microstructure and pathways for the release of decomposition products. The analysis of the particle morphologies of washed samples will be provided later.

Table 6: TGA weight loss due to decomposition of IBU and correlated estimated loading of IBU

Sample	TGA Weight Loss (%)	Estimated Relative Loading (mg IBU/mg ZnO)
1 mg/mL	2.18%	0.022
2 mg/mL	2.46%	0.025
10 mg/mL	3.66%	0.038
10 mg/mL, 1 wash	2.82%	0.029
10 mg/mL, 3 wash	1.20%	0.012

Despite the complications arising from the presence of unknown quantities of citric acid in the samples, the estimated loading IBU was calculated according to the procedure outlined in the previous chapter in order to provide a comparison for the tool for the results of the drug release experiments. These data are presented in table 6. The general trend shows that the increased IBU concentration in the ethanol loading solution enables a higher uptake of drug into the delivery system, which is observed by the larger weight loss step at 300 °C. By comparing the samples of 10 mg/mL and 1 mg/mL, for example, it is shown that a ten-fold increase in the loading concentration results in a 70% increase in drug uptake. Similarly, the washing procedures clearly show that some of the drug is removed from the loaded samples, and an expected reduction in drug release will be seen. However, because of the step observed in the virgin sample attributed to decomposition of citric acid is located in a similar range as the expected step due to the decomposition of ibuprofen, the accuracy of the loading values presented in the right-hand column of table 5 cannot be claimed with high confidence.

It would be of high interest to develop a method in order to more accurately perform these calculations so that a relationship could be made between the loading concentration and the loading amount, as well as to determine the maximum amount of loading that is possible for this materials. Firstly, the potential for this material in biomedicine can be evaluated based on the drug loading potential. In other words, the more drug that can be

stored in the system affords the most useful system. However, that is not to say that the system would need to be loaded at it's maximum potential in all applications. By being able to fine-tune the amount of drug loaded, it would be possible to vary the drug dosage stored in the system for customization of the therapeutic application of the DDS.

4.2. Characterization of ZnO/PU Composites

4.2.1. Scanning Electron Microscopy

SEM micrographs were produced for the composite ZnO/PU DDSs and are shown in figure 44, in which images for both the 25 wt% and 50 wt% samples are shown at magnifications of x500 and x10000. Here, as in the rest of this work, the wt% designation refers to the relative amount of loaded ZnO present in the composite system. In the left side of the figure can clearly be seen the effect of increased quantities of ZnO. Namely, the density of nanostructured particles is much higher for the 50 wt% sample. On the right side can be seen a magnified view of the ZnO particles. There is an apparent lack of sharpness for these particles, which is due to the fact that these images were taken from the top surface of the composite. During the solvent evaporation procedure the particles towards the upper surface became completely covered by polyurethane and their nanostructured morphologies can therefore not be distinguished on the SEM images of the composite materials.

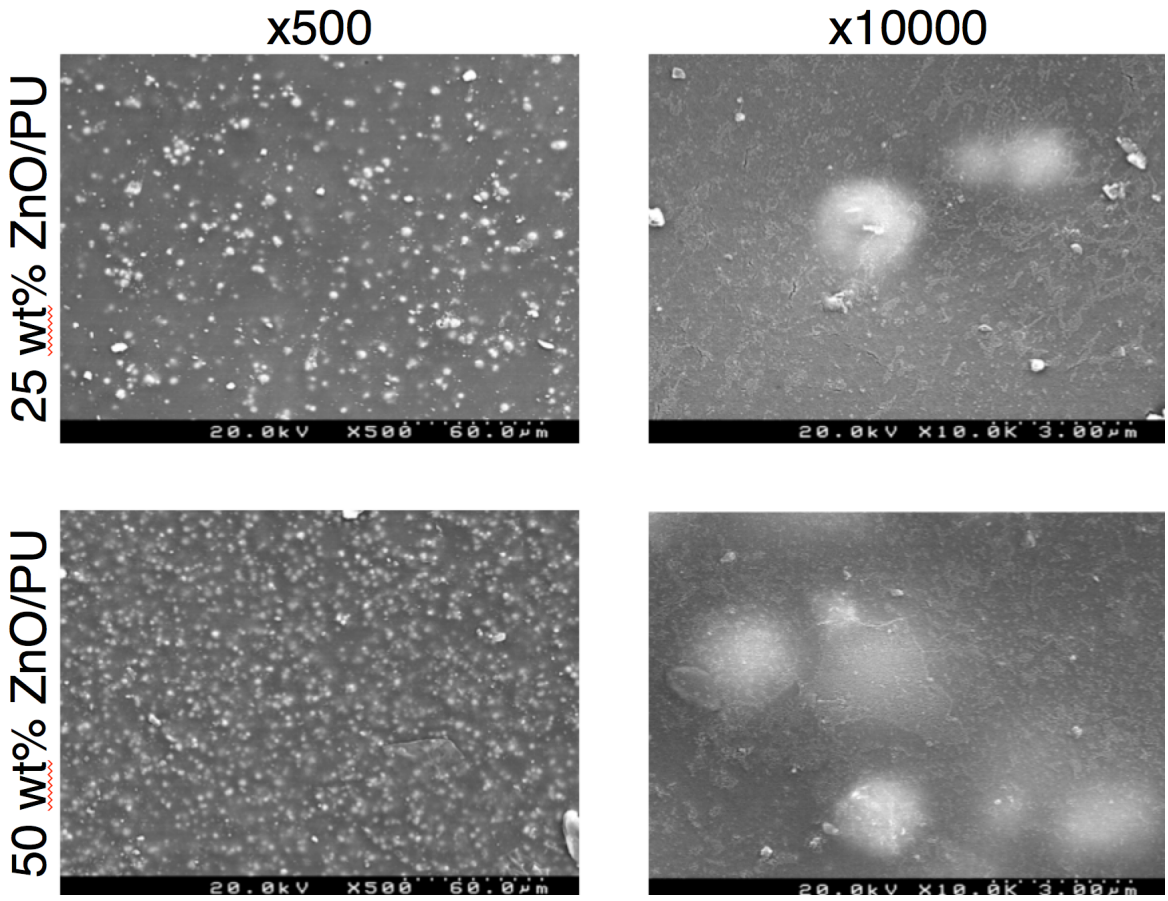

Figure 46: SEM images of ZnO/PU composite DDSs at magnifications of x500 and x10000. Top row: 25 wt% ZnO; bottom row: 50 wt% ZnO.

For the ZnO particles, it can be observed that they are evenly distributed across the sample. The polyurethane itself is rather featureless, but in the more highly magnified view in the figure one can observe that it is not perfectly smooth. This will be discussed in more detail in the section regarding composite degradation during drug release. Suffice it say, the composite serves to embed the ZnO nanostructured particles in a homogenous fashion.

4.2.2. Fourier Transform Infrared Spectroscopy

FTIR analyses were performed on the composite samples in order to investigate the chemical interaction between the various components of the composite systems. These

are presented in figures 45-47. The spectrum for pure, commercial PU is shown in figure 45 with the corresponding peak assignments provided in table 7.

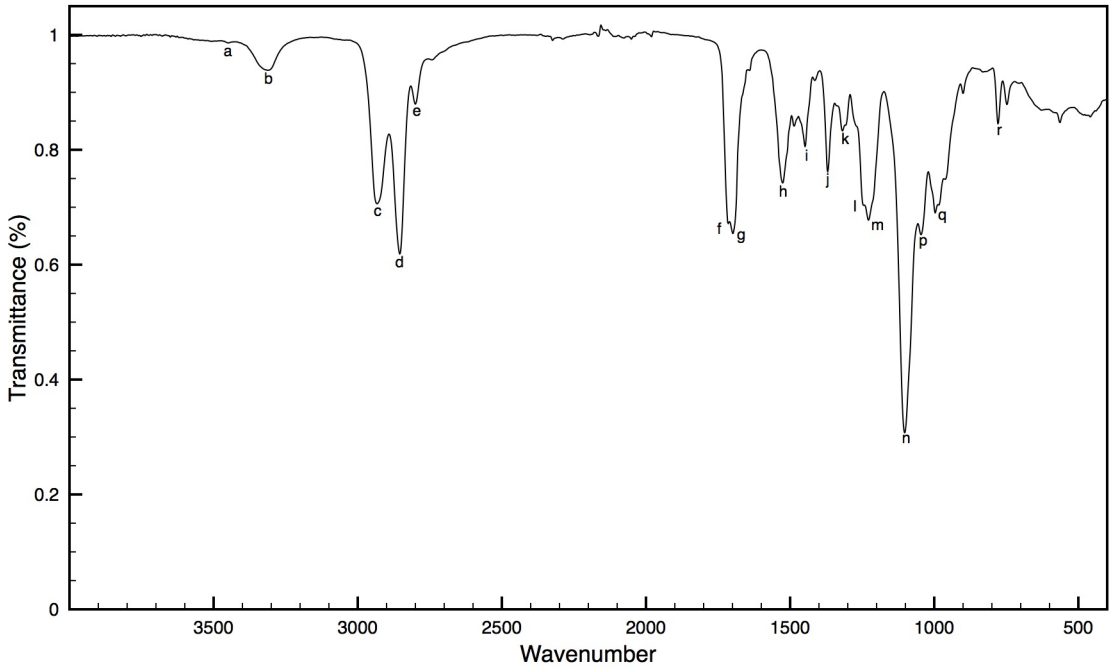

Figure 47: FTIR spectrum of pure, commercial PU

Table 7: Absorption peak assignments for FTIR spectrum of PU

Designation	wavenumber (cm	Assignment [59]
a	3449	Free NH stretching
b	3310	H-bounded NH stretching
c	2931	Asymmetric β CH_2 Stretching (polyether) + asymmetric CH_2 stretching (cyclohexane)
d	2851	Asymmetric α CH_2 stretching (polyether) + symmetric β CH_2 stretching (polyether) + symmetric CH_2 stretching (cyclohexane)
e	2800	Symmetric α CH_2 stretching (polyether)
f	1714	Free C=O stretching (amide I region)
g	1699	H-bounded C-O stretching (amide I region)
h	1525	C-N stretching + N-H bending (amide II band)
i	1448	CH_2 bending
j	1369	CH_2 wagging

k	1319	C-C stretching (cyclohexane)
l	1248	CH_2 wagging
m	1228	C-N stretching (Amide III band)
n	1103	Asymmetric C-O-C stretching (polyether)
p	1045	Asymmetric C-O-C stretching (urethane)
q	900	Asymmetric ring stretching (cyclohexane)
r	779	Cyclohexane ring breating

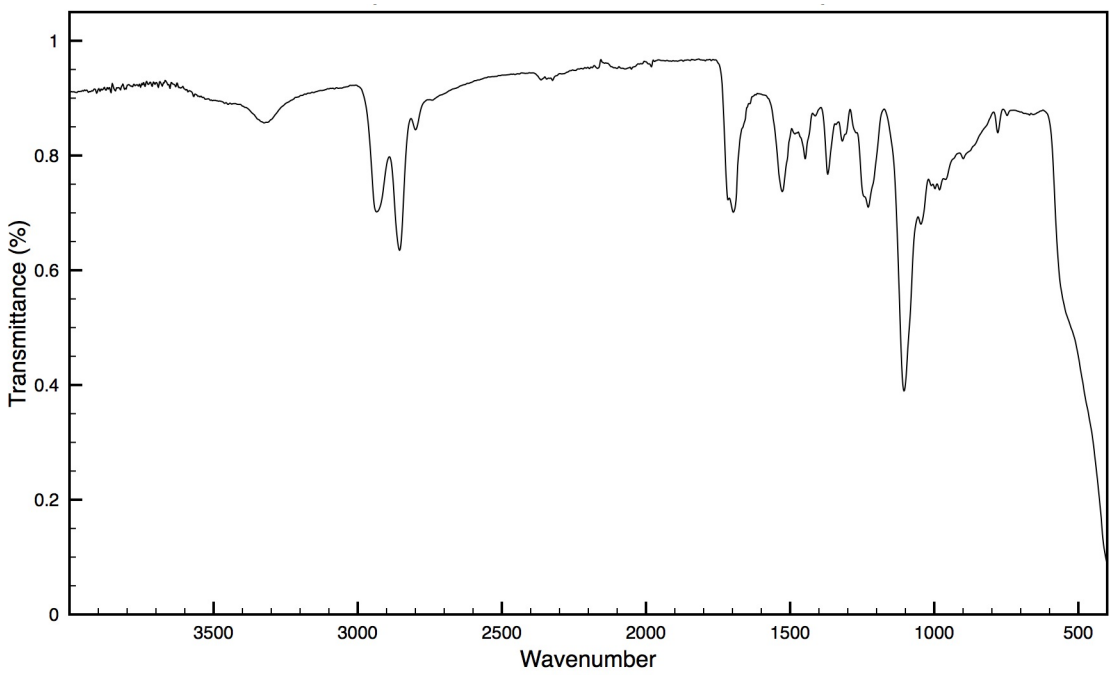

Figure 48: FTIR spectra of ZnO/PU composite DDSs with 25 wt% ZnO content

As was observed in the FTIR spectra for the ZnO powders, a strong absorption peak is partially seen in the experimental range near 400 cm^{-1} due to the Zn—O bond for the composite samples shown in figure 46. The peaks shown near 2900 cm^{-1} can be attributed to C—H bonds. The assortment of peaks between 1000 and 2000 cm^{-1} can be assigned by interactions between carbon, nitrogen, and oxygen atoms in the polyurethane component of the composites, which are specifically detailed in table 7. Similar to the powder spectra, a broad peak around 3500 cm^{-1} is observed due to O—H bonds of hydroxyl components for the composite samples.

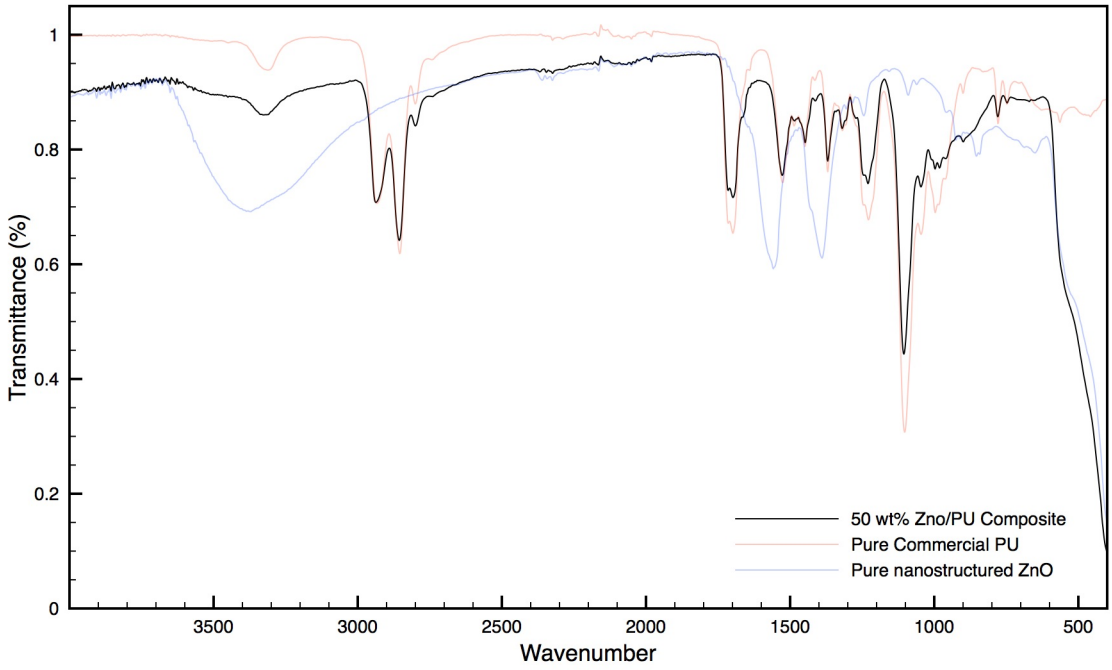

Figure 49: FTIR spectra of 50 wt% ZnO/PU composite DDS showing spectra of both pure ZnO and PU

Referring to figure 47 enables comparison of the spectra between the composite DDS and its individual components (pure PU and pure ZnO). The black line, showing the data for the composite sample, shows no deviation in terms of peak positions compared to the red (PU) and blue (ZnO) lines. This suggests that there is little chemical interaction between the ZnO and PU, as no additional peaks arise in for the composite sample, nor do the peak positions shift in the composite sample from their positions in the spectra of the individual components.

4.3. Drug Release Studies

4.3.1. Variations in Drug Loading Concentration

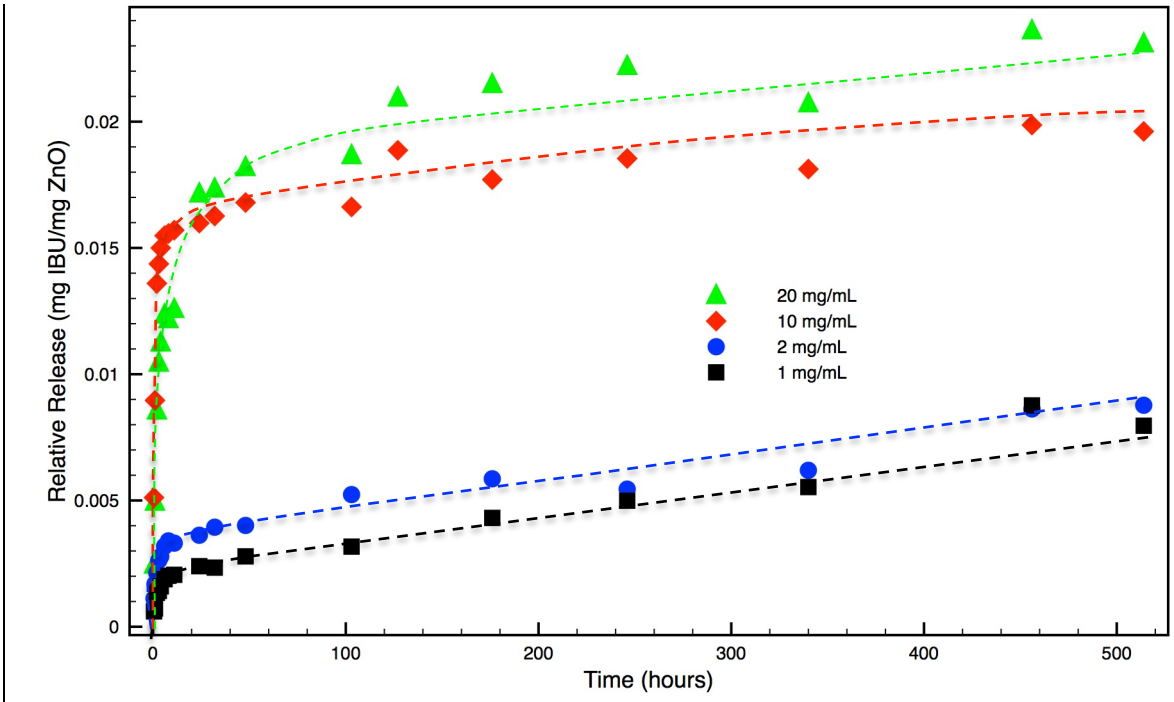

Figure 50: Drug release curves for nanostructured ZnO loaded with different amounts of IBU. IBU loading was performed by soaking ZnO in ethanolic solutions of IBU with different IBU concentrations (mg of IBU/ml of ethanol).

Drug release studies were completed to investigate various influences based on variation preparation methods of different DDSs. In the first investigation, the powders were loaded in ethanol solutions containing different concentrations of ibuprofen (1, 2, 10, and 20 mg/mL). It can be seen in figure 48 that an increase in loading concentration corresponds to an increase in the relative amount of drug released. This means that the drug uptake was higher for samples loaded in solutions of higher ibuprofen concentration, as one would expect. In applications where dosage is an important parameter for a drug delivery system, it is useful to be able to control the amount of drug stored in the DDS. The results from this study show that it is possible to control the drug uptake during the loading procedure simply by adjusting the drug concentration in the loading solution.

However, it should be noted from the figure that doubling the loading concentration does not result in a doubling of the maximum amount of drug released. In fact, changing the loading concentration from 1 to 2 mg/mL has only a small effect in the maximum drug released. Similarly, a tenfold increase in concentration from 1 to 10 mg/mL results in slightly more than double the amount of drug released.

Comparing the relative shape of the release profiles reveals a consistency in the generic behavior of the drug release systems. Namely, an initial burst release occurs over the first 24 hours followed by a slower release stage that continued over the course of the study. Additionally, the slope of this second stage is quite comparable between the studies. This could suggest that a certain amount of drug is strongly connected to the ZnO surface which is slowly released over a long time period and that the increase in loading concentration provides additionally loosely bound ibuprofen, which can be observed by the increase in the amount of drug released in the initial burst stage.

4.3.2. Influence of Post-Loading Washing Procedure

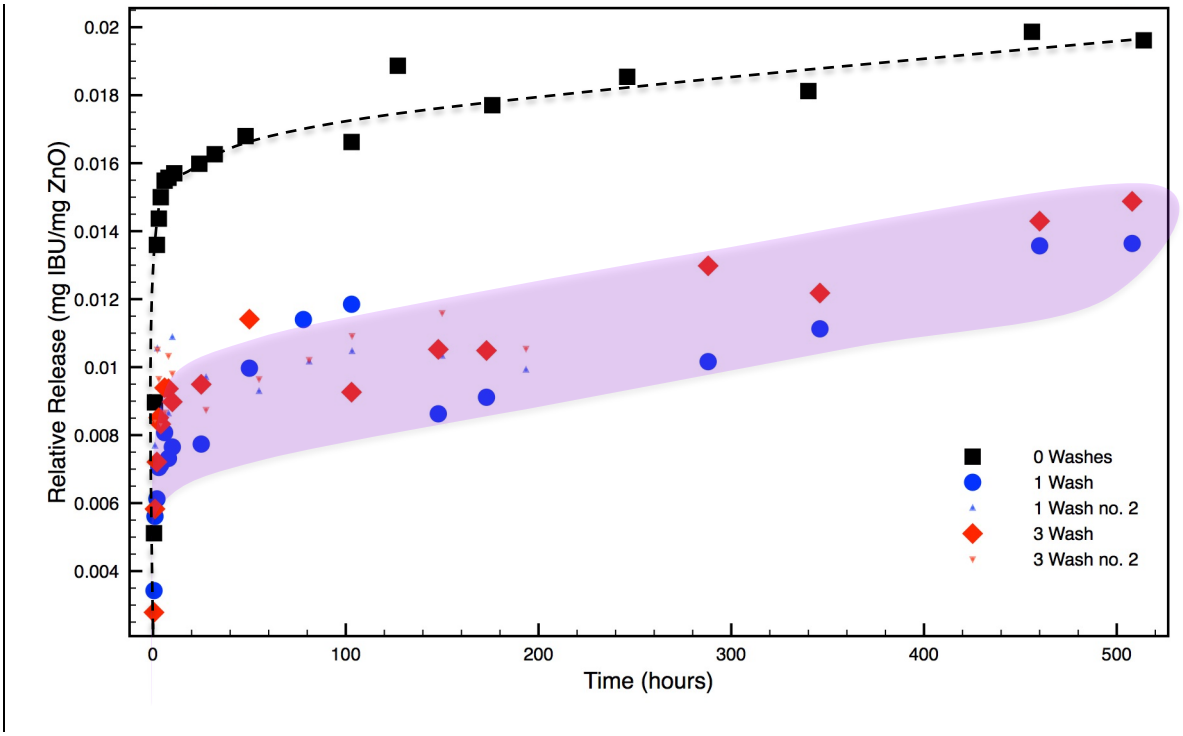

Figure 51: Drug release curves for nanostructured ZnO showing the effect of washing post-loading

The second study on drug loading was complete in order to investigate the effect of washing the samples after loading in ethanol with an ibuprofen concentration of 10 mg/mL. This was completed as the procedure described in literature is often unclear and no standard practice as to handling the loaded powder exists; some papers report washing the samples while others forego a washing procedure. For this study, the samples were washed through centrifugation.

It can be seen in figure 49 that the washing procedure has a detrimental effect on the maximum amount of drug released. Namely, after the first wash cycle, the maximum drug released and thus the drug present in the carrier dropped nearly in half. However, after the third wash cycle the relative amount of drug released remained consistent. This suggests that a loosely bound layer of ibuprofen exists on the loaded sample that is easily removed during the first wash cycle. Then, the remaining drug is strongly enough bound so that its removal is not induced by subsequent wash cycles.

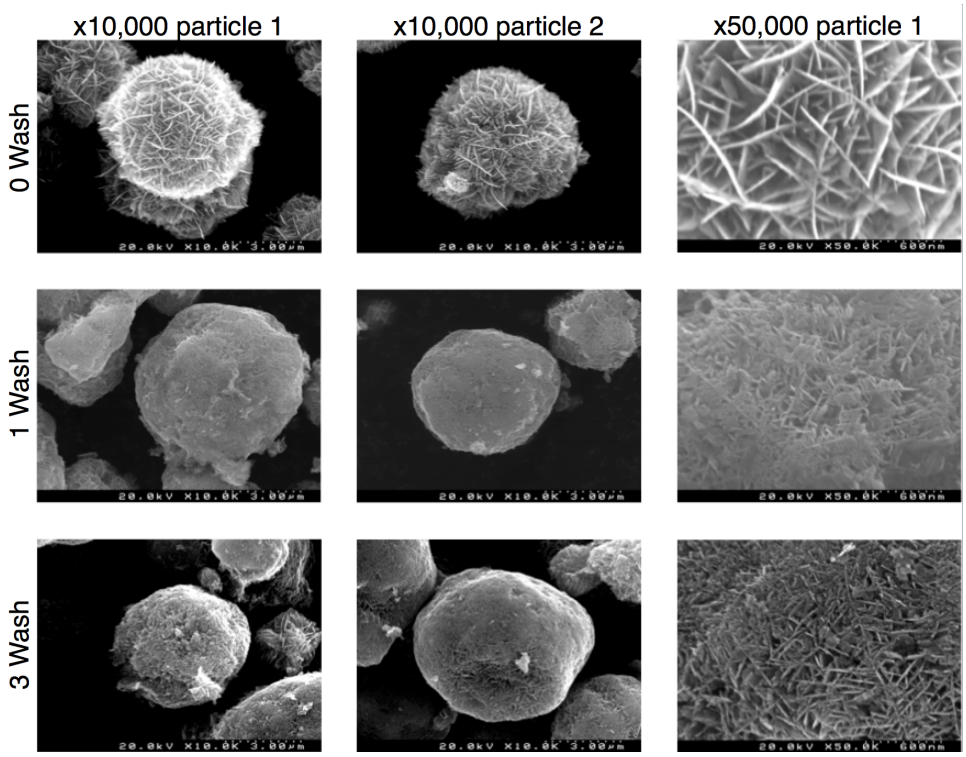

Figure 52: SEM Images of samples loaded in ethanol with IBU concentration of 10 mg/mL. Top row: particles with no post-loading wash cycles; second row: particles with 1 post-loading wash cycle; row 3: particles with 3 post-loading wash cycles

The effects of the washing cycles on the particle morphologies are shown in figure 50, which depicts SEM images of the three samples at various magnifications. For each sample, two particles are shown in order to demonstrate the consistency of the washing effect on the particles. It can be seen that the washing cycles affect the particle surface structure. Where the unwashed sample can be characterized by the typical assembly of distinct nanoplatelets, the surface of the washed particles is much smoother. In the images at magnification of x10000, the nanostructure of the washed particles can barely be distinguished. Because of this effect on the structure of the particles themselves, it can be easily imagined that the washing procedure removes the loosely attached ibuprofen.

Practical implications of these results are clear, which can be understood by the fact that additional procedural steps in the creation of a DDS can impact the drug release profile of the system. Here it has been seen that washing the samples after loading unsurprisingly reduces the amount of drug released from the system due to removal of the adsorbed drug molecules during the wash procedure. Whether a washing procedure can be recommended for use or not is largely dependent on the application in mind with respect to the intended dosage. However, as common DDS applications typically benefit from larger loading capacities, it would be recommendable that the washing step is eliminated from DDS production procedures.

4.3.3. Drug Release from Composite Delivery Systems

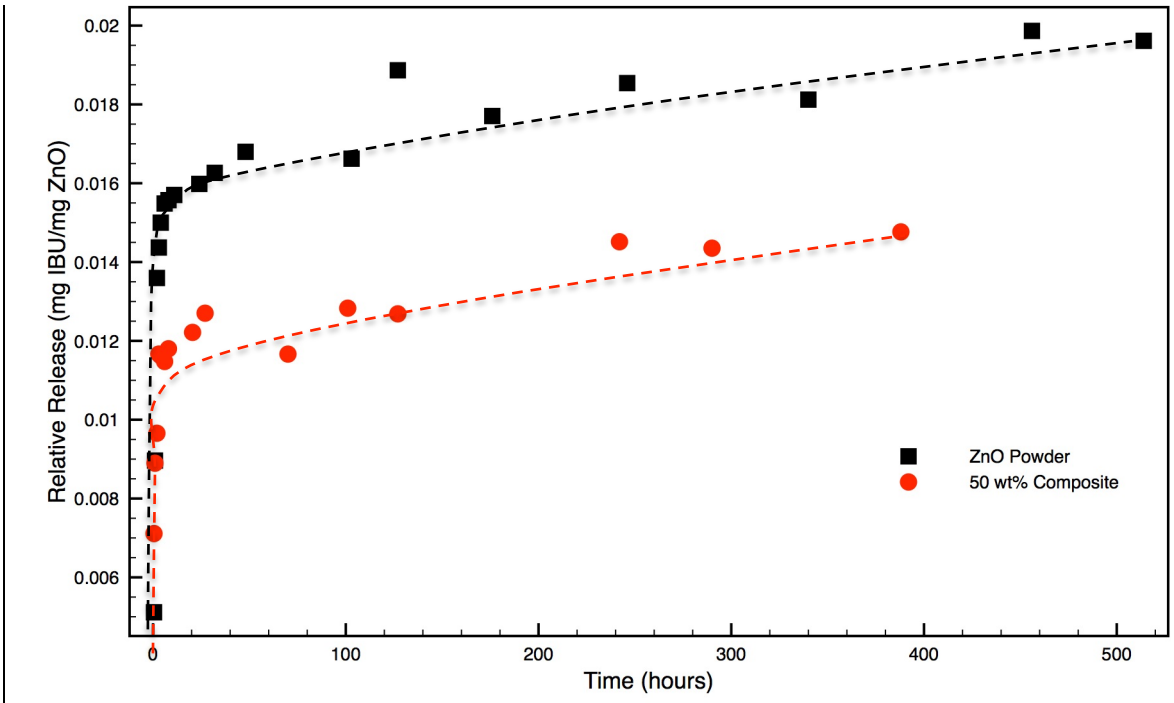

Figure 53: Drug release curves comparing powder to composite DDS

The final study examined the drug release from the composite DDSs. These samples were prepared from unwashed ZnO powders that were loaded in ethanol with ibuprofen concentrations of 10 mg/mL. Figure 51 illustrates the typical behavior of the composite system as compared to the powder systems. It can be seen by comparison to figure 48 that the drug release depicted for the composite samples in figure 52 shows a maximum release that is lower than that corresponding to the ZnO powder DDS, due to the diffusion barrier presented by the polymeric material. The burst-effect can also be observed for the composite samples, suggesting the presence of a large amount of loosely bound drug molecules.

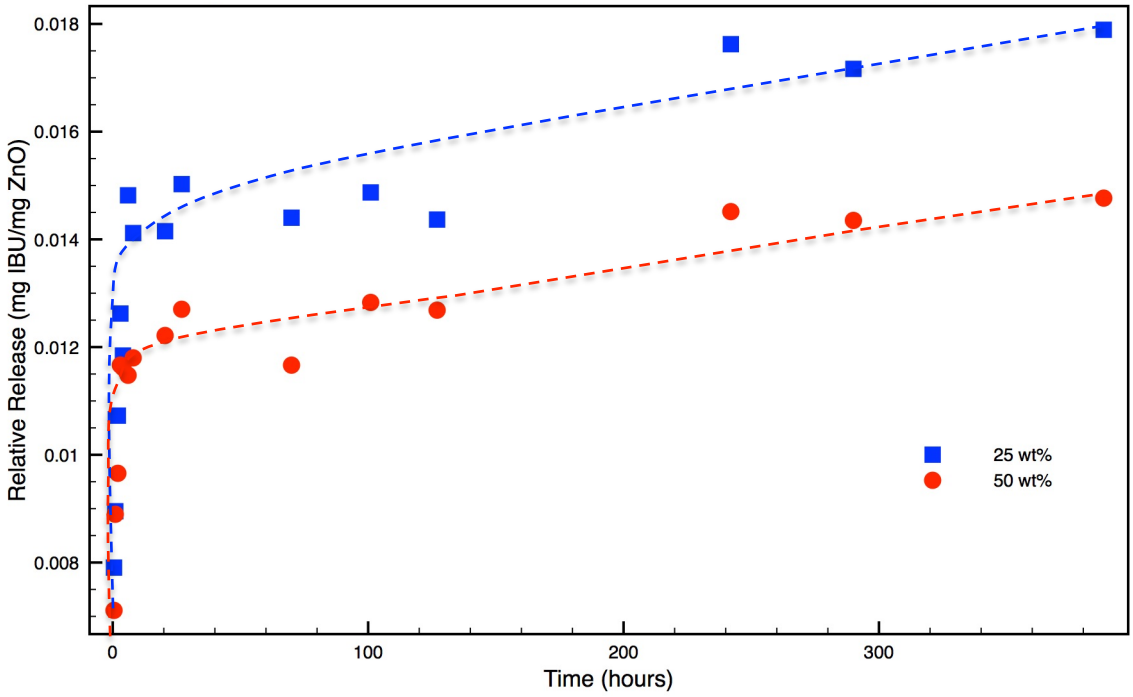

Figure 54: Drug release curves for ZnO/PU composite drug delivery systems

A comparison of the release profiles for the two produced composite systems (25 and 50 wt%) is shown in figure 52. Upon initial interpretation, the results might seem contrary to the expectation that the 50 wt% should have a larger amount of drug released as the larger proportion of PU in the 25 wt% would suggest the presence of longer diffusion pathways for the drug during release. However, a few observations can be made to explain this seemingly contradictory result. Firstly, the y-axis of the graph is given in reference to the amount of ibuprofen released relative to the weight of ZnO in the composite. In terms of IBU loading with respect to the weight of the composite, the 50 wt% is higher and the drug release in terms of mg IBU/mg composite is higher for this sample. Though, this does not explain the fact that figure 52 shows the 25 wt% sample to release a higher percentage of the loaded IBU. As was mentioned previously, it was observed in the solvent evaporation process that the loaded ZnO powder tended to settle in the mixture with PU so that the final composites would not be characterized by an even distribution of powder across the height of the cylindrical samples. For the 25 wt% sample, a larger proportion of the powder was located towards the bottom surface of the composite, which would be associated by short diffusion pathways for the IBU to release from the DDS. Although the 25 wt% composite had more polymer to serve as hindrance to IBU diffusion, the system was not arranged in a way for the PU to serve its expected

purpose. Thus, a higher percentage of the drug could be released during the experiment. For the 50 wt% sample, on the other hand, a larger percentage of the loaded powder was located within the bulk of the sample, where the drug diffusion would be have the longest pathway.

4.3.4. Modeling of Release Curves

Assigning proposed mathematical models to the drug release curves was done in order to better predict the properties of drug release for the DDSs. Figure 53 shows the fitting of the different models to the IBU release profile corresponding to the sample loaded at 10 mg/mL. Five models have been selected in an attempt to match the data to established models, which have been presented in the introduction: first order, Higuchi, Korsmayer-Peppas, Baker-Lonsdale, and Makoid-Banaker.

It can be seen that the Korsmeyer-Peppas model as well as the Makoid-Banaker model fit the data quite well. The Korsmeyer-Peppas model was selected as the best fit to the drug releases of this study based on the combination of a good fit to the data and its simplicity. The Korsmeyer-Peppas model is given by the equation:

$$F = k_{KP} t^n$$

where k_{KP} and n are constants. This model is quite similar to that given by the Higuchi model. However, for the Higuchi model, the power is given by a constant as opposed to being restricted to 0.5. To reiterate from the introduction, this model was designed for polymeric DDSs to account for simultaneous drug release and swelling due to water absorption. For this reason, it is surprising that the model fits well to the data, as the drug was loaded into inorganic nanostructured particles. Thus, while the equation can generally fits the data, as seen in figure 53 and 54, it should be taken as an empirical fit as opposed to drawing conclusions to the physical properties of the material based on the constants in the equation. In other words, as the system under study (loaded ZnO particles) does not fall under the realm of intended use for the Korsmeyer-Peppas model, one should be careful to infer significant meaning from the constants.

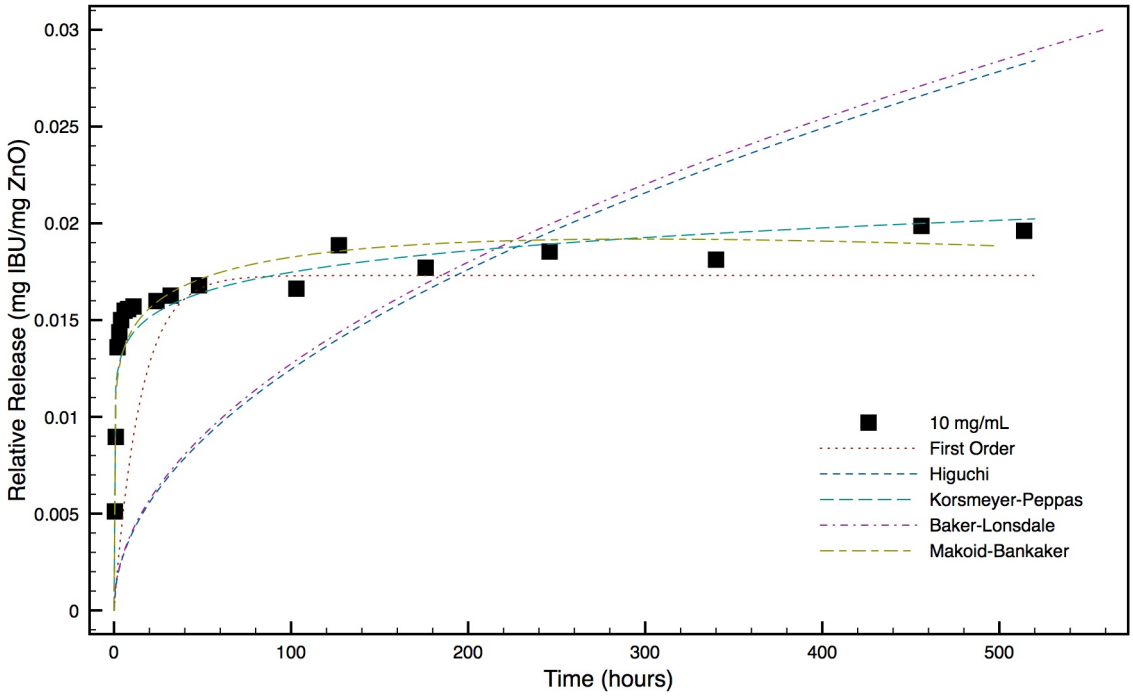

Figure 55: Release curve for nanostructured ZnO loaded at 10 mg/mL and selected models

In a similar light, the Higuchi model, while commonly used in DDS studies, fails to accurately represent the present data. Here, however, it is rather expected to see shortcomings in the fitting ability of the Higuchi model, as its intention was to model the diffusion of drug out of a thin film matrix, such as an ointment.

Closely mirroring the Higuchi model, the Baker-Lonsdale model, shown as the purple line in figure 53, also fails to accurately represent the experimental data. This is disappointing, as the model offered the most promise with regards to describing the drug release based on physical properties of the system, such as diffusion coefficient of the drug, drug loading concentration, and size of the carrier. Had it more closely modeled the data, it could have been used as another measure to estimate a quantitative value for the ibuprofen drug loading.

The Makoid-Banaker model fits the data set nicely, however this is an unsurprising result due to the inclusion of three empirical constants in the model. To restate from the introduction, the model includes both power and exponential relationships with time, each including their own empirical constant. In this way, the Makoid-Banaker model can be

applied to an array of drug release profiles. However, it offers little insight into the release mechanisms.

Lastly, the first order model, while not perfectly fitting the data, can be seen to closely approximate the release profile. This suggests that the drug release occurs through a Fickian diffusion process, where a large concentration gradient exists between the nanostructured ZnO particles and the PBS release medium.

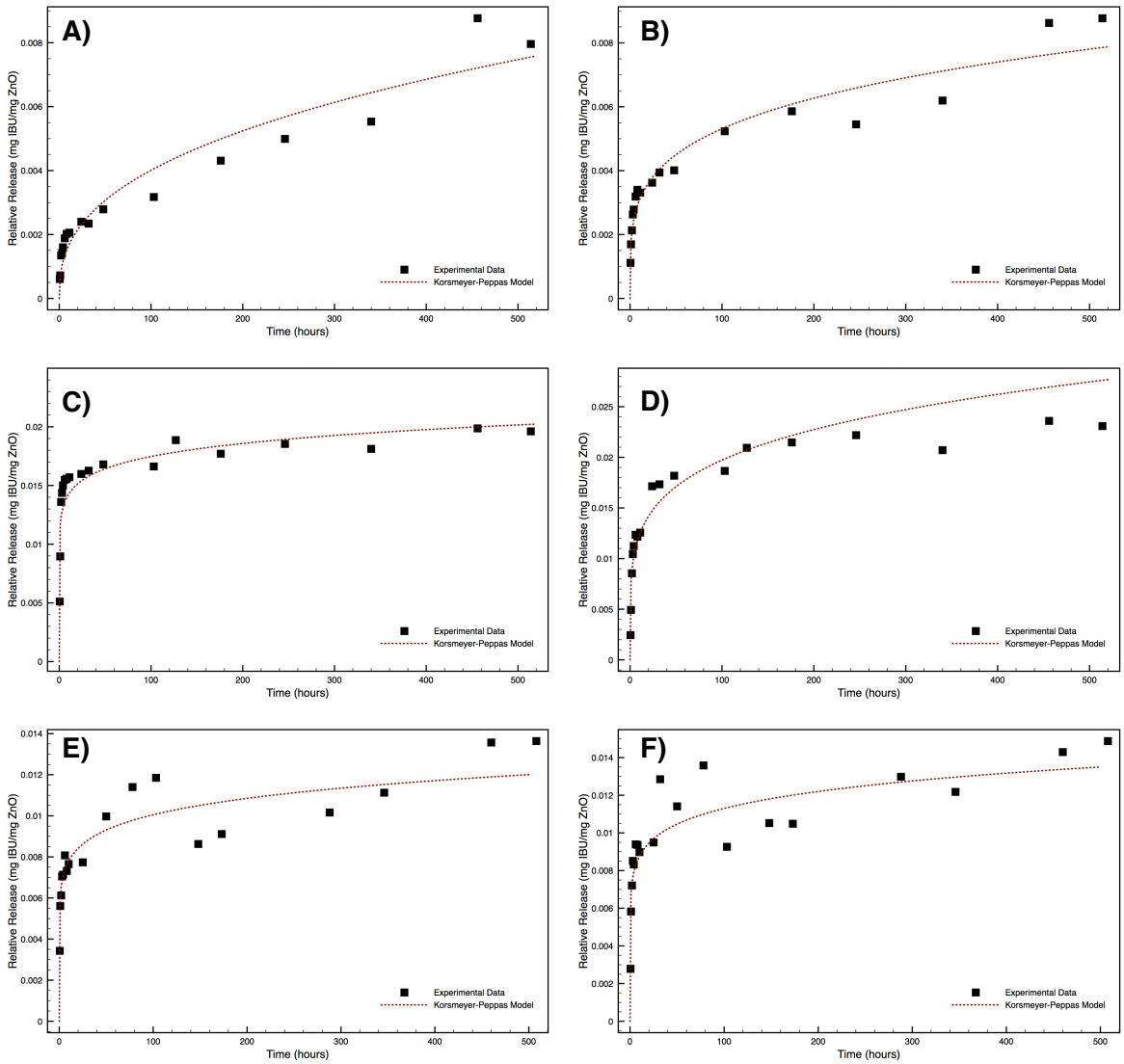

Figure 56: Korsmeyer-Peppas model applied to various drug releases of nanostructured ZnO loaded with IBU. A: 1 mg/mL; B: 2 mg/mL; C: 10 mg/mL; D: 20 mg/mL; E: 10 mg/mL 1 wash; F: 10 mg/mL 3 wash

4.4 Degradation of the Drug Delivery Systems

SEM images were created to look at the microstructure of the DDSs before and after the drug release in order to gain insight into possible release mechanisms. These are shown in figure 55 for the nanostructured ZnO particles and figure 56 for the composite drug delivery systems.

4.4.1 Degradation of Nanostructured ZnO

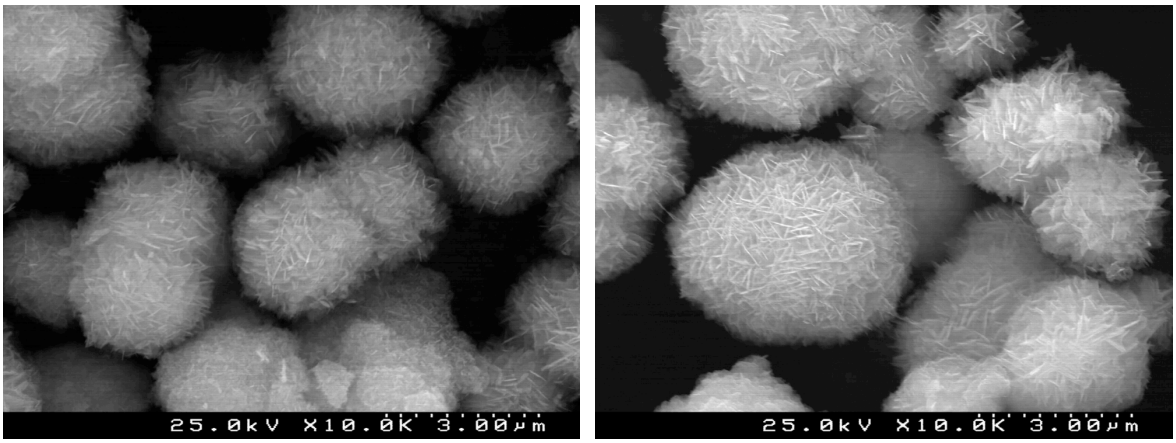

Figure 57: SEM of nanostructured ZnO before (left) and after (right) being subjected to shaking at 125 rpm in PBS at 37 °C for 14 days during a drug release experiment

Comparison of the left and right sections of figure 45, showing the nanostructured ZnO before and after the drug release experiments, respectively, shows that the structural integrity of the particles is maintained, even after being subjected to shaking at 125 rpm in PBS for 2 weeks. It can be seen that the particles post-release can still be characterized by an agglomeration of nanoplatelets that form spherical particles of roughly 4 microns in diameter. This observation suggests that the drug release occurs primarily by desorption of the drug from the particle surface, and that other mechanisms based on the particle degradation do not occur.

4.4.2 Degradation of ZnO/PU Composites

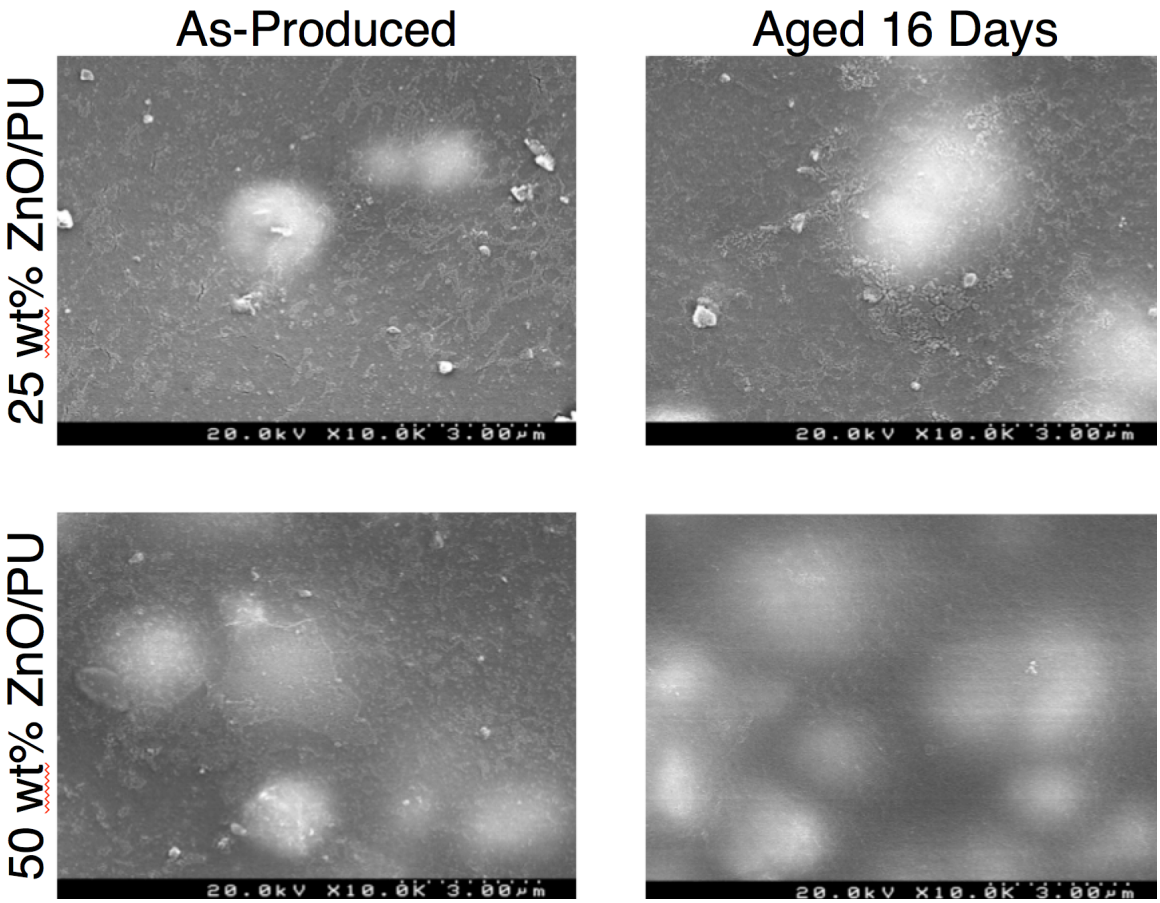

Figure 58: SEM image of ZnO/PU composite DDSs before and after being subjected to drug release medium for 16 days

Similar to the situation of the ZnO particle degradation (or lack thereof), the ZnO/PU composites also withstand the drug release environment. As documented in figure 56, the images taken before and after the drug release experiments are nearly indistinguishable from each other. This suggests that the composites are physically robust, and do not easily degrade in solutions with high salt concentration (e.g. PBS). This offers practical significance in applications for where the structure of the DDS should be maintained, as would be useful for bone or vascular implants. Furthermore, this observation offers insight into the drug release mechanisms. Namely, the polymer plays little role in the drug release process aside from serving as a diffusion barrier. As no swelling or degradation of the system was observed, it is indicative that, even in the more complex composite system,

the drug release occurs through desorption from the ZnO particles and diffusion throughout the composite into the release medium.

Chapter 5

Conclusions and Future Work

5. Conclusions and Future Work

In this work, drug delivery systems based on nanostructured zinc oxide as well as composite DDSs based on nanostructured zinc oxide embedded in polymeric matrices of polyurethane were successfully created. It has been shown that the chemical precipitation of the nanostructured ZnO powders allows particles to form with uniform morphologies and narrow size distributions as well as providing a simple and repeatable method for synthesizing an oxide material without the need of high temperatures for calcination processes.

Various characterization techniques have been used on both loaded and unloaded samples of the zinc oxide powders in order to examine the role of loaded ibuprofen. It was confirmed that it is possible to control the drug loading in the samples by controlling the ibuprofen concentration in the loading solutions. It was also found that washing the samples post loading resulted in a decrease in the amount of drug loaded, likely caused by the removal of a loosely bound layer of ibuprofen. An associated smoothing of the particle surfaces was observed for the washed samples.

Finally, the composite samples were able to reduce the drug release by providing barriers to the diffusion of ibuprofen out of the zinc oxide nanostructures. In both systems (particle and composite DDSs), subjecting the carriers to the release medium had little effect on the overall structural integrity of the samples. No degradation was observed.

Suggestions for future work would be to further investigate the role of variations in drug loading and how composites created with powders of different loadings behave. Experiments performed in release media of various acidities would also be interesting and could provide information pertaining to the material's use in response-driven drug release. Additionally, it would be desirable to develop a method to accurately and quantitavely determine the amount of ibuprofen loading in the samples so a relationship could be develop between the concentration in the loading solution and drug release potential.

Bibliography

[1] H. Liu, T.J. Webster, Ceramic/polymer nanocomposites with tunable drug delivery capability at specific disease sites. Journal of Biomedical Materials Research Part A. 93A, 1180-1192 (2009)

[2] A.L.M. Pires, Sistemas compósitos de PU/ZnO para entrega da fármacos. MA Thesis. Universidade de Aveiro (2012)

[3] J. Louro. Compósitos PU/ZnO para aplicações biomédicas. MA Thesis. Universidade de Aveiro (2012)

[4] T.M. Allen, P.R. Cullis, Liposomal drug delivery systems: From concept to clinical applications, Medicinal applications of fullerenes, The application of carbon nanotubes in target drug delivery systems for cancer therapies. Advanced Drug Delivery Reviews. 65, 36-48 (2013)

[5] V.J. Venditto, F.C. Szoka Jr., Cancer nanomedicines: So many papers and so few drugs!. Advanced Drug Delivery Reviews. 65, 80-88 (2013)

[6] S. Sershen, J. West, Implantable, polymeric systems for modulated drug delivery. Advanced Drug Delivery Reviews. 55, 439 (2003)

[7] J.S. Boateng, K.H. Matthews, H.N.E. Stevens, G.M. Eccleston, Wound Healing Dressings and Drug Delivery Systems: A Review. Journal of Pharmaceutical Sciences. 97, 2892-2923 (2008)

[8] M. Biondi, F. Ungaro, F. Quaglia, P.A. Netti, Controlled drug delivery in tissue engineering. Advanced Drug Delivery Reviews. 60, 229-242 (2008)

[9] X. Huang, P.K. Jain, I.H. El-Sayed, M.A. El-Sayed, Gold nanoparticles: interesting optical properties and recent applications in cancer diagnostics and therapy. Nanomedicine. 2, 681-693 (2007)

[10] Y. Shi, S. Xu, A. Dong, Design and in vitro evaluation of transdermal patches based on ibuprofen-loaded electrospun fiber mats. Journal of Materials Science: Materials Medicine 24, 333-341 (2013)

[11] http://www.nlm.nih.gov/medlineplus/druginfo/meds/a682159.html, Access: Dec, 2014

[12] S. Lederkanchanaporn, D. Dollimore, A Thermal Analysis Study of Ibuprofen, Journal of Thermal Analysis. 49, 879-886 (1997)

[13] K.D. Rainsford, Ibuprofen: pharmacology, efficacy and safety. Inflammopharmacology. 17, 275-342 (2009)

[14] J. Wu, Y.J. Zhu, S.W. Cao, F. Chen, Hierarchically Nanostructured Mesoporous Spheres of Calcium Silicate Hydrate: Surfactant-Free Sonochemical Synthesis and Drug-Delivery System with Ultrahigh Drug-Loading Capacity. Advanced Materials. 22, 749-753 (2010)

[15] M.P. Ferraz, A.Y. Mateus, J.C. Sousa, F.J. Monteiro, Nanohydroxyapatite microspheres as delivery system for antibiotics: Release kinetics, antimicrobial activity, and interaction with osteoblasts. Journal of Biomedical Materials Research Part A. 81, 994-1004 (2007)

[16] S.A. Gittens, H. Uludag, Growth Factor Delivery for Bone Tissue Engineering, Journal of Drug Targeting. 9, 407-429 (2001)

[17] B. Palazzo et al., Controlled drug delivery from porous hydroxyapatite grafts: An experimental and theoretical approach. Materials Science and Engineering C. 25, 207-213 (2005)

[18] M. Öner, E. Yetiz, E. Ay, U. Uysal, Ibuprofen release from porous hydroxyapatite tablets. Ceramics International. 37, 2117-2125 (2011)

[19] J. Andersson, J. Rosenholm, S. Areva, M. Lindén, Influences of Material Characteristics on Ibuprofen Drug Loading and Release Profiles from Ordered Micro- and Mesoporous Silica Matrices. Chemistry of Materials. 16, 4160-4167 (2004)

[20] I. Izquierdo-Barba, Á. Martinez, A.L. Doadrio, J. Pérez-Pariente, M. Vallet-Regí, Release evaluation of drugs from ordered three-dimensional silica structure. European Journal of Pharmaceutical Sciences. 26, 365-373 (2005)

[21] T. Ukmar, U. Maver, O. Planinšek, V. Kaučič, M. Gaberšček, A. Godec, Understanding controlled drug release from mesoporous silicates: Theory and experiment. Journal of Controlled Release. 155, 409-417 (2011)

[22] P. Horcajada, A. Rámila, J. Pérez-Pariente, M. Vallet-Regí, Influence of pore size of MCM-41 matrices on drug delivery rate. Microporous and Mesoporous Materials. 68, 105-109 (2004)

[23] B. Palazzo, M. Iafisco, M. Laforgia, N. Margiotta, G. Natile, C.L. Bianchi, D. Walsch, S. Mann, N. Roveri, Biomimetic Hydroxyapatite–Drug Nanocrystals as Potential Bone Substitutes with Antitumor Drug Delivery Properties. Advanced Functional Materials. 17, 2180-2188 (2007)

[24] M.Y. Ma, Y.J. Zhu, L. Li, S.W. Cao, Nanostructured porous hollow ellipsoidal capsules of hydroxyapatite and calcium silicate: preparation and application in drug delivery. Journal of Materials Chemistry. 18, 2722-2727 (2008)

[25] Q.L. Tang, Y.J. Zhu, J. Wu, F. Chen, S.W. Cao, Calcium phosphate drug nanocarriers with ultrahigh and adjustable drug-loading capacity: One-step synthesis, in situ drug loading and prolonged drug release. Nanomedicine: Nanotechnology, Biology, and Medicine. 7, 428-434 (2011)

[26] A. Dubnika, D. Loca, L. Berzina-Cimdina, Functionalized hydroxyapatite scaffolds coated with sodium alginate and chitosan for controlled drug delivery. Proceedings of the Estonian Academy of Sciences. 61, 193-199 (2012)

[27] D. Loca, J. Locs, K. Salma, J. Gulbis, I. Salma, L. Berzina-Cimdina Porous Hydroxyapatite Bioceramic Scaffolds for Drug Delivery and Bone Regeneration. IOP Conference Series: Materials Science and Engineering. 18, 192019 (2011)

[28] H.W. Kim, J.C. Knowles, H.E. Kim, Hydroxyapatite/poly(ε-caprolactone) composite coatings on hydroxyapatite porous bone scaffold for drug delivery. Biomaterials. 25, 1279-1287 (2004)

[29] A.K. Dash, R. Suryanarayanan, An Implantable Dosage Form for the Treatment of Bone Infections. Pharmaceutical Research. 9, 993-1002 (1992)

[30] M.T. Ethell, R.A. Bennett, M.P. Brown, K. Merritt, J.S. Davidson, T. Tran, In Vitro Elution of Gentamicin, Amikacin, and Ceftiofur From Polymethylmethacrylate and Hydroxyapatite Cement. Veterinary Surgery. 29, 375-382 (2000)

[31] A.S. Hassan, A. Sapin, A. Lamprecht, E. Emond, F.E. Ghazouani, P. Maincent, Composite microparticles with in vivo reduction of the burst release effect. European Journal of Pharmaceutics and Biopharmaceutics. 73, 337-344 (2009)

[32] K.C. Barick, S. Nigam, D. Bahadur, Nanoscale assembly of mesoporous ZnO: A potential drug carrier. Journal of Materials Chemistry. 20, 6446-6452 (2010)

[33] J. Rasmussen, E. Martinez, P. Louka, D.G. Wingett, Zinc Oxide Nanoparticles for Selective Destruction of Tumor Cells and Potential for Drug Delivery Applications. Expert Opinion on Drug Delivery. 7, 1063-1077 (2010)

[34] J.Y. Cherng, T.Y. Hou, M.F. Shih, H. Talsma, W.E. Hennink, Polyurethane-based drug delivery systems. International Journal of Pharmaceutics. 450, 145-162 (2013)

[35] Ü. Özgür, Y.I. Alivov, C. Liu, A. Teke, M.A. Reshchikov, S. Dogan, V. Avrutin, S.J. Cho, H. Morkoç, A comprehensive review of ZnO materials and devices. Journal of Applied Physics. 98, 041301 (2005)

[36] Y.B. Hahn, Zinc oxide nanostructures and their applications. Korean Journal of Chemical Engineering 28, 1797-1813 (2011)

[37] A. Moezzi, A.M. McDonagh, M.B. Cortie, Zinc oxide particles: synthesis, properties and applications. Chemical Engineering Journal. 185-186, 1-22 (2012)

[38] H.M. Xiong, ZnO nanoparticles applied to bioimaging and drug delivery. Advanced Materials. 25, 5329-5335 (2013)

[39] Y. Fu, W.J. Kao, Drug Release Kinetics and Transport Mechanisms of Non-degradable and Degradable Polymeric Delivery Systems. Expert Opinion on Drug Delivery. 7, 429-444 (2010)

[40] R. Adhikari, P.A. Gunatillake, I. Griffiths, L. Tatai, M. Wickramaratna, S. Houshyar, T. Moore, R.T.M. Mayadunne, J. Field, M. McGee, T. Carbone, Biodegradable injectable polyurethanes: Synthesis and evaluation for orthopaedic applications. Biomaterials. 29, 3762-3770 (2008)

[41] T. Amna, M.S. Hassan, F.A. Sheikh, H.K. Lee, K.S. Seo, D. Yoon, I.H. Hwang, Zinc oxide-doped poly(urethane) spider web nanofibrous scaffold via one-step electrospinning: a novel matrix for tissue engineering. Applied Microbiology and Biotechnology 97, 1725-1734 (2013)

[42] H.B. Bakrudeen, J. Tsibouklis, B.S.R. Reddy, Facile fabrication of mesoporous ZnO nanospheres for the controlled delivery of captopril. Journal of Nanoparticle Research 15, 1505 (2013)

[43] Z.Y. Zhang, Y.D. Xu, Y.Y. Ma, L.L. Qiu, Y. Wang, J.L. Kong, H.M. Xiong, Biodegradable ZnO@polymer Core–Shell Nanocarriers: pH-Triggered Release of Doxorubicin In Vitro. Angewandte Chemie International Edition 52, 4127-4131 (2013)

[44] S. Hillaert, W. Van den Bossche, Determination of captopril and its degradation products by capillary electrophoresis. Journal of Pharmaceutical and Biomedical Analysis. 21, 65-73 (1999)

[45] A.M. Nyström, B. Fadeel, Safety assessment of nanomaterials: Implications for nanomedicine. Journal of Controlled Release. 161, 403-408 (2012)

[46] W.I. Hagens, A.G. Ooman, W.H. de Jong, F.R. Cassee, A.J.A.M. Sips, What do we (need to) know about the kinetic properties of nanoparticles in the body?. Regulatory Toxicology and Pharmacology. 49, 217-229 (2007)

[47] S. Chibber, S.A. Ansari, R. Satar, New vision to CuO, ZnO, and TiO2 nanoparticles: their outcome and effects. Journal of Nanoparticle Research 15, 1492 (2013)

[48] Y.N. Chang, M. Zhang, L. Xia, J. Zhang, G. Xing, The Toxic Effects and Mechanisms of CuO and ZnO Nanoparticles. Materials. 5, 2850-2871 (2012)

[49] Y. Zhang, M. Huo, J. Zhou, A. Zou, W. Li, C. Yao, S. Xie, DDSolver: An Add-In Program for Modeling and Comparison of Drug Dissolution Profiles. The AAPS Journal. 12, 263-271 (2010)

[50] J. Siepmann, F. Siepmann, Mathematical modeling of drug delivery. International Journal of Pharmaceutics. 368, 328-343 (2008)

[51] R.A.K. Arza, C.S.R. Gonogunta, P.R. Veerareddy, Formulation and Evaluation of Swellable and Floating Gastroretentive Ciprofloxacin Hydrochloride Tablets. AAPS PharmSciTech. 10, 220-226 (2009)

[52] J.T. Seil, T.J. Webster, Decreased astroglial cell adhesion and proliferation on zinc oxide nanoparticle polyurethane composites. International Journal of Nanomedicine. 3, 523-531 (2008)

[53] S. Ramukutty, E. Ramachandran, Reaction Rate Models for the Thermal Decomposition of Ibuprofen Crystals. Journal of Crystallization Process and Technology. 4, 71-78 (2014)

[54] Owen, Tony. Fundamentals of UV-visible Spectroscopy: A Primer. Germany: Hewlett-Packard Company, 1996. Print

[55] V. Srivastava, D. Gusain, Y.C. Sharma, Synthesis, characterization and application of zinc oxide nanoparticles (n-ZnO). Ceramics International. 39, 9803-9808 (2013)

[56] L. Alexander, H.P. Klug, Determination of crystallite size with the x-ray spectrometer. Journal of Applied Physics. 21, 137-142 (1950)

[57] R. Hariharan, S. Senthilkumar, A. Suganthi, M. Rajarajan, Synthesis and characterization of doxorubicin modified ZnO/PEG nanomaterials and its photodynamic action. Journal of Photochemistry and Photobiology B: Biology. 116, 56-65 (2012)

[58] V. Parthasarathi, G. Thilagavathi, Synthesis and characterization of zinc oxide nanoparticle and its application on fabrics for microbe resistant defence clothing. International Journal of Pharmacy and Pharmaceutical Sciences. 3, 392-398 (2011)

[59] C. Guignot, N. Betz, B. Legendre, A. Le Moel, N. Yagoubi, Degradation of segmented poly(etherurethane) Tecoflex® induced by electron beam irradiation: Characterization and evaluation. Nuclear Instruments and Methods in Physics Research B. 185, 100-107 (2001)

[X] C. Yao, M. Hedrick, G. Pareek, J. Renzulli, G. Haleblian, T.J. Webster, Nanostructured polyurethane-poly-lactic- co-glycolic acid scaffolds increase bladder tissue regeneration: an in vivo study. International Journal of Nanomedicine. 8, 3285-3296 (2013)

Appendix

Table 8: R^2 values for the various mathematical models

Sample	First Order	Higuchi	Korsmeyer-Peppas	Baker-Lonsdale	Mankoid-Banaker
1 mg/mL	.75	.90	.93	.92	.97
2 mg/mL	.59	.52	.93	.09	.96
10 mg/mL	.87	-.51	.73	.32	.76
20 mg/mL	.88	.07	.92	.80	.95
1 Wash	.57	-2.8	.63	.24	.72
3 Washes	.73	-2.8	.66	.30	.71